Available online at www.sciencedirect.com

ScienceDirect

Nuclear Data Sheets 148 (2018) 214–253

Nuclear Data Sheets

www.elsevier.com/locate/nds

Evaluation of Neutron Reactions on Iron Isotopes for CIELO and ENDF/B-VIII.0

M. Herman,[1,*] A. Trkov,[2] R. Capote,[2] G.P.A. Nobre,[1] D.A. Brown,[1] R. Arcilla,[1] Y. Danon,[3] A. Plompen,[4] S.F. Mughabghab,[1] Q. Jing,[5] G. Zhigang,[5] L. Tingjin,[5] L. Hanlin,[6] R. Xichao,[6] L. Leal,[7,8] B.V. Carlson,[9] T. Kawano,[10] M. Sin,[11] S.P. Simakov,[12] and K. Guber[13]

[1] *National Nuclear Data Center, Brookhaven National Laboratory, Upton, NY 11973, USA*
[2] *NAPC-Nuclear Data Section, International Atomic Energy Agency, A-1040 Vienna, Austria*
[3] *Rensselaer Polytechnic Institute, Troy, NY, USA*
[4] *European Commission, Joint Research Center, Retieseweg 111, B-2440, Geel, Belgium*
[5] *China Nuclear Data Center, P.O. Box 275-41, Beijing 102413, P.R. China*
[6] *China Institute of Atomic Energy, P.O. Box 275-41, Beijing 102413, P.R. China*
[7] *Oak Ridge National Laboratory, Oak Ridge, TN 37831-6171, USA*
[8] *Institut de Radioprotection et de Surete Nucleaire, Paris, France*
[9] *Departamento de Física, Instituto Tecnológico de Aeronáutica, 12228-900, SP, Sao José dos Campos, Brazil*
[10] *Los Alamos National Laboratory, Los Alamos, NM 87545, USA*
[11] *Nuclear Physics Department, Bucharest University, Bucharest-Magurele, Romania*
[12] *Karlsruhe Institute of Technology, 76344 Eggenstein-Leopoldshafen, Germany*
[13] *Oak Ridge National Laboratory, Oak Ridge, TN 37831-6354, USA*

(Received 7 September 2017; revised received 26 October 2017; accepted 16 November 2017)

A new suite of evaluations for ^{54,56,57,58}Fe has been developed in the framework of the CIELO international collaboration. New resolved resonance ranges were evaluated for ^{54}Fe and ^{57}Fe, while modifications were applied to resonances in ^{56}Fe. The low energy part of the ^{56}Fe file is almost totally based on measurements. At higher energies in ^{56}Fe and in the whole fast neutron range for minor isotopes the evaluation consists of model predictions carefully adjusted to available experimental data. We also make use of the high quality and well experimentally-constrained dosimetry evaluations from the IRDFF library. Special attention was dedicated to the elastic angular distributions, which were found to affect results of the integral benchmarking. The new set of iron evaluations was developed in concert with other CIELO evaluations and they were tested together in the integral experiments before being adopted for the ENDF/B-VIII.0 library.

CONTENTS

* Corresponding author: mwherman@bnl.gov

https://doi.org/10.1016/j.nds.2018.02.004

I. INTRODUCTION

Iron is obviously one of the most common elements in the structural materials in nuclear technology applications, and yet the iron evaluations available from various libraries were deemed deficient in certain important respects. One particular concern was the inelastic scattering cross sections: the recommendations by WPEC Subgroup 26 indicate that the inelastic scattering cross sections on ^{56}Fe should be significantly improved to meet target accuracy estimated for innovative reactor systems. At the same time, the ENDF/B-VII.1 [1] inelastic uncertainties close to threshold were increased up to 16% to account for discrepancies among various libraries. Another concern was the angular distributions for elastic and inelastic channels which are expected to play a significant role in shielding, reflection and leakage (in the case of small systems). Therefore it is no surprise that iron is included in the Collaborative International Evaluated Library Organization (CIELO) [2, 3] pilot project.

The evaluations described in the present paper have been created primarily by the combined BNL and IAEA team of evaluators. Within the CIELO project, there is a parallel work on ^{56}Fe conducted by the Chinese team. These are two distinct efforts carried out by different groups which use their own specific tools (*e.g.*, nuclear reaction codes) and make independent decisions. Both groups, however, work in harmony by contributing components of the evaluation effort, by offering specific expertise which is unique to one of the groups, and by comparing performance of preliminary versions of the evaluations. While adopting parts of the evaluations and comparing their performance is a routine practice within the nuclear data community, the novelty of the CIELO project is that this exchange occurs *during* the evaluation process rather than solely after one of the evaluations is already completed. This means that both evaluations benefit from sincere exchange of information and expertise. As a result, they are likely to be similar or even identical in some parts, while different performance priorities, alternative opinions, or different evaluation strategies might drive the two evaluations apart.

The ^{56}Fe evaluation described in the current paper builds on the previous accomplishments including ENDF/B-V file [4] with LANL high energy extension [5], and JEFF evaluations descending from the original work documented in Refs. [6, 7]. For further details we refer readers to the reconstruction of the history of iron evaluations, including links among various national projects, outlined in a BNL report [8].

Even though iron is a very common structural material, unfortunately it is also very difficult to evaluate. There are several strong scattering resonances in ^{56}Fe, with very deep interference minima, where the cross section is nearly zero. In these energy intervals (*e.g.*, the most well known one around 24 keV) the cross sections of the minor isotopes, as well as the alloying constituents (*e.g.*, in stainless steel) dominate. For this reason the evaluation of ^{56}Fe nuclear data cannot be separated from the evaluations of the minor isotopes and alloying materials. On top of it, the nearly closed shell ^{56}Fe is known to have a very small capture cross section. Due to the vicinity of the shell closure and the odd-even effect, capture on the minor isotopes might be higher than that on ^{56}Fe. Therefore validation results for iron containing benchmarks are sensitive to minor isotopes of iron even though ^{56}Fe makes up 91.8% of natural iron. Thus, we have reevaluated minor iron isotopes ^{54}Fe (5.8%), ^{57}Fe (2.1%), and ^{58}Fe (0.3%), modifying the resolved resonance region and recalculating the fast neutron region with the EMPIRE [9] code.

It is worth noting that the new Fe evaluations have to be in sync with the changes in ^{238}U, ^{235}U and ^{239}Pu. In particular, lowering of capture in ^{235}U would greatly increase the reactivity of benchmark assemblies from Argonne National Laboratory like ZPR-9/34 and ZPR-6/10 since many benchmarks (including the latter two) are highly sensitive to the capture cross section below 25 keV.

For obvious reasons, natural iron and ^{56}Fe are among the best measured materials. Many measurements exist for the natural element, as well as for the major isotopic constituent ^{56}Fe. This wealth of precise and high resolution experiments on a relatively light (A $<$ 60) target reveals strong fluctuations that persist in total, and inelastic cross sections up to about 7 MeV. Indeed fluctuations are also present in all of the minor iron isotopes, but are less well resolved experimentally. These fluctuations have to be incorporated in the new evaluation and there is currently no theoretical model capable of reproducing such fluctuating behavior. Therefore, the experimental data, which always form the basis for the evaluation work, are even more critical in the case of iron.

As iron is one of the most important materials in experimental accelerator facilities, many evaluations go beyond 20 MeV. ENDF/B-VII.1 includes the LA-150 evaluation [10] that goes up to 150 MeV, and JEFF-3.1 contains TALYS calculations all the way up to 200 MeV. Other libraries (JENDL-4.0, CENDL-3.1, and ROSFOND) contain evaluations that just go up to 20 MeV, but JENDL-4.0 has a separate file for high energy applications (JENDL/HE). The current evaluation extends up to 150 MeV, which on its own poses a number of formatting issues. We refer to Sec, VI for the adopted file structure and explain our unusual choices (*e.g.*, our treatment of the (n, α) channel).

Development of the new iron evaluations can be

traced with the 'CIELO-iron' project on the NNDC GForge server (https://ndclx4.bnl.gov/gf/project/cielo_iron). All elements of the evaluation, such as experimental datasets, EMPIRE inputs and outputs, intermediate ENDF files and plots can be found there in chronological order. This not only allows an interested person to follow all stages of the evaluation development but makes it possible to reproduce, and therefore also modify, the current evaluation.

Although ^{56}Fe is the most important of the iron isotopes, the evaluation process for all the naturally occurring isotopes proceeded in parallel. This aspect drives then the organization of this paper. First we describe the experimental data generally available for all iron isotopes and which sets we based our evaluations upon. Following this, we describe the resonance region evaluations of each isotope. Next, we describe the common fast region modeling for all the isotopes. Then we discuss evaluated results for cross sections, angular distributions, energy spectra and double-differential cross sections. Our non-standard formatting choices are detailed in a dedicated section. Next we discuss covariances and the results of the validation. In the conclusions we summarize our achievements but also point to possible future improvements.

The evaluations reported in this paper have been adopted by the ENDF/B-VIII.0 library [11] and therefore we often refer to them as ENDF/B-VIII.0. Regarding the ^{56}Fe evaluation, which is part of the CIELO project, we also refer to it as CIELO.

II. RESOLVED RESONANCE REGION

A. Resonances in ^{56}Fe

The fluctuations in the ^{56}Fe cross sections continue to rather high energy, well past the thresholds of the first two (n, n') states. Therefore the resonance region could be extended to much higher energy than what has been done in earlier evaluations. Unfortunately, our attempts to extend the resolved resonance region (RRR) beyond 2 MeV did not result in improvements over the original Froehner evaluation used in JEF-2.2. Therefore we decided to adopt the Froehner evaluation, correcting the original evaluation for typos (a resonance energy was changed from 767.240 keV to 766.724 keV and the spurious resonance at 59.9 keV was deleted). Froehner's evaluation has also been adopted in subsequent JEFF libraries and in JENDL-4.0.

Froehner's resonance evaluation uses the Reich-Moore formula and ranges from 0.01 meV to 850.0 keV and there is no unresolved resonance range. The JENDL-4.0 capture background near 800 keV was reduced by 40%, with the difference assigned to the elastic. This background is needed to compensate for the missing resonances at the end of the resonance region (the lack of such background in JEFF-3.2 creates an unphysical dip in the capture cross section).

An artificial "background" was added to capture between 10 eV and 100 keV. Originally, this addition was motivated by the criticality benchmarking in which the HEU-MET-INT-001 (ZPR-34/9) eigenvalue was overpredicted by more than 1000 pcm. There is an extraordinary sensitivity of this benchmark to capture around 24 keV and a relatively minor correction in this range allows for bringing the HEU-MET-INT-001 result within the experimental uncertainty, practically without affecting other benchmarks. The adjusted capture cross section nearly follows the $1/v$ behavior as shown in Fig. 1. The difference was compensated in the total cross section. It is important to check the impact of this background on the well-known dip around 24 keV in the ^{56}Fe total cross section that is extremely important for the calculation of the shielding properties of iron. This cross section in ENDF/B-VII.1 is 3.43 mb while ENDF/B-VIII.0 rises it up to 6.82 mb, in perfect agreement with the result of Ref. [12] (7.5 ± 4.2 mb).

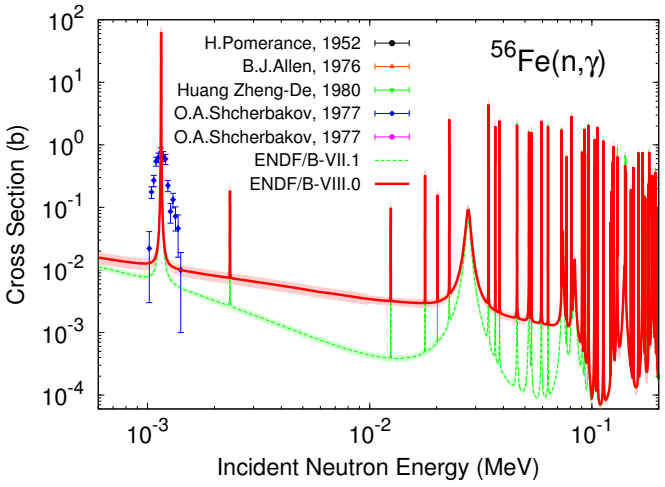

FIG. 1. (Color online) ^{56}Fe(n, γ) cross sections in the resonance region. The present evaluation is compared with ENDF/B-VII.1 to show the effect of the added low-energy background.

Fig. 2 shows that the well-known dip in the total cross section, that leads to strongly enhanced transmission of 24 keV neutrons through iron, is better described in the current evaluation than in ENDF/B-VII.1 providing strong justification for the added background (at least until a better description by resolved resonance parameters is provided).

Additionally, the capture width of the resonance at 28 keV was increased to better match the data by Spencer (ORELA) [13] that are available in EXFOR [14] (see Fig. 3).

Thermal cross section, resonance integral (RI) and Maxwellian averaged cross sections (MACS) integral metrics for ^{56}Fe are shown in Table I. In this set of tables, we compare to values from the Atlas [15], KADoNiS [19] and EXFOR. In this table, we note that the KADoNiS values are based on the Kaeppeler reference for gold capture

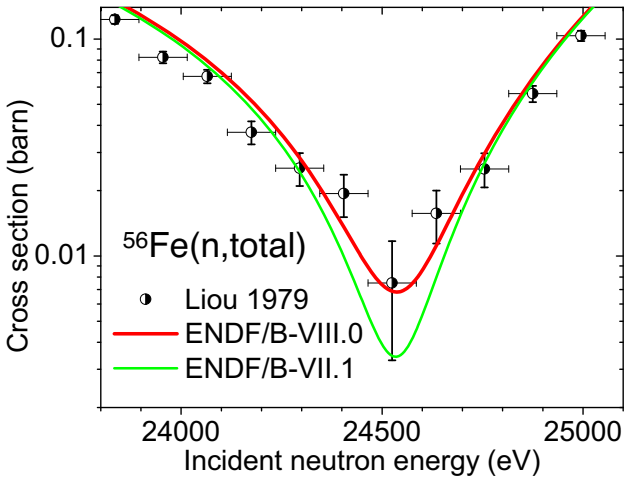

FIG. 2. (Color online) ^{56}Fe(n,tot) cross sections in the resonance region around 24 keV. Present evaluation is compared with ENDF/B-VII.1 showing a much better agreement with the experimental data in this critical energy region ("iron filter").

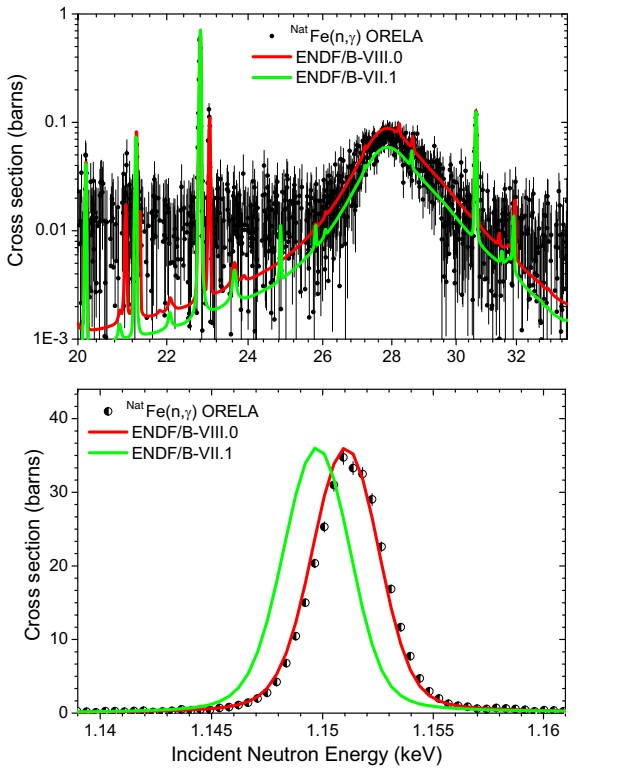

FIG. 3. (Color online) Effect of the two specific changes made in the resolved resonance region for ^{56}Fe. The upper panel shows the result of adding a low energy background and increasing the γ-width for the resonance at 28 keV on the capture cross sections and compares the results to Spencer's data. The lower panel shows the shift between ENDF/B-VII.1 and Spencer's energy calibration.

MACS(30 keV) which is now 8% below the calculated value from gold reference cross section [11]. That affects all renormalizations in KADoNiS and the affected values are marked. This, coupled with issues with the flux profile used in these measurements, lead us to use the MACS data for validation purposes only.

We comment that R. Firestone *et al.* advocate for a lower thermal capture (2.394 ± 0.019 b) value based on EGAF results [16]. Unfortunately this result became available only after the current version of the evaluation was complete. A preliminary version of this result advocated for a much higher result (2.71 b), going in exactly the wrong direction from what is needed according to our integral benchmarking. However this new result, once included, may help to push our results into better agreement with the LCT benchmarks.

B. Resonances in ^{54}Fe

The resonance region evaluation for ^{54}Fe was initially evaluated at IRSN, up to 1.036 MeV, by using SAMMY to fit Pandey *et al.* [27] and Cornelis *et al.* [28] data. In both cases a time of flight correction [29] was applied, accounting for energy shifts between fits and unmodified data retrieved from EXFOR. The evaluation uses the Reich-Moore approximation and the LRF=7 format. The initial J^π assignments of resonances were taken from the Atlas of Neutron Resonances [30]. The original fit included direct/semi-direct contributions that were later removed in favor of bound levels taken from the new edition of the Atlas. As neither Cornelis *et al.* nor Pandey *et al.* resolved all resonances (especially the smaller p- and d-wave resonances), the IRSN fits were supplemented with 64 resonances compiled in the newest edition of the Atlas. The largest number of these smaller resonances were measured by Giubrone *et al.* [31].

Even with the addition of these p- and d-wave resonances, the average capture cross section was substantially lower than the measured average capture data of Allen *et al.* (1976) [26]. We computed the capture background from 100 keV-1 MeV by subtracting the group-wise cross section determined from the resonance parameters from the Allen *et al.* data. This not only brought the average cross section into agreement with Allen *et al.* [26] data, but also with the new Wallner data [32] shown in Table III and discussed below. To ensure a proper match of the fast region capture onto the average resonance region capture cross section, we extended our EMPIRE calculations to 10 eV and tuned our calculation to match the average data of Allen *et al.* (1976) [26]. Fig. 4 shows the background determination and the comparison to the EMPIRE calculations.

We comment that while our evaluation compares favorably with Atlas values for both the thermal cross sections and resonance integrals, it does not match the KADoNiS-0.3 recommended value for MACS(30 keV) [19] (see Table II). This is no surprise: the KADoNiS recommendation was based on a preliminary version of the Wallner *et*

TABLE I. ^{56}Fe resonance region integral metrics. KADoNiS values are based on the Kappeler reference for gold capture MACS(30 keV) which is now 8% below the calculated value from the gold reference cross section [11]. That affects all renormalizations in KADoNiS and the affected values are marked with an asterisk (*). Atlas results marked with ?exp? refer to the Mughabghab's evaluation based on the experimental data, while Atlas values derived from systematics are marked with ?sys?.

σ_{therm} (b)	$(n$,tot)	$(n$,el)	(n,γ)
ENDF/B-VIII.0	14.69	12.1	2.6063
Atlas (2018) [15]		12.6	2.59 ± 0.14
Firestone, *et al.* (2017) [16]			2.394 ± 0.019

RI (b)	$(n$,tot)	$(n$,el)	(n,γ)
ENDF/B-VIII.0	138.84	133.83	1.379
Atlas (2018) [15]			1.37 ± 0.15

MACS(30 keV) (mb)	(n,γ)
ENDF/B-VIII.0	13.97
JENDL-4.0 [17]*	11.84 ± 1.17
ENDF/B-VII.1 [1]*	11.50 ± 1.18
JEFF-3.1 [18]*	11.48
Atlas (exp) (2018) [15]	15.1 ± 1.3
Atlas (sys) (2018) [15]	11.3 ± 1.2
KADoNiS-0.3 [19]*	11.7 ± 0.5
Wang *et al.* (2009) [20]*	12.22 ± 2.06
Corvi *et al.* (1991,1992) [21, 22]*	11.7 ± 0.5
Käppeler *et al.* (1983) [23, 24]	13.9 ± 0.7
Allen *et al.* (1976,1977) [25, 26]	14.4 ± 2.0
Allen *et al.* (1976) [26]	13.2 ± 2.0
Allen *et al.* (1976) [26]	15.1 ± 1.3

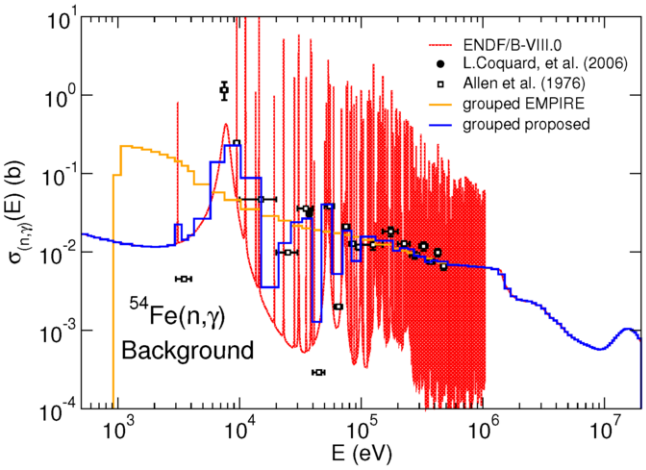

FIG. 4. (Color online) ^{54}Fe(n,γ) cross sections in the resonance region, showing our treatment of the background cross section.

al. data [33]. This data has since been superseded with the results from Ref. [32]. The new Wallner *et al.* results are tabulated in Table III and consist of a measurement of the thermal capture cross section, the MACS(25 keV) (and not the MACS(30 keV) as reported in Refs. [19, 33]), and an average over a roughly triangular spectrum peaked at 481 keV. Issues with the flux profile used in these measurements lead us to use the MACS and similar data for validation purposes only.

TABLE II. ^{54}Fe resonance region integral metrics. The results from Coquard *et al.* [33] form the basis for the KADoNiS recommendation however this set has been superceded. See the text for more discussion.

σ_{therm} (b)	$(n$,tot)	$(n$,el)	(n,γ)
ENDF/B-VIII.0	4.417	2.162	2.25
Atlas (2018) [15]	4.47 ± 0.12	2.17 ± 0.10	2.30 ± 0.07

RI (b)	$(n$,tot)	$(n$,el)	(n,γ)
ENDF/B-VIII.0	125.96	121.60	1.21
Atlas (sys) (2018) [15]			1.27 ± 0.10

MACS(30 keV) (mb)	(n,γ)
ENDF/B-VIII.0	27.13
Atlas (exp) (2018) [15]	27.7 ± 1.0
Atlas (sys) (2018) [15]	28.3 ± 1.3
KADoNiS-0.3 [19]	29.6 ± 1.3
Coquard *et al.* (2006) [33]	30.3 ± 3.0
Brusegan *et al.* (1982) [34]	27.6 ± 1.8
Allen *et al.* (1977) [35]	33.6 ± 2.7
Beer *et al.* (1974,1975) [36, 37]	28 ± 9

TABLE III. ^{54}Fe comparison with Wallner *et al.* [32] neutron capture results. See text for discussion.

	Wallner *et al.*	ENDF/B-VIII.0
$\sigma_{\gamma,\text{therm}}$ (b)	2.30±0.07	2.25
MACS(25 keV) (mb)	30.3±1.2	30.75
σ_γ(481±53 keV) (mb)	6.01±0.23	7.83

C. Resonances in ^{57}Fe

As all modern ^{57}Fe evaluations trace back to the 1981 edition of the Atlas [38] and have at most modest changes, we decided it was best to start from the version of the Atlas that was still in development at the time our evaluation was performed [15]. At that time, the Atlas provided Multi-Level Breit-Wigner for ^{57}Fe. However, the compilation in the Atlas appeared to use parameters generated in Reich-Moore approximation. Because the Atlas also contained resonance parameters for resonances in the first (n,n') state, we realized it was wise to convert the Atlas compilation to the LRF=7 format using Reich-Moore approximation, including the first inelastic state.

While the change from MLBW Atlas parameters to LRF=7 parameters necessitated a refitting of the bound levels and R' in ^{57}Fe, the change did improve agreement between the evaluation and experiment in the minima between resonances. The capture widths were known only from the area under each resonance. Additionally we added several resonances at the upper end of the RRR to improve agreement of the RRR with data in the region of 140-165 keV. The list of added/modified resonances

TABLE IV. Resonance changes from the Atlas compilation [15] for the present ^{57}Fe evaluation.

		Before			After		
E_R (keV)	J	Γ_{tot} (eV)	Γ_n (eV)	Γ_γ (eV)	Γ_{tot} (eV)	Γ_n (eV)	Γ_γ (eV)
-55.00	0				27,000.8	27,000.0	0.8
-2.33	1	66.62	64.89	1.73			
-1.22	1				11.51	9.51	2.00
6.22	1	381.15	380.00	1.15	401.15	400.00	1.15
169.31	0				1801.38	1800	1.38
176.30	0	701.20	700.00	1.20	501.20	500	1.20
185.00	1	3903.00	3500.00	3.00	5203.00	4800	3.00
189.50	0	3201.50	3200.00	1.50	4201.50	4200	1.50
194.25	0				703.55	700	3.55
197.30	0				702.57	700	2.57
198.90	0				701.18	700	1.18
200.10	0				700.99	700	0.99

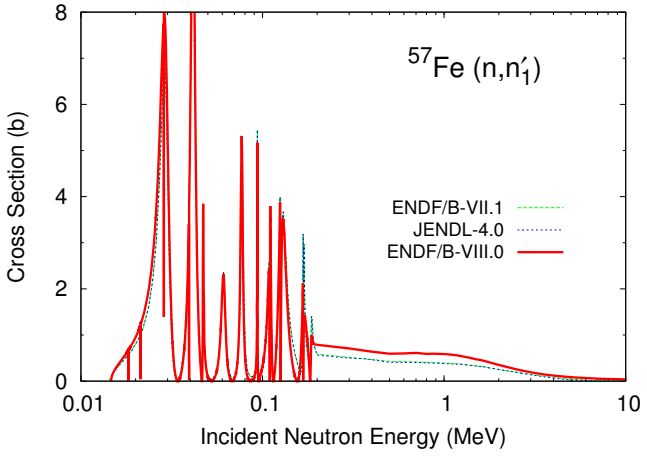

FIG. 5. (Color online) Evaluated ^{57}Fe(n,n'_1) cross section compared with JENDL-4.0 and with the previous ENDF evaluation. The fluctuating structure below 200 keV is the inelastic cross section reconstructed from the resonance parameters stored in the evaluated file using LRF=7 option.

TABLE V. ^{57}Fe resonance region integral metrics.

$\sigma_{\rm therm}$ (b)	$(n$,tot)	$(n$,el)	(n,γ)
ENDF/B-VIII.0	3.087	0.604	2.484
Atlas (2018) [15]	3.16 ± 0.31	0.68 ± 0.06	2.48 ± 0.3

RI (b)	$(n$,tot)	$(n$,el)	(n,γ)
ENDF/B-VIII.0	94.48	82.25	1.508
Atlas (2018) [15]			1.51 ± 0.15

MACS(30 keV) (mb)	(n,γ)
ENDF/B-VIII.0	35.98
JENDL-4.0 [17]	30.3
Atlas (exp) (2018) [15]	37.7 ± 2.3
Atlas (sys) (2018) [15]	42.1 ± 4.2
KADoNiS-0.3 [19]	40 ± 4
KADoNiS-1.0 [41]	26.8 ± 4.4
Giubrone (2014) [31]	26.8 ± 4.4
Wang *et al.* (2010) [20]	44.48 ± 7.56
Rohr *et al.* (1983) [42]	39.9 ± 4.0
Allen *et al.* (1977) [43]	36.0 ± 2.3
Beer (1975) [36, 37]	28 ± 6, 28.8 ± 6.2

is given in Table IV. The (n,n') resonances were determined by identifying capture resonances with no elastic counterpart and subtracting the capture width from the total width determined from $(n$,tot) measurements. The (n,n') resonances were assumed to be s-wave only. This choice was supported by the experimental results of Ref. [39] and Ref. [40]. The final ^{57}Fe(n,n') cross section is shown in Fig. 5. We note that prior evaluations placed the resonance structure directly in the pointwise ^{57}Fe(n,n') cross section, and the competition between inelastic, elastic and capture was handled with the use of a "competitive" channel.

The translation to LRF=7 also forced us to implement several checks and changes to FUDGE including checks for convergence of partial waves with respect to the orbital angular momentum ℓ and for complete enumeration of open R-matrix channels in the ENDF file.

Our thermal cross section and computed resonance integral values are in excellent agreement with the Atlas recommendations [15], see Table V. However, the MACS(30 keV) results deserve more discussion. We note that our value lies roughly in between the JENDL-4.0 and KADoNiS-0.3 values and is generally consistent with the experimental averaged value given in the new Atlas (marked with "exp"). The Atlas value derived from systematics (marked with "sys") is more consistent with the KADoNiS-0.3 value. We note that the in-development version of KADoNiS-1.0 recommends a value basically taken from the Giubrone thesis [31], measured at CERN n_TOF. We note that this measurement does not span the whole energy range of the resonance region. Therefore Giubrone omits several low energy resonances that would have provided a smooth background to the 30 keV region, lowering the MACS(30 keV) value obtained from the consideration of that set alone. As before, we only use the MACS data for validation purposes only.

D. Resonances in ^{58}Fe

The resolved resonance parameters were adopted from the JEFF-3.2. For convenience of the reader, we summarize below the documentation of the JEFF-3.2 evaluation.

Moxon's evaluation was performed as part of the IAEA project on the IRDFF library and is documented in https://www-nds.iaea.org/publications/indc/indc-uk-0089/, following his earlier work [44], and is documented in Ref. [45]. The resonances are given in the Reich-Moore representation covering the energy range from 10^{-5} eV to 350 keV. The unresolved region is adopted for self-shielding only. In the current evaluation all angular distributions, including Resolved and Unresolved Resonance Regions, were calculated by EMPIRE.

The thermal cross section value of 1.315 b for radiative capture agrees very well with 1.30 and 1.31 b, values reported in Refs. [44, 46] respectively. The radiation width of the first bound level was adjusted to reproduce the evaluated thermal capture cross section. Several negative energy resonances were invoked to ensure $1/v$ dependence of the capture cross section below the first positive resonance.

JEFF-3.2 documentation reports that resonance parameters up to 150 keV originate directly from experiment. Additional ℓ=2,3,4 resonances were added to reproduce the observed average capture cross sections between 150 and 350 keV (therefore the detailed shape of the cross sections in this energy range is not reliable, but is probably correct on average). Further details on the adjustments and assumptions on the raw experimental data can be found in Ref. [45].

Table VI lists the publications that were considered in the JEFF-3.2 evaluation to obtain Reich-Moore parameters. The resonance integrals at T=300 K between 0.55 eV and 2 MeV reported in the JEFF-3.2 documentation are listed in Table VII.

TABLE VI. Sources used to determine resonance parameters for ^{58}Fe.

Energy range	Exp. type	1st author	Ref.
	Capture	Hockenbury+	[47]
7 - 325 keV	Capture, transmission	Hong+	[48]
0 - 500 keV	Transmission	Garg+	[49]
2.5 - 200 keV	Capture	Allen+	[50]
10 - 100 keV	Capture	Kaeppeler+	[23]
359 eV	Capture	Gayther+	[51, 52]
230 & 359 eV	Capture	Borella+	[53]

TABLE VII. Resonance integrals at T=300 K between 0.55 eV and 2 MeV for ^{58}Fe.

Total	115.5 b
Elastic scattering	113.6 b
Radiative capture	1.246 b

TABLE VIII. ^{58}Fe resonance region integral metrics. Entries marked with a single asterisk (*) indicate use of the incorrect Au standard. Entries marked with a double asterisk (**) correspond to MACS(25 keV) corrected to MACS(30 keV) by the authors of KADoNiS.

$\sigma_{\rm therm}$ (b)	$(n$,tot)	$(n$,el)	(n,γ)
ENDF/B-VIII.0	8.796	7.476	1.315
Atlas (2018) [15]			1.32 ± 0.03

RI (b)	$(n$,tot)	$(n$,el)	(n,γ)
ENDF/B-VIII.0	121.282	115.944	1.279
Atlas (exp) (2018) [15]			1.50 ± 0.07
Atlas (sys) (2018) [15]			1.34 ± 0.16

MACS(30 keV) (mb)	(n,γ)
ENDF/B-VIII.0	15.058
JENDL-4.0 [17]	14.06
Atlas (exp) (2018) [15]	12.0 ± 0.06
Atlas (sys) (2018) [15]	13.7 ± 1.5
KADoNiS-0.3 [19]	13.5 ± 0.7
KADoNiS-1.0 [41]	14.3 ± 0.9
Heil+ (2008) [54]*,**	13.5 ± 0.7
Kaeppeler+ (1983) [23], Allen+ (1980) [50]*	12.1
Allen+ (1980) [50]	15.4 ± 1.5

Thermal cross section values for T=0 are given in Table VIII. We note that the thermal cross section values are in good agreement with the Atlas [15], but the resonance integral values are 15% - 4% below the two Atlas recommendations. Furthermore, our MACS(30 keV) is 2 mb ($\sim$ 13%) larger than either the Atlas or KADoNiS recommendations. Given the dearth of experimental data on ^{58}Fe capture around 30 keV, recommendations are based either on one direct measurement [50] near 30 keV or extrapolations from MACS(25 keV) measurements [23, 54]. To complicate matters, the KADoNiS recommendations were corrected using the wrong gold standard. Given this situation, we agree with the only direct measurement in this energy range.

III. EXPERIMENTAL DATA IN THE FAST NEUTRON REGION

There is an extraordinary abundance of experimental data for elemental iron and its four major isotopes ^{54}Fe, ^{56}Fe, ^{57}Fe, and ^{58}Fe. At the time of writing this paper, the EXFOR database contained 799 entries (papers) with 2552 datasets. Analyzing this amount of information is a daunting task and we greatly benefited from our Chinese collaborators sharing with us their detailed analysis of the experimental data. This CIELO-facilitated cooperation sped up the initial phase of the evaluation process and is reflected in the authorship of this paper.

Table IX lists the most relevant of the 799 references grouped according to the physical quantities appearing in the evaluation. In doing this selection we favored: (i) broad energy range covered by the experiment, (ii)

high energy resolution, and (iii) high (but reasonable) accuracy of the experiment. Thus the measurements providing possibly wide and reliable picture were given precedence over single energy-point experiments, especially if the latter were taken within the energy range where strong fluctuations were observed. On the other hand, many single- or a few-point measurements ended up in Table IX when no extended datasets were available.

Some of the measured datasets were renormalized to account for changes in the reference cross sections since they were used in the analysis of the experiments. These renormalizations are built into the EXFOR retrieval system and are documented in the descriptive part of the evaluations.

In a few cases we took advantage of the existing high quality evaluations available from the IRDFF library [55, 56] and used these data instead of the actual measurements (these cases are indicated as IRDFF in Table IX).

Our evaluation was informed by the preliminary results of the RPI semi-integral measurement that has been published recently [57]. While the integral data usually involve broad energy averages taken over several materials, the semi-integral experiments yield an energy average for a single material (although it can be a natural element) removing ambiguity related to the variety of materials. The semi-integral experiments do not provide differential cross sections that can be directly included in the evaluation but constitute a stringent test of a new evaluation. Comparing results of the transport calculations that use the new evaluation to simulate the semi-integral experiment with the measured values checks the performance of the new evaluation on the specific material. The most useful semi-integral measurements probe a specific reaction on a target element (or even isotope).

Finally, we took into consideration feedback from the integral (mostly criticality) experiments. Details will be discussed in the validation section VIII.

TABLE IX. Most relevant measurements used in the evaluations of the fast neutron region. "x-sect." stands for cross section, "Double-diff. x-sect." refers to energy-angle correlated distributions (*e.g.*, neutron emission spectra at a given angle) and "Partial ang. distr." refers to components of the reaction measured at given angle(s) (*e.g.*, γ-transitions following inelastic scattering to a discrete level measured at a given angle). The data used in the resonance evaluations are not included here because they are described in the previous section.

Isotope	Reaction or Quantity	References
^{Nat}Fe	Total x-sect.	[58–72]
	Elastic x-sect.	[72–77]
	Inelastic x-sect.	[73, 78–82]
	Capture x-sect.	[13, 47, 83–86]
	Angular distr.	[72–75, 81, 87–102]
	Energy spectra	[102–115]
	Double-diff. x-sect.	[100, 102, 108–111, 113, 114, 116–128]
^{56}Fe	Total x-sect.	[12, 129–132]
	Elastic x-sect.	[133–139]
	Inelastic x-sect.	[140–145]
	Capture x-sect.	[146, 147]
	(n,p) x-sect.	IRDFF
	$(n,2n)$ x-sect.	[148–153]
	(n,α) x-sect.	[154, 155]
	$(n$, charged) x-sect.	[154–158]
	Angular distr.	[70, 92, 134–136, 139, 159–163]
	Energy spectra	[112, 118, 154, 164–173]
	Double-diff. x-sect.	[169–172, 174, 175]
	Partial ang. distr.	[75, 123, 133–136, 156, 176–189]
^{54}Fe	Total x-sect.	[37, 190–194]
	Elastic x-sect.	[30, 133, 134, 138, 195, 196]
	Inelastic x-sect.	[193]
	Capture x-sect.	[26, 30, 33, 35, 197–199]
	(n,p) x-sect.	IRDFF
	$(n,2n)$ x-sect.	[152, 200–216]
	(n,α) x-sect.	IRDFF
	Angular distr.	[133, 134, 161, 193, 195, 217–219]
	Energy spectra	[154, 156]
	Double-diff. x-sect.	[175]
	Partial ang. distr.	[133, 134, 156, 180, 181, 185, 193, 195, 218, 220, 221]
^{57}Fe	Total x-sect.	[39, 222–225]
	Capture x-sect.	[36, 37, 147]
	(n,p) x-sect.	[151, 206, 216, 226–232]
	Partial ang. distr.	[181]
^{58}Fe	Total x-sect.	[233]
	(n,p) x-sect.	[151, 216, 230, 232, 234–236]
	(n,α) x-sect.	[89, 237]

IV. MODELING THE FAST NEUTRON RANGE

It is a common practice in modern nuclear reaction evaluation to rely on the reaction modeling to provide a complete and internally consistent set of physical observables for the evaluated material. In this schema, experimental data are used to select the most appropriate models and constrain their parameters to reproduce experimental data as close as possible. In the case of iron, persistent fluctuations in the fast neutron region modify this approach at lower incident energies. Since no fast neutron reaction model is capable of predicting fluctuations and even external scaling of the calculations, which could simulate fluctuation, is impractical because of the size of the resulting file we decided to make direct use of experimental data in the evaluations. Even in such cases we have tried to adjust parametrization of the models as to reproduce averages of the fluctuating experimental data in order to complete the file with quantities that were not experimentally available.

The fast region calculations were performed using the EMPIRE code [9], which is a comprehensive package that integrates into a single system a number of impor-

tant physical modules and evaluation tools. In particular, it offers usually a choice of reaction models and/or parametrizations. We have tried to find an optimum balance between good physics and performance with the latter taking precedence in case of conflict (this is the "Anglo Saxon" (empirical) approach as opposite to "Gallic" (theory)). Below we list and justify our choices.

We have adopted coupled channel (CC) calculations in the incident channel and for the direct inelastic scattering to collective levels. In addition, we have allowed for the Distorted Wave Born Approximation (DWBA) to populate presumably collective levels which are not included in the ground state band used in the CC calculations. This allows to adjust neutron emission spectra in the high energy range which is essential for proper modeling of the neutron-target system. The optical model potentials used in the calculations are listed in Table X.

TABLE X. Optical model potentials used in the EMPIRE calculations.

Ejectile	Type	RIPL #	Reference
n (inelastic)	CC	614	Li+ [238],Sun+ [239]
n (inelastic)	CC	615 for ^{57}Fe	Li+ [238]
n (outgoing)	Spher.	2405	Koning+ [240]
p	Spher.	5405	Koning+ [240]
α	Spher.	9600	Avrigeanu+ [241]
d	Spher.	6200	Haixia+ [242]
t	Spher.	7100	Becchetti+ [243]
^{3}He	Spher.	8100	Becchetti+ [243]

We note that the sophisticated optical potential used for the CC calculations on ^{56}Fe was not designed for incident neutrons with energies below 4 MeV. In order to match averaged experimental cross sections, the CC predictions were scaled down by a factor of 0.78 from 1 keV to 0.5 MeV and later modulated by factor varying between 0.68 and 0.9 up to 2.5 MeV and eventually increased to gradually reach 1.0 at 4 MeV . This had very little impact on the evaluation since practically all major cross sections below 4 MeV were determined by the measurements. There was no evidence that a similar reduction is necessary for other iron isotopes.

For the preequilibrium (PE) emission we decided to employ the classical exciton model (PCROSS module) because of its higher flexibility in modeling neutron spectra compared with the use of physically more advanced, but also more rigid models, as multistep compound and multistep direct. The same module was also used for the PE emission of protons and gammas as well as for PE emission of clusters, the latter taking advantage of the Iwamoto-Harada model [244]. For PE angular distributions, the well known Kalbach-Mann [245, 246] systematics was used for all ejectiles except γ's.

The Hauser-Feshbach formulation of the statistical model was employed to follow sequential emission of particles from highly-excited but equilibrated nuclei, as compound nucleus (CN). The elastic and inelastic angular distributions of neutrons emitted from the CN were calculated using the Blatt-Biedenharn formalism [247]. The width fluctuation factor was accounted for within HRTW formalism [248] applied up to 12.0 MeV incident neutrons. We have found that HRTW and Moldauer [249] approaches are practically equivalent. The 12 MeV upper limit could be lower for the width fluctuation correction but we intentionally kept it at this level to extend the range of angular distributions of CN neutrons. In the EMPIRE code the T_{lj} transmission coefficients are used only within the width fluctuation correction module while pure Hauser-Feshbach mode switches to T_l's, making Blatt-Biedernharn formalism inapplicable. Compound nucleus and direct cross sections were added incoherently, *i.e.*, the Engelbrecht-Weidenmüller transformation [250] was not invoked. As a matter of fact, there was no need for it since the direct component is relatively weak in the very spherical iron isotopes and then, at least for the most important ^{56}Fe, between the first inelastic threshold and 4 MeV the optical model cross sections were externally rescaled to bring calculated total cross section to agree with the average of the experimental results.

Different level-density models were tested, such as EMPIRE-specific level densities (adjusted to RIPL-3 [251] experimental $D_{\rm obs}$ and to discrete levels), Generalized Superfluid Model (GSM), microscopic combinatorial (HFBM) and the Gilbert-Cameron model. This testing has been mostly influenced by the performance of a given model on the ^{56}Fe(n,p) reaction that is extremely sensitive to level densities. We found that the HFBM and the Gilbert-Cameron models described better the observed shape of the cross sections. Ultimately the Gilbert-Cameron model was adopted to describe the level densities for all isotopes, as the HFBM would lead to oscillations in the double-differential spectra at low outgoing neutron energies that are not confirmed by measurements.

The excitation energy cut-off of discrete levels was chosen to ensure a smooth transition from the discrete region to level densities. Level density parameters were fitted to reproduce the asymptotic behavior of discrete levels, as well as to correctly describe the observed cross sections, especially for those reactions for which dosimetry IRDFF evaluation exists. This was done for all relevant nuclei within each isotope-evaluation. Consistency for level-density parameters across the different evaluations was aimed and approximately achieved.

Complete γ-ray cascades for every excited nucleus were calculated. In all nuclei γ-strength functions for E1 transitions initiated from the continuum were determined from the RIPL3 MLO1 formulation by Pluyko (the only exception was made for ^{56}Fe, as will be discussed in Sec. V A). M1, E1 and E2 electromagnetic transitions were considered.

Discrete-level energies and transitions between discrete levels were governed by experimental branching ratios and electron conversion coefficients taken from the up-

dated version of RIPL-3 [251]. Therefore, γ-ray emission, including discrete γ's, could be directly compared with measured γ's following inelastic scattering. We note that RIPL-3 used to contain a spurious low-lying 3^- level at 3.076 MeV in ^{56}Fe originating from the ENSDF library. Inclusion of this spurious level destroys the modeling of inelastic cross sections in ^{56}Fe. This level was thoroughly refuted by Fotiades, Nelson and Devlin [252] and has since been removed both from RIPL-3 and ENSDF.

There were only a few adjustments of the model parameters for the individual isotopes. The mean free-path multiplier in the exciton model, which by default is set at 1.5, was changed to 2.3 for ^{54}Fe, 1.9 for ^{56}Fe, 2.2 for ^{57}Fe, and 1.9 for ^{58}Fe. These modifications were done to adjust PE contributions in order to optimize the description of inelastic high energy tail, (n,p) and (n,α) reactions as well as neutron emission spectra. It is also a typical practice to tune PE γ-emission to simulate semi-direct capture mechanism and bring calculated capture cross section in the GDR region to about 1 mb. These tune factors were 5.1 for ^{55}Fe, 10.97 for ^{57}Fe, 5.68 for ^{58}Fe, and 5.5 for ^{59}Fe.

A detailed account of the reaction models choices and parameter adjustment is given in the descriptive part of the evaluation and even more details can be found in the input and output files available from the GForge server. The parameters that were not explicitly mentioned were taken from the RIPL-3 library and additional datasets included in the EMPIRE code. Occasionally, we resorted to energy-dependent parameter scaling or tuning factors, available in the EMPIRE code, to account for model deficiencies. Apart from the correction of the CC results for ^{56}Fe discussed above, these corrections were typically on the level of 1-2% or less and can be found in the input files.

All calculations were carried out considering 7 subsequent neutron emissions, 3 proton emissions and a single α-particle, deuteron, triton, and ^{3}He for a total of 146 residual nuclei. Only 5 of these were treated as exclusive, *i.e.*, had an explicit reaction assigned to them along with the corresponding exclusive spectra for all particles and γ's included in the reaction. The exclusive reactions were (n,γ), $(n$,elas$)$, (n,n'), $(n,2n)$, (n,p), and $(n,2p)$. For all the remaining we provide cross sections for residua production which represent a sum of contributions from all possible reactions populating a given residue. Their respective spectra are lumped together providing only seven cumulative spectra (for γ's, neutrons, protons, α-particles, deuterons, tritons, and ^{3}He) for all the inclusive channels.

V. EVALUATED RESULTS

A. Cross Sections

In this section we discuss cross sections for the major reactions on isotopes of iron. For the reactions that are not mentioned explicitly we accepted EMPIRE results without modifications. In general, there were no data to compare with, or the calculated results were close to those measured.

1. Total Cross Sections

^{56}Fe(n,total) - The adopted cross sections above the resonance range up to 10 MeV were the ones from JEFF-3.2, which is essentially the Vonach-Tagesen evaluation with superimposed fluctuations that correspond to the Berthold measurement [61]. This ultra-high resolution transmission measurement on natural iron was taken on a 387.739 meter flight path at the 150 MeV GELINA linac. The results extend from 0.75 up to 22 MeV and are available from EXFOR Entry #22276 as a private communication since they have never been published in detail.

Measurements of high resolution on an enriched sample of ^{56}Fe were made by Cornelis (1995, EXFOR #22316) [253]. They are in good agreement with the Berthold data, except for a slight shift in energy. After careful review we realized that the energy calibration of the Berthold data is more reliable. In addition, Cornelis data show fluctuations increasing with energy above 19 MeV, *i.e.*, to the end of the covered energy region. The amplitude of these fluctuations is unphysical and therefore the Cornelis data were not considered in the evaluation. Therefore, the total cross sections between the resolved resonance region and 10 MeV were fully determined by the Berthold data with a correction for the minor isotopes.

Above 10 MeV, the total cross sections were provided by coupled channel calculations with the soft-rotor dispersive potential by Soukhovitskiĩ-Capote [238] with minor adjustments (factor of 0.997 up to 20 MeV and less than +1.5% above) to reproduce the measurement by Abfalterer [59]. We remind that below 4 MeV the optical model total (and absorption) cross sections were reduced up to 30%. In this energy range the reduction has no effect on the evaluated total since it was defined either by the resonance parameters or by the experimental values.

^{54}Fe(n,total) - The cross sections were calculated with the EMPIRE code using an optical potential specified in Table X. The energy-dependent scaling was applied below 2 MeV to reproduce elastic Guenther data [193] and to improve agreement with averaged ENDF-VII.1 between 700 keV and 1.2 MeV. The scaling applied below 4 MeV in ^{56}Fe was not used in the ^{54}Fe case. Fig. 6, top-right panel, shows the comparison of the recommended total cross sections with existing experimental values. We note that data points above 10 MeV [192] deviate drastically from our coupled-channel calculations and are completely out of phase with the general shape resonance predictions of the optical model. We excluded this data set from consideration.

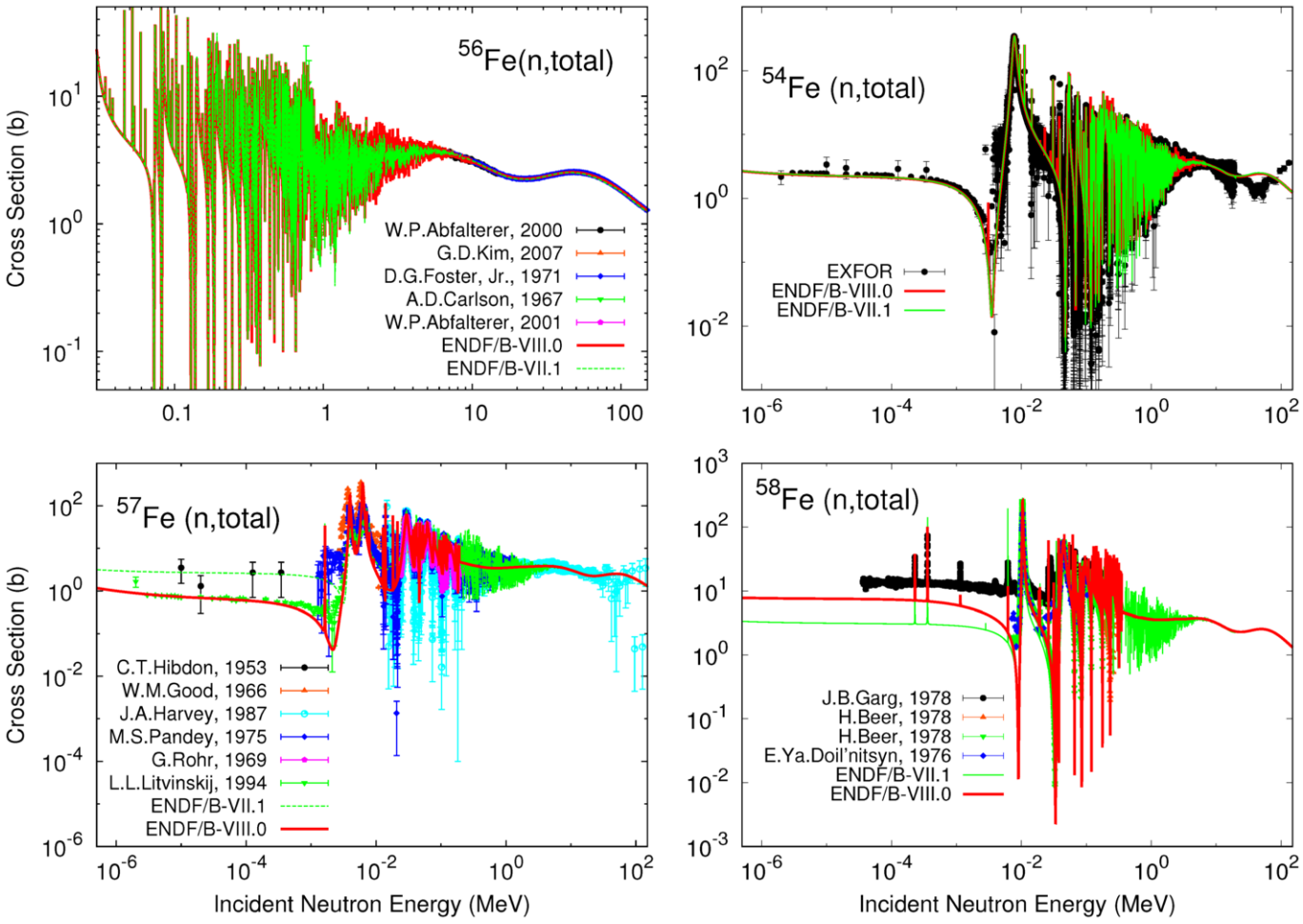

FIG. 6. (Color online) Evaluated ^{54,56,57,58}Fe(n,total) cross sections compared with data retrieved from EXFOR and with the ENDF/B-VII.1 evaluation.

^{57}Fe(n,total) - Fluctuations in the region from the higher-energy end of the RRR until roughly 4 MeV are present in the ENDF/B-VII.1 evaluation's total cross section. These fluctuations are derived from the abundance-weighted ^{56}Fe(n,total) cross section. To "restore" the fluctuations, we performed a generalized least-square linear spline fit to the data of Harvey [223] and that of Pandey [225] in the region from 190 keV to 8 MeV. Both sets were in excellent agreement, differing only slightly in their treatment of the neutron time-of-flight. At the energy resolution of our spline fit, this difference was not observable. The fluctuations were distributed to the ^{57}Fe(n,elas) and ^{57}Fe(n,γ) cross sections such that both the energy average elastic and capture cross sections were preserved and so that they sum to the fluctuating total cross section. The results are shown in Figs. 6, 7, 13. The data of Hibden *et al.* [254] is not trustworthy as the target was an isotopically-enriched iron oxide target and the target composition was not given to enough precision to extract meaningful data.

^{58}Fe(n,total) - The fluctuations in ENDF/B-VII.1's (n,elas), (n,total) and (n,γ) cross sections were not preserved in the current evaluation. The ENDF/B-VII.1 fluctuations are the abundance weighted $^{\text{Nat}}$Fe cross sections from ENDF/B-IV and are not based on ^{58}Fe data. The data of Garg *et al.* [255] is not trustworthy as the target was an isotopically-enriched iron oxide target and the target composition was not given to enough precision to extract meaningful data.

2. *Elastic Cross Sections*

The elastic cross sections were generally defined as the difference between the total and the sum of the remaining partial cross sections.

^{56}Fe(n,elas) - Shown in Fig. 7 (upper panel), the elastic cross section was also obtained using subtraction of the inelastic (see below) from the total. Berthold's total and Dupont's inelastic have a higher resolution than Kinney's elastic. After reconstructing the elastic by sub-

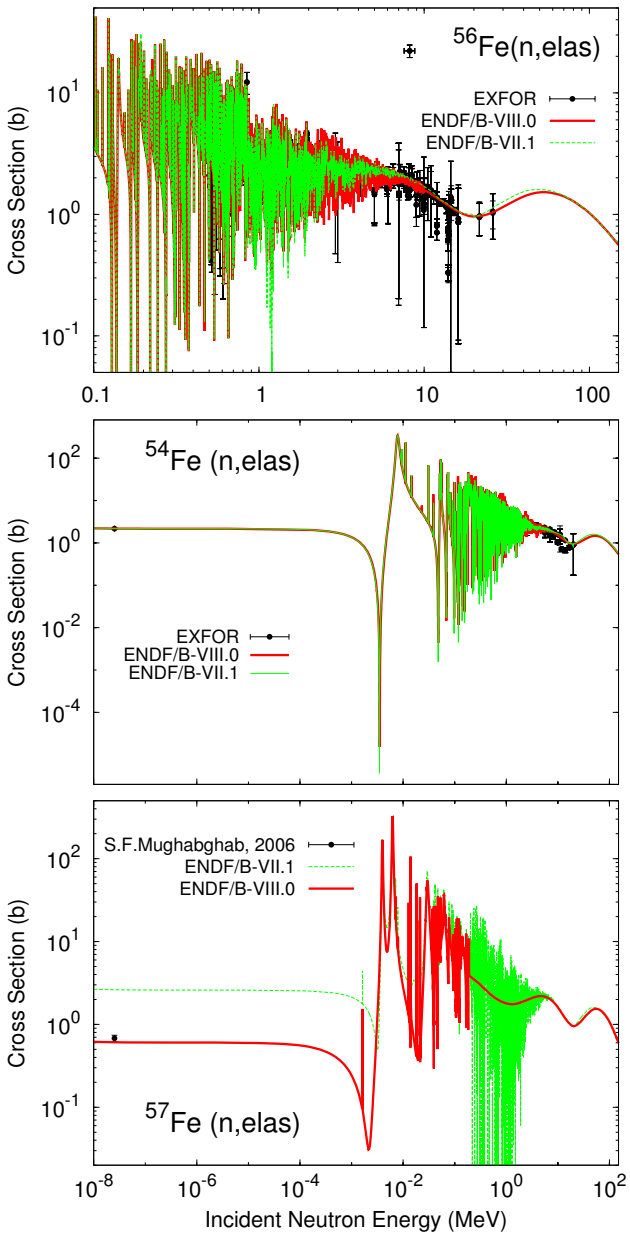

FIG. 7. (Color online) Evaluated neutron elastic cross section on ^{54,56,57}Fe compared with data retrieved from EXFOR and with the ENDF/B-VII.1 evaluation.

traction and resolution-broadening of the fluctuations, good agreement with the Kinney data is observed (see Fig. 8), although the resolution-broadened curve is systematically lower compared to the Kinney data. If there is a problem of an under-prediction of the elastic cross section in this energy range one should weigh the reliability of the absolute normalization of the Kinney measurements and the Negret measurements, since the capture cross section in this energy region is only about 3 mb, which is more than an order of magnitude smaller than the inelastic cross section.

^{54}Fe(n,elas) - The elastic cross section for ^{54}Fe is shown in Fig. 7, middle panel. As already mentioned, EMPIRE results were adjusted to reproduce the Guenther data.

^{57}Fe(n,elas) - As is shown in Fig. 7, bottom panel, it is distinctly different from the ENDF/B-VII.1 evaluation. Apart from the lower thermal region, the new evaluation adopts smooth EMPIRE calculations above the resonance region, contrary to ENDF/B-VII.1 which propagated ^{56}Fe fluctuations up to several MeV.

3. *Inelastic Cross Sections*

^{56}Fe(n,inelastic) - Two sets of inelastic cross section data were produced at Geel. The older one, by Dupont [141], was never published in a peer-reviewed journal, because the authors found normalization problems in the measurement that could not be resolved. A newer measurement by Negret [144] was performed with a new experimental set-up, but the resolution was lower than that of the Dupont data. In the current evaluation, data from both datasets were binned over a suitable energy mesh. A piecewise linear scaling parameter was constructed to adjust Dupont data such that they agree on average with the Negret data. It was also found that the energy calibration of the Negret data did not match the resonances in the total cross section. Since the evaluated elastic cross section is calculated as the difference between the total and the remaining partial cross sections, any mismatch in the position of resonances can have catastrophic consequences. To force agreement in the resonance peaks the energy scale of the Negret data was scaled linearly, amounting to 2.5 keV at 1.8 MeV. The main concern was whether to trust the energy calibration of Berthold (done on a 400 m flight path) and Dupont, or to adopt the calibration by Cornelis and Negret. From a private communication with P. Schillebeeckx, it was found that a 2.5 keV shift in the Negret data corresponds to an error in timing of 5 ns, which is possible. So, the obtained inelastic was subtracted from the total to produce the elastic cross sections. A comparison of the evaluated total, elastic and inelastic cross sections is shown in Fig. 8. We note that choosing an absolute scale according to Negret results in higher inelastic, and consequently lower elastic, compared to JEFF-3.2 and ENDF/B-VII.1.

Fluctuations were imposed on the inelastic scattering to the first and the second excited state in ^{56}Fe. The Negret data show some structure also for the higher levels but the cross sections are small enough to disregard them (at a certain level it is difficult to judge whether the fluctuations represent physics effect or simply statistical noise). Up to 2.5 MeV the rescaled Dupont data were used on MT=51 and 52. Between 2.5 and 3.5 MeV the lower resolution Negret fluctuations were applied. Smooth EMPIRE calculations were adopted above 3.5 MeV for the first two inelastic levels and in the whole energy range for the remaining levels.

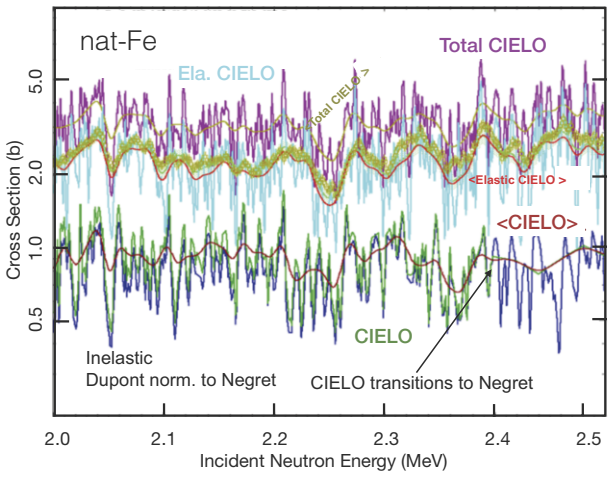

FIG. 8. (Color online) Example of fluctuating structure in total, elastic and inelastic on ^{nat}Fe illustrating consistent construction of the recommended CIELO (ENDF/B-VIII.0) cross sections. Lines indicated with <> represent energy averages.

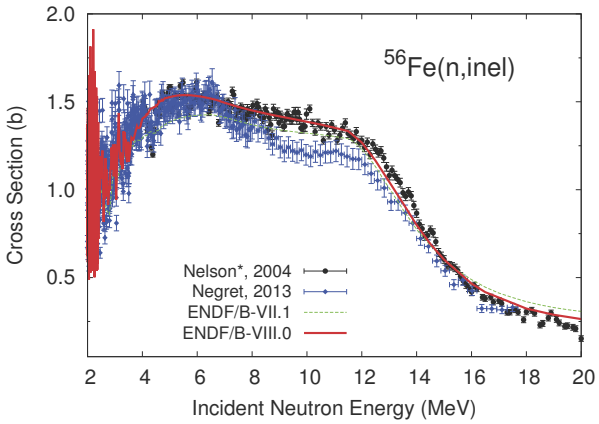

FIG. 9. (Color online) Evaluated ^{56}Fe(n, n') neutron inelastic cross section compared with data retrieved from EXFOR and with previous evaluation. The asterisk on the Nelson data indicates renormalization described in the text.

Fig. 9 compares total inelastic cross sections in the CIELO evaluation with experimental data by Negret and Nelson [143]. Both experiments derived total inelastic cross sections from the intensity of the 847 keV γ-line through which the first excited state in ^{56}Fe decays to the ground state. The Nelson results were corrected for the contribution of the ^{57}Fe$(n, 2n)$ reaction and monitor cross section updated in 2004. For the more recent Negret measurement carried out on an enriched sample these corrections were not needed. Both experiments agree perfectly up to around 6 MeV while at higher energies the Negret data tend to be lower. Authors consider, however, their data accurate only up to 4.5 MeV where there is no model-dependent contribution from the continuum. Above that limit the Negret data represent a lower limit. Our new evaluation reproduces very well the Negret data up to about 7 MeV and then follows the results of Nelson. In the plateau of the inelastic cross section no adjustment of the model parameters was needed. Above 12 MeV EMPIRE calculations, adjusted to reproduce the ^{56}Fe(n, p) reaction, were slightly lower than measurements and other libraries. To remove this discrepancy, without upsetting agreement for other channels, we increased the γ-strength function in ^{56}Fe which makes it more likely for γ's to win the competition with neutrons just above the threshold of the ^{56}Fe$(n, 2n)$ reaction. To this end, E1 γ-strength in ^{56}Fe was switched from the GDR default to Weisskopf single-particle estimates with the scaling factor set to 0.1 instead of the default 0.01.

^{54}Fe, ^{57}Fe, ^{58}Fe(n,inelastic) - For the three minor isotopes results of EMPIRE calculations were adopted.

Limited experimental data, available only for ^{54}Fe(n,inelastic), indicate the possibility of a fluctuating structure similar to the one observed in the case of ^{56}Fe (see Fig. 10). Such a pattern is expected in all isotopes of iron, at least in the even ones, as the nuclear structure of these nuclei is similar. The data, however, are not sufficient to unambiguously establish the shape of the fluctuating cross sections, thus we resort to smooth model calculations. Fig. 10 shows that the calculations are in fair agreement with the experimental data and that the new evaluation agrees with ENDF/B-VII.1 up to 6 MeV and then it is consistently higher.

^{57}Fe is a special case since the inelastic threshold lies inside the resonance region requiring the Reich-Moore formalism and the ENDF-6 option LRF=7. The details were already described in Sec. II C. The cross sections for scattering to the first excited state in ^{57}Fe are displayed in Fig. 5.

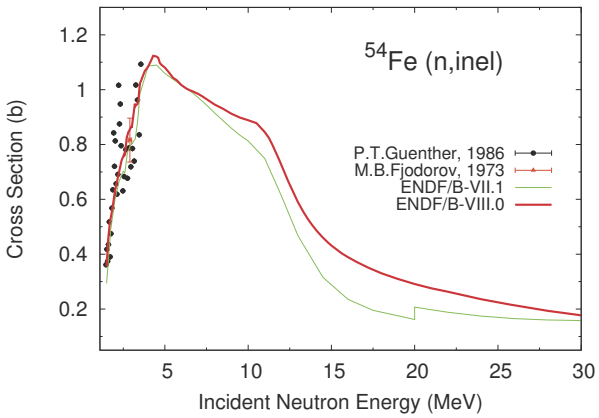

FIG. 10. (Color online) Evaluated ^{54}Fe(n, n') neutron inelastic cross section compared with data retreived from EXFOR and with the previous evaluation.

4. Capture Cross Sections

For all isotopes, capture was provided by the EMPIRE code. The pre-equilibrium was tuned to yield about 1 mb cross section in the GDR region. By default, EMPIRE scales the γ-ray strength function to reproduce the experimental or systematics value at thermal energy. In the cases mentioned below, energy-dependent tuning was employed to improve agreement with experimental data.

$^{56}Fe(n,\gamma)$ - Capture cross sections are shown in Fig. 11. Above 860 keV the evaluation was adjusted to the RPI data presented by Y. Danon at the ND2016 Conference. Fig. 12 compares performance of the current evaluation, ENDF/B-VII.1, and JEFF-3.2 with the semi-integral experiments at RPI. One notes underestimation of capture between 700 and 850 keV by JEFF-3.2 (lack of background) and overestimation by ENDF/B-VII.1 (too high background). Also above the resonance region the CIELO evaluation is a clear winner in this contest.

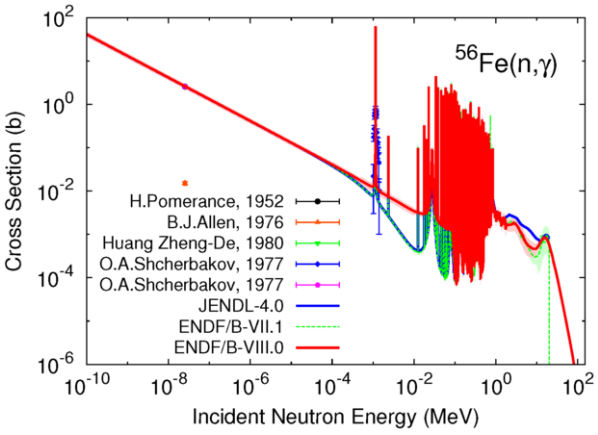

FIG. 11. (Color online) Evaluated ^{56}Fe(n,γ) cross section compared with data retrieved from EXFOR and with the previous evaluation.

$^{54}Fe(n,\gamma)$ - Fig. 13, top panel, shows the capture cross section for ^{54}Fe compared to ENDF/B-VII.1. Neutron capture between 200 and 500 keV was tuned to agree with Allen data [35]. This resulted in the ^{54}Fe CIELO capture between 1 and 2 MeV to be about twice of that in ENDF/B-VII.1, which could be a reason for over-prediction of the RPI semi-integral results on natural iron shown in Fig. 14. Considering that in the discussed energy range capture for all other isotopes is close to ENDF/B-VII.1, it was natural to assume that ^{54}Fe would be the culprit for the discrepancy. We have realized that benchmarks are not helpful in solving the issue since their sensitivity to capture on ^{54}Fe is very small. Thus, having to choose between semi-integral and differential experiment we decided to adopt the latter.

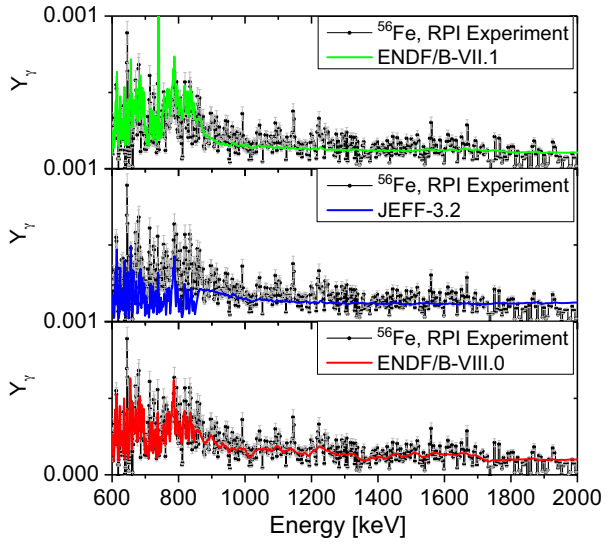

FIG. 12. (Color online) Comparison of calculated yields of γ from a semi-integral (thick target) experiment at RPI on ^{56}Fe.

5. $(n,2n)$ Cross Sections

$^{56}Fe(n,2n)$ - Level densities for ^{55}Fe and other parameters that impact ^{56}Fe$(n,2n)$ cross sections were fitted taking into account not only $(n,2n)$ experimental data but also data for (n,p) and (n,α) reactions, in order to simultaneously improve the agreement with data for the three reactions through the minimization of global χ^2. For the fits we kept only the $(n,2n)$ data used in the Vonach evaluation, which includes the corrected version of Frehaut. The final curve, as can be seen in the upper panel of Fig. 15, agrees well with the trend of Frehaut and is sufficiently close to the other points to allow us to state that a good agreement was reached, especially considering that the different $(n,2n)$ experiments are not fully consistent with each other. It is reassuring that the most recent measurement by Wallner [152] supports the new evaluation. This experiment makes use of the very precise mass spectroscopy method, but being still preliminary, has not been used in the evaluation procedure.

$^{54}Fe(n,2n)$ - Again, the ^{54}Fe$(n,2n)$ channel was fitted simultaneously with (n,p) and (n,α) reactions. In this case, since the IRDFF [55, 56] dosimetry evaluation was available for all three reactions, IRDFF was used as fitting guidance instead of actual experimental data. As can be seen in the lower panel of Fig. 15, around 15 to 20 MeV the experimental data present two conflicting trends. Our evaluation follows the lower trend and the data above 20 MeV. Ultimately, the total ^{54}Fe$(n,2n)$ (ground plus meta-stable states) was replaced by the IRDFF evaluation. In the energy region close to the reaction threshold the new evaluation is significantly lower than all other evaluations, which is again well supported by the results of Wallner's experiment.

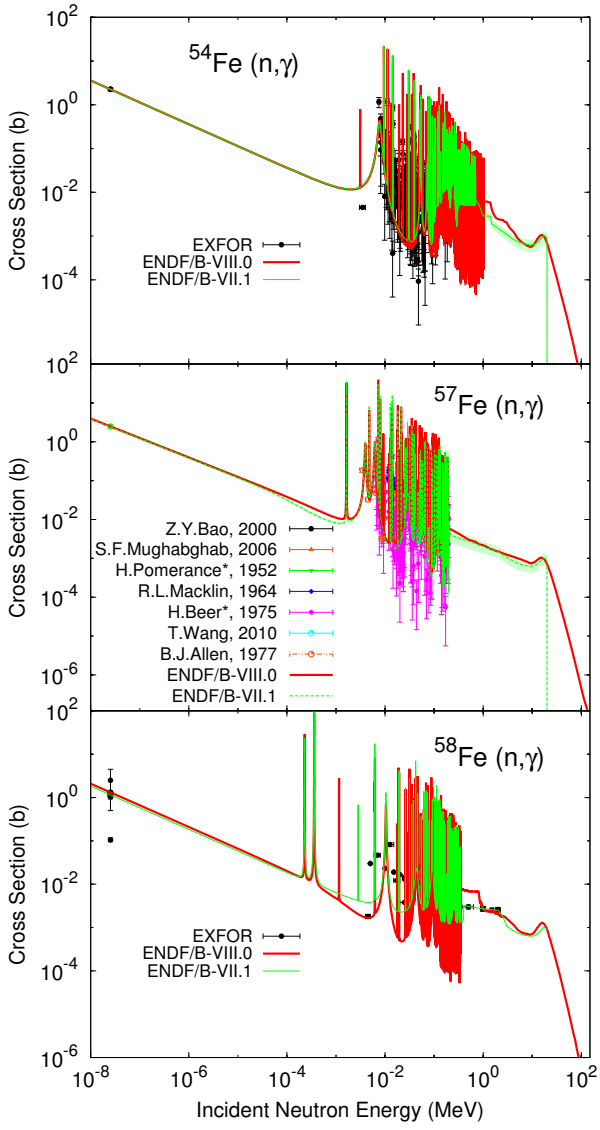

FIG. 13. (Color online) Evaluated ^{54,57,58}Fe(n,γ) neutron capture cross section compared with data retrieved from EXFOR and with the previous evaluation.

6. (n,p) Cross Sections

$^{56}Fe(n,p)$ - This was one of the key factors defining the whole ^{56}Fe evaluation in the fast neutron energy range. Although, at the very end, the IRDFF recommended cross sections were adopted for the CIELO iron file, we adjusted EMPIRE code calculations to reproduce IRDFF values as close as possible. Because of the extraordinary sensitivity of the ^{56}Fe(n,p) reaction to the level densities, this very well measured reaction essentially determined the choice of the level-density model and its parametrization. With the adjustment of the additional parameters we managed to reproduce the dosimetry file within its own uncertainties (except at energies very close to the threshold, which actually are probably

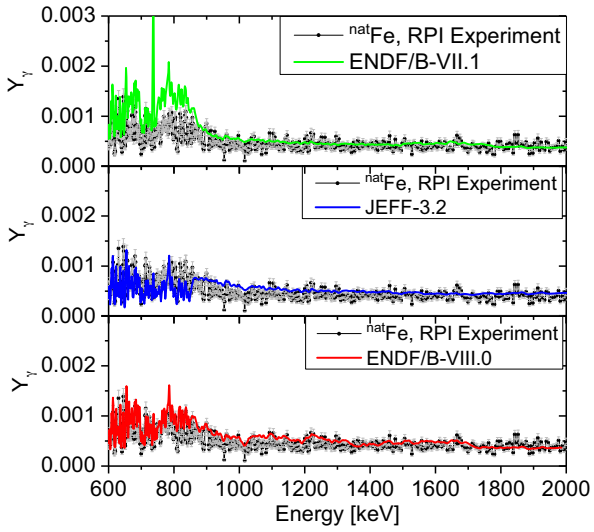

FIG. 14. (Color online) Comparison of calculated yields of γ from a semi-integral (thick target) experiment at RPI on ^{nat}Fe.

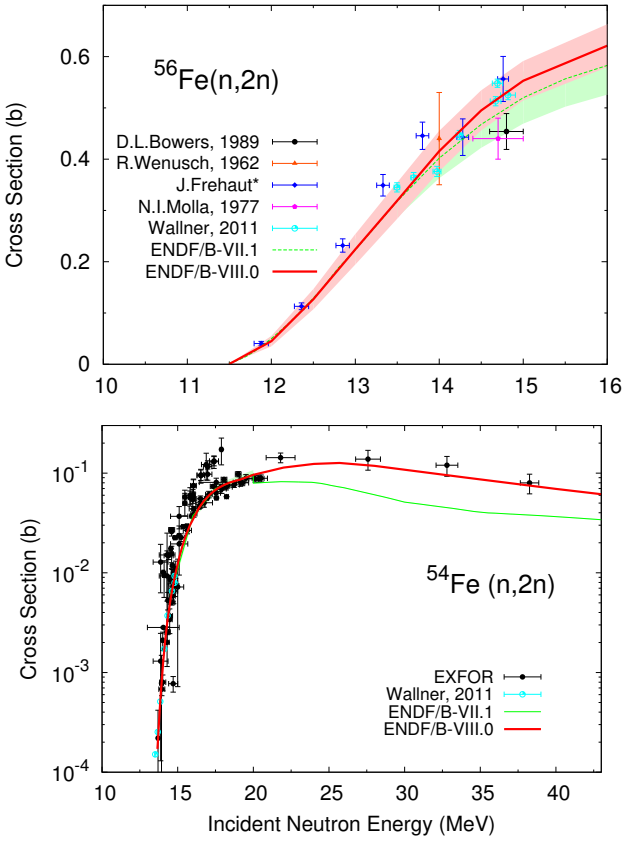

FIG. 15. (Color online) Evaluated ^{54,56}Fe$(n,2n)$ cross section compared with data retrieved from EXFOR and with ENDF/B-VII.1 evaluations.

better determined by the model calculations than experimental data). EMPIRE calculations were adopted above

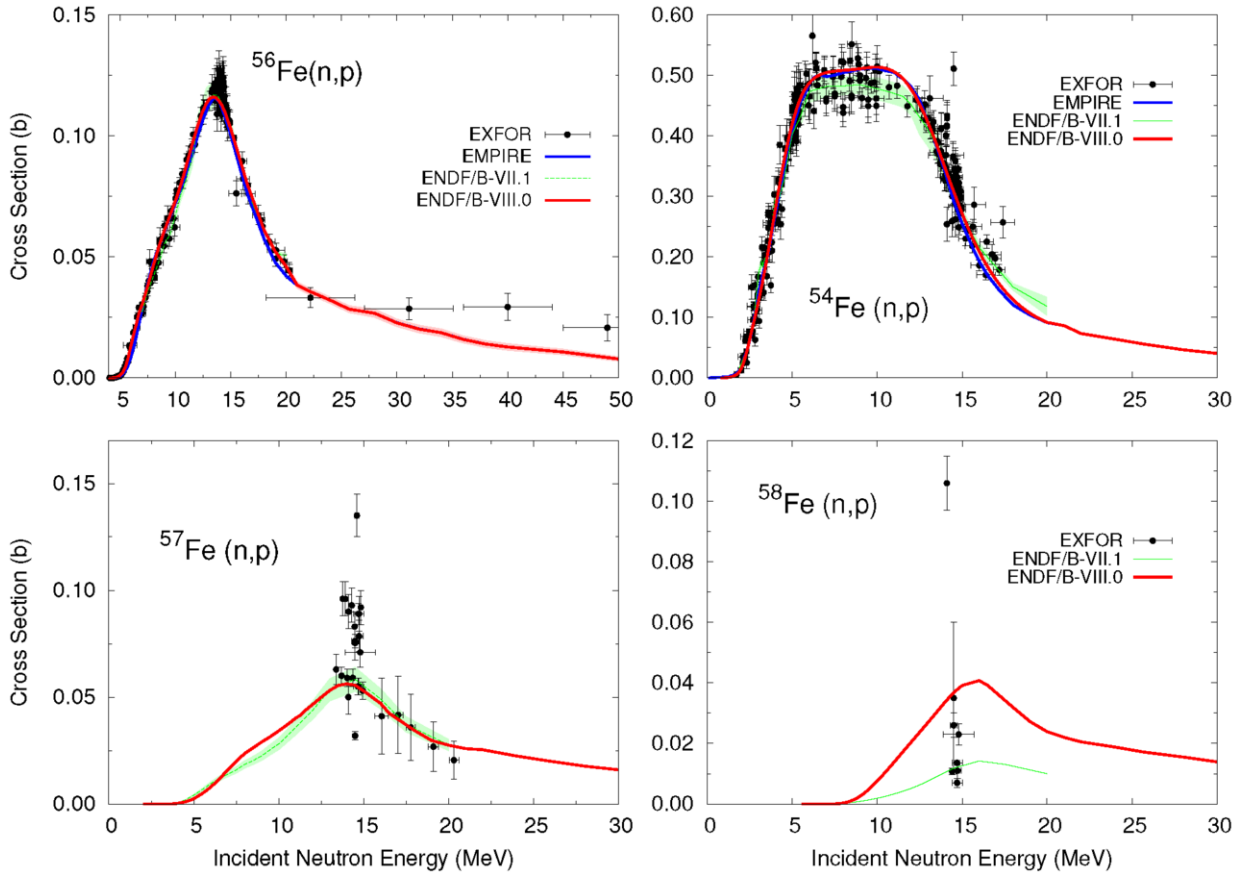

FIG. 16. (Color online) Evaluated ^{54,56,57,58}Fe(n,p) cross section compared with data retrieved from EXFOR and with the ENDF/B-VII.1 evaluation. In case of ^{56}Fe we also include results of EMPIRE calculations to show how close they reproduce the adopted IRDFF evaluation.

20 MeV since the original IRDFF was extended with old TENDL results. In Fig. 16, upper-left panel, we show how well EMPIRE calculations agree with the IRDFF evaluation below 20 MeV and compare to the ENDF/B-VII.1 file. Good agreement of EMPIRE calculated cross sections with the IRDFF library (the one adopted for the CIELO evaluation) ensures that use of the IRDFF cross sections does not break consistency of model calculations.

^{54}*Fe*(n,p) - This reaction has been adjusted to reproduce the IRDFF evaluation by fitting level-density parameters. In addition, the optical model parameters for the residue nucleus ^{54}Mn were changed globally up to 10%. To obtain a particularly good fit around the (n,p) peak, an energy-dependent fit of optical potential parameters was introduced between 4.5 and 9.5 MeV. These results can be seen in Fig. 16, upper-right panel.

^{57}*Fe*(n,p) - Proton emission from the compound nucleus was tuned above the neutron incident energy of 15.0 MeV in order to improve the agreement with experimental data. Results can be seen in Fig. 16, bottom-left panel.

^{58}*Fe*(n,p) - Due to the scarcity of data, ^{58}Fe(n,p) is obtained directly from model calculations (Fig. 16, bottom-right panel)

7. (n,α) Cross Sections and α Production

^{56}*Fe*(n,α) - Below 20 MeV production of ^{53}Cr and α production come exclusively from the ^{56}Fe(n,α) reaction. There are experimental data for ^{56}Fe$(n,x\alpha)$ available in the literature going all the way up to ~150 MeV. In order to reach a good agreement above ~50 MeV without compromising the lower-energy fits for other reactions, we fitted the level densities and α emission of nuclei reached from compound only after multiple emissions, such as ^{48,49}Ti, ^{46,47}Sc, ^{51}V, ^{55}Mn, ^{51,52,53}Cr. In Fig. 17 we show the result of such fit as compared to experimental data and ENDF/B-VII.1.

^{54}*Fe*(n,α) - Alpha emission (from both discrete levels and continuum) from the compound nucleus was tuned between 5 and 20 MeV in order to closely reproduce the (n,α) cross section from IRDFF. Additionally, the optical model parameters for the residue nucleus of the ^{54}Fe(n,α) reaction, ^{51}Cr, were changed up to 6% and the α emission from the compound nucleus was tuned between 5 and 21 MeV, leading to an excellent agreement with IRDFF. Since, as for ^{56}Fe, we do not provide cross sections for the ^{54}Fe(n,α) reaction Fig. 18 shows cumulative produc-

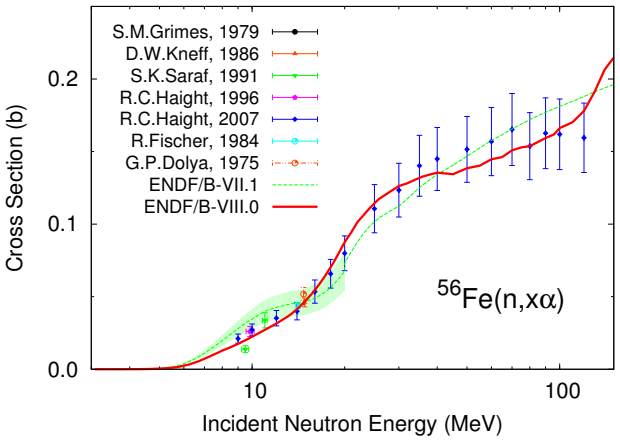

FIG. 17. (Color online) Total α production for ^{56}Fe as a function of neutron incident energy.

tion of the ^{51}Cr residue in all possible reactions. The two-hump shape of the excitation function results from different reactions contributing to the production of the residue. The first hump is due to the (n,α) while multi-particle emission reactions, on top of the (n,α) tail, are responsible for the the second one. Our evaluation agrees very well with the ENDF/B-VII.1 (and IRDFF) in the (n,α) part of the excitation function and predicts higher cross sections in the second hump.

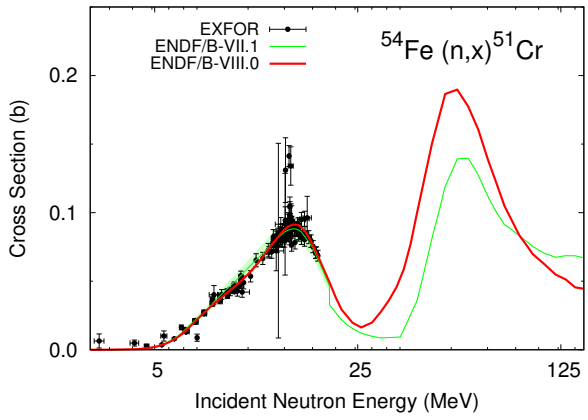

FIG. 18. (Color online) Evaluated ^{51}Cr production cross sections. Up to 20 MeV these cross sections coincide with ^{54}Fe(n,α) and therefore (n,α) data retrieved from EXFOR are included in the plot. The ENDF/B-VII.1 evaluation is also shown.

B. Elastic Angular Distributions

In this section we discuss elastic angular distributions for ^{56}Fe, since for the minor iron isotopes elastic angular distributions were well described by the EMPIRE calculations, which were adopted. In the resolved resonance range of ^{56}Fe, the elastic angular distributions are taken from the resolution-broadened Perey data [70]. From 847 keV up to 2.5 MeV the angular distributions correspond to re-fitted Kinney [135] data with some adjustments based on the comparison with the Perey data in the overlapping region. In the range 2.5-4.0 MeV the angular distributions are taken from Smith [81]. Above 4.0 MeV the angular distributions are from the EMPIRE calculation.

The adjustments in fitting the Kinney data were partially motivated by a discontinuity observed in the Kinney data between scattering into forward and backward hemisphere as illustrated at the incident energy of 0.501 MeV in Fig. 19, upper-left panel. We note that the similar-resolution Perey data do not show such discontinuity. Unfortunately, the Perey data do not cover the upper range of the Kinney experiment so we used the latter trying, within the experimental uncertainties, to follow the pattern at lower energies by lowering the anisotropy. In addition, an increase of the backward scattering also improved fast plutonium criticality benchmarks.

In general, we have found that elastic angular distributions have a significant impact on criticality. There are several experimental data sets for elastic angular distributions. Out of these only Perey and Kinney were taken with high energy resolution (apart from the Cierjacks measurement [256] which, due to unfortunate mislabeling in data classification, was not taken into account in our evaluation). The remaining low energy-resolution experiments agree pretty well, and are also in good agreement with optical model calculations. The essential issue is how important detailed elastic angular distributions between the end of the resonance region and the incident energy of around 3 MeV are for applications. We have not addressed this issue in the present work. Generally, our agreement with Perey and Kinney data is better than the one provided by ENDF/B-VII.1 as demonstrated by Fig. 19. We also avoid dramatic changes as those seen in ENDF/B-VII.1 at 0.729 MeV (Fig. 19, upper right panel). The willingness to follow the most detailed experimental data has, however, influenced our reproduction of lower resolution experiments as can be seen in Fig. 36. Our results are comparable to ENDF/B-VII.1 but optical model calculations from EMPIRE provide better agreement with data.

The elastic angular distributions at higher energies are so well described by our coupled-channel calculations (Figs. 20 and 21) that we are quite confident to be able to discriminate unreliable experimental results as shown in the middle panel of Fig. 20. We note, that in the high energy range (Fig. 21) our evaluation is either compatible to or provides better data agreement than ENDF/B-VII.1.

C. Energy Spectra

There are several measurements of neutron energy spectra concentrated around 14 MeV and some measure-

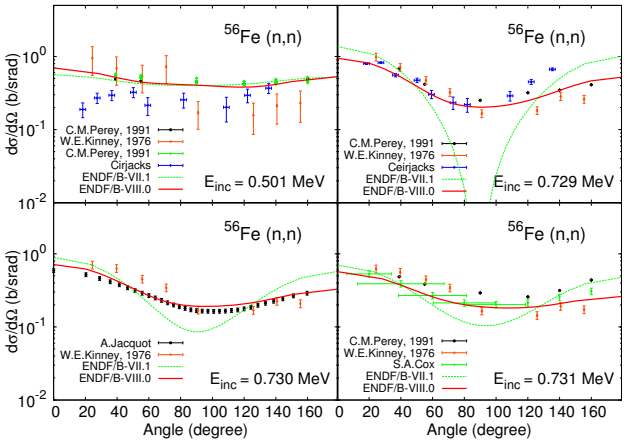

FIG. 19. (Color online) Elastic angular distributions for the neutron incident energies of 0.501, 0.729, 0.730 and 0.731 MeV. The two upper plots include also data by Cierjacks [256] which were not included in the evaluation.

ments at 18, 25.7, and 96 MeV. At these incident energies, the high outgoing-energy end of the spectra is dominated by the elastic peak and direct transitions to the collective levels that are modeled by CC and DWBA calculations. The middle part of the spectrum is governed by the PE emission, while the low energy peak is the statistical model domain. Proper description of the neutron spectra is thus a very good overall test of the quality of the modeling used in the evaluation. Fig. 22 compares CIELO and ENDF/B-VII.1 evaluations (for ^{56}Fe) with the experimental data taken on natural iron or ^{56}Fe. Both evaluations reproduce measurements at the three lower energies quite well, with CIELO being systematically closer to experimental data. This is probably due to the CC modeling of the inelastic scattering and careful selection of the levels and parameters with which DWBA calculations were performed in the CIELO evaluation.

Both evaluations underpredict neutron spectrum measured at 96 MeV by Sagrado Garcia [172]. In this case we trust evaluations more than the measurement. Our confidence is based not only on the good prediction of lower energy spectra but also, as it will be shown in the next section, on the good description of the shape of double-differential spectra at the same incident energy which, however, were measured in a different experiment.

ENDF-6 format requires that all reactions treated in the exclusive way are accompanied by the exclusive spectra of all ejectiles. The exclusive spectra are understood as those that would be measured if one could experimentally identify neutrons that were associated with a given reaction. For example, in the case of the ^{56}Fe$(n,2n)$ reaction the exclusive neutron spectrum should include the first and the second neutron that produced ^{55}Fe residue in a state that it could emit only γ-rays. EMPIRE includes a special algorithm to calculate such spectra. In Fig. 23 we show exclusive neutron spectra for the (n,n'), $(n,2n)$, and $(n,3n)$ reactions at the incident energy of 96 MeV.

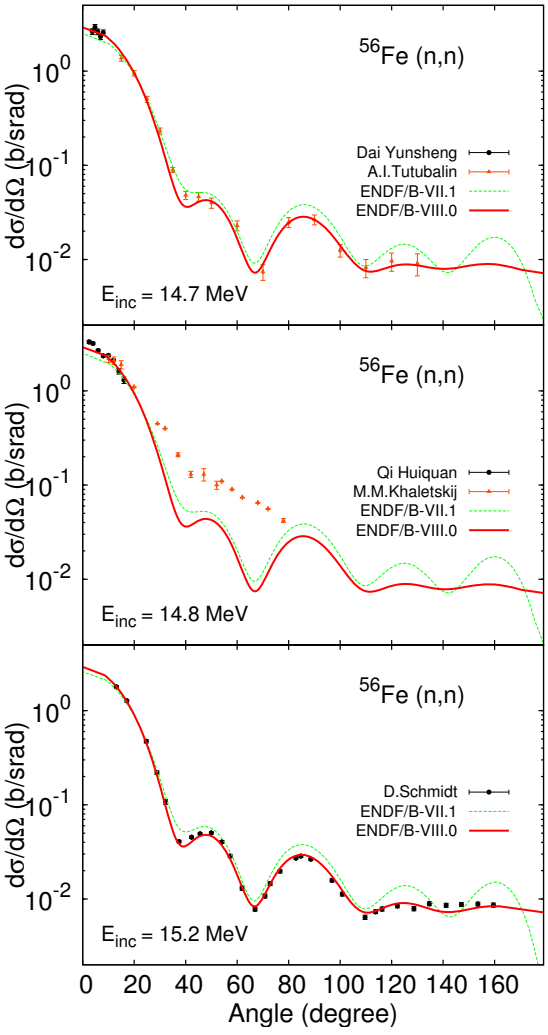

FIG. 20. (Color online) Elastic angular distributions for the neutron incident energies of 14.7, 14.8 and 15.2 MeV. The middle panel shows a case in which the experimental data are most likely wrong.

The high incident energy exacerbates peculiar features of such spectra - inelastic spectrum has one hump close to the incident energy, while multiple emission reactions produce two humps one at high energy and the other in a few MeV region. The physics interpretation of this shape is quite straightforward. In order to produce an inelastic residue the first neutron must take away so much energy to leave the residue below neutron binding energy. If it would not, other particles would be most likely emitted leading to $(n,2n)$, (n,np), *etc.*, or more complicated reactions if there is enough excitation energy. In the $(n,2n)$ reaction the high energy hump is lower than in the inelastic scattering by about the neutron binding energy in the first residue. Most of the energy left in the system is taken out by the second neutron which has an evaporation spectrum that forms the low energy hump. The same reasoning can be iterated for other multiple emis-

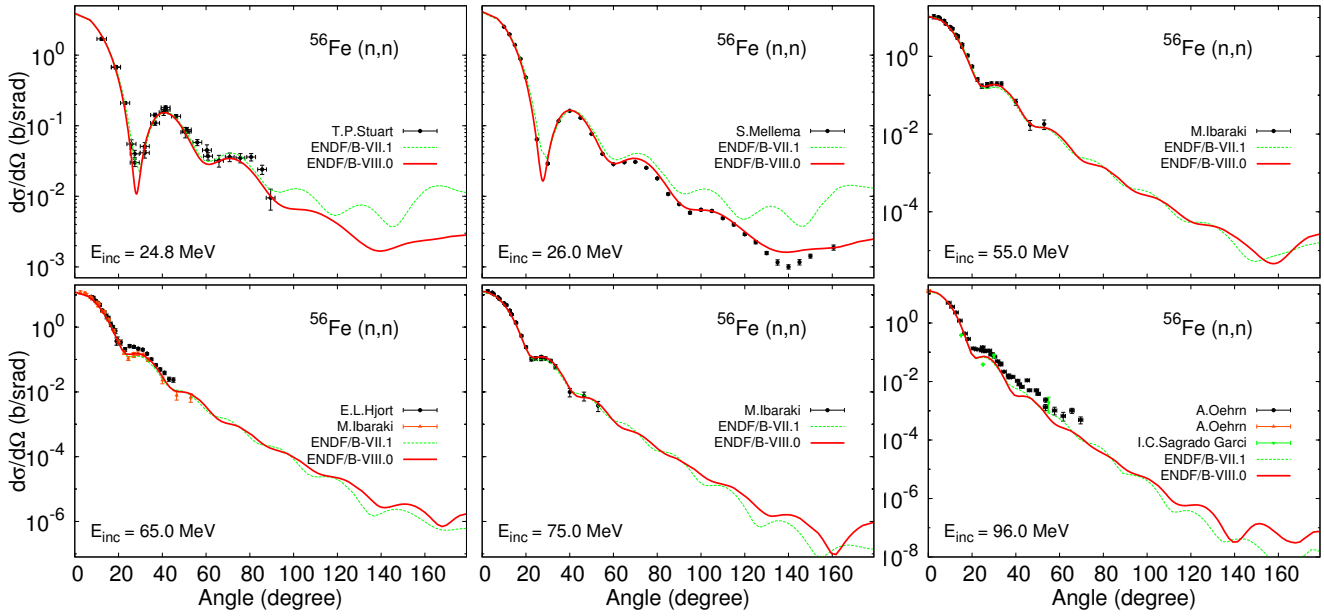

FIG. 21. (Color online) Elastic angular distributions for the neutron incident energies of 24.8, 26.0, 55.0, 65.0, 75.0 and 96.0 MeV.

sion reactions, *e.g.*, $(n, 3n)$. The effect of γ competition is to smooth transitions between the high energy humps as can be seen in Fig. 23.

From the reaction mechanism point of view, the high energy hump is exclusively due to the preequilibrium emission (at least at 96 MeV), while the low energy one is the result of statistical evaporation of nucleons from the equilibrated residua. The latter explains why the $(n, 3n)$ reaction still produces two and not three humps. This picture would change slightly if we would allow multiple preequilibrium emission in our calculations. Most likely the effect of the multiple preequilibrium emission would be adding small tails to the two humps which would tend to fill the gap between them.

D. Double Differential Cross Sections

1. *Neutron Double-Differential Spectra*

Energy-angle correlated cross sections add another (angular) dimension to the energy spectra. In some sense these are even more direct measurements since energy spectra are usually obtained by integrating double-differential ones which unavoidably involves some approximations related to interpolation and extrapolation of angular distributions. Therefore, comparison of an evaluation with double-differential cross sections provides for an additional stringent test of the modeling employed in the evaluation procedure. Again, both ENDF/B-VII.1 and the new CIELO evaluations pass this test successfully. Fig. 24 shows double-differential cross sections of both libraries compared with experimental data taken at 8.17, 14.06, and 18.0 MeV. The agreement of both evaluations with the measurement by Xichao Ruan at 8.17 MeV is quite remarkable. For the 14.06 MeV experiments, the CIELO evaluation follows very closely the data of Takahashi [102] while at 18 MeV the best agreement is found with the measurement by Soda [111]. Once again, the CIELO evaluation proves to reproduce experimental data slightly better than ENDF/B-VII.1.

In Fig. 25 we present a comparison of double-differential cross sections with experimental data taken with incident neutrons of 95 and 150 MeV. Taking into account that in this energy range angular distributions change by several orders of magnitude, the agreement between the evaluations and experimental data can be considered as fair. Performances of the ENDF/B-VII.1 and CIELO are comparable. At backward angles both evaluations are nearly identical at 95 as well as at 150 MeV, except the elastic peak which is considerably higher in CIELO than in the ENDF/B-VII.1 evaluation. At 60 degrees the results are mixed with CIELO being better at 95 MeV and ENDF/B-VII.1 reproducing quite closely the experimental data at 150 MeV.

We note that for the incident neutrons of 95 MeV, the spectra of the neutrons ejected with energies above 20 MeV are dominated by the scattering in forward angles. Thus the angle-integrated spectrum at 95 MeV should have a shape close to the one shown in the upper left panel of Fig. 25, *i.e.*, compound nucleus peak below 10 MeV followed by a slowly declining plateau between 20 and 80 MeV. This contradicts results for energy spectra by Sagrado Garcia discussed in the previous section enforcing our trust in the calculations.

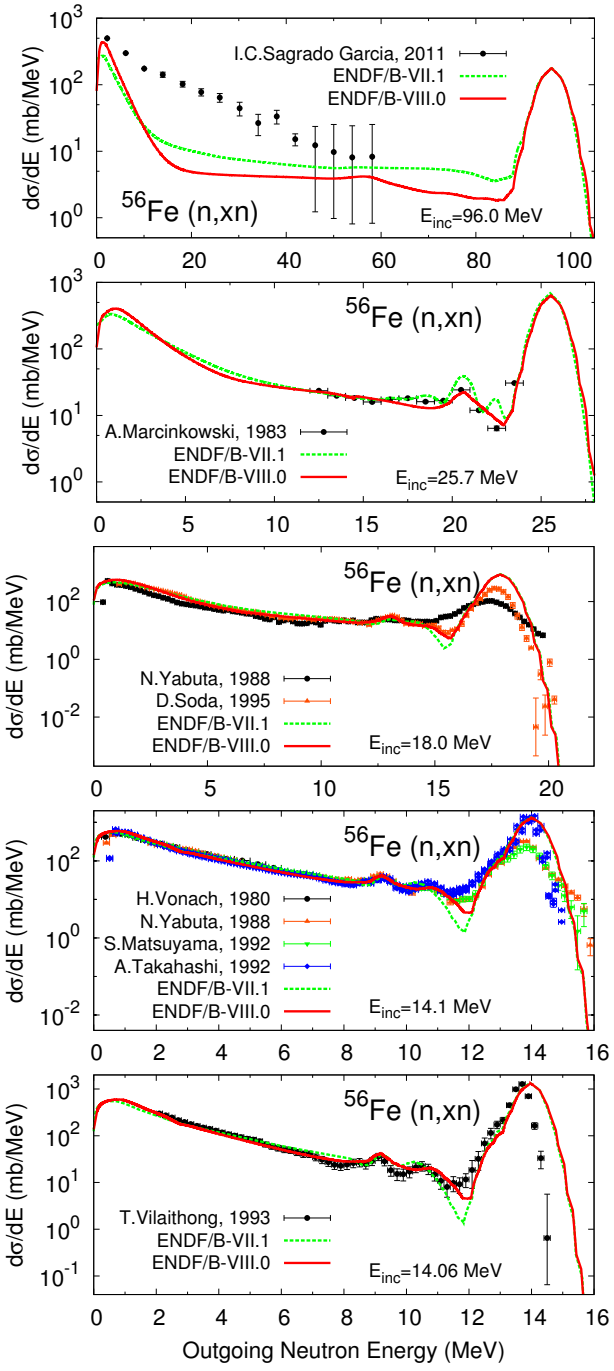

FIG. 22. (Color online) Angle-integrated neutron spectra as a function of the outgoing energy for the incident energies of 14.06, 14.1, 18.0, 25.7 and 96.0 MeV. Except for the two highest energies, for which experiments were done on ^{56}Fe, all other measurements were performed on natural targets. The plotted evaluations are for ^{56}Fe but one does not expect that introducing exact mixtures of isotopes would make any essential difference.

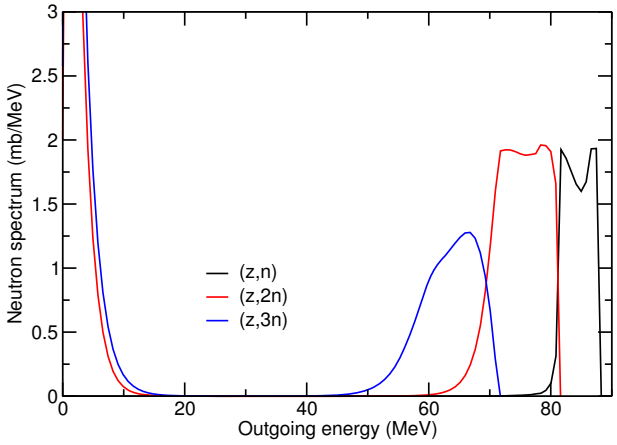

FIG. 23. (Color online) Exclusive neutron spectra for the (n,n), $(n,2n)$, and $(n,3n)$ reactions on ^{56}Fe at incident neutron energy of 96 MeV.

2. *Charged-Particle and γ Spectra*

Proton and alpha double-differential spectra are taken directly from the EMPIRE calculations. The overall behavior of the experimental data is reproduced even though the agreement is not exceptionally good. Also, such agreement with experimental data is not particularly better or worse than that of ENDF/B-VII.1: depending on the incident energy, scattering angle, and neutron outgoing energy, either ENDF/B-VII.1 or ENDF/B-VIII.0 may provide a better agreement with data. In particular, in the case of proton spectra, there is a somewhat clear pattern at high outgoing energies where the proton double-differential data show approximately linear decrease in the logarithmic scale on energy of the secondary particle while both ENDF/B-VII.1 and ENDF/B-VIII.0 drops abruptly at the end of the outgoing energy range. This should be investigated further in the next release.

In Fig. 26 we present the double-differential γ spectra for two different incident energies, 5.26 and 8.27 MeV, at the same scattering angle of 125 degrees. In the case of 5.26 MeV (upper panel), we can see that both ENDF/B-VII.1 and ENDF/B-VIII.0 reproduce well the peak at 846 keV corresponding to the decay of the first inelastic state. Above that both curves have the same overall behavior, even though ENDF/B-VII.1 seems to provide a slightly better agreement with data. At the neutron incident energy of 8.27, however, we see that ENDF/B-VIII.0 has an excellent agreement with experimental data while ENDF/B-VII.1, even though presenting a similar shape, clearly has a scaling issue, indicating that the current evaluation has more consistent multi-reaction modeling.

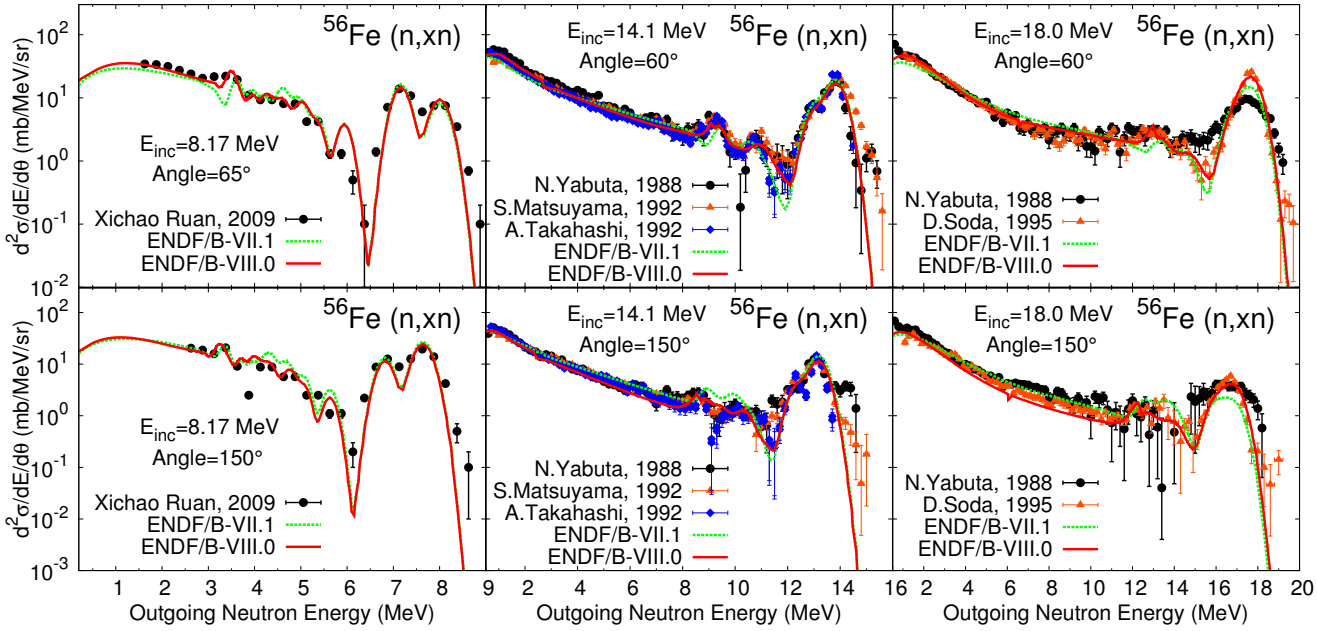

FIG. 24. (Color online) Double-differential neutron spectra for intermediate incident energies at forward and backward angles.

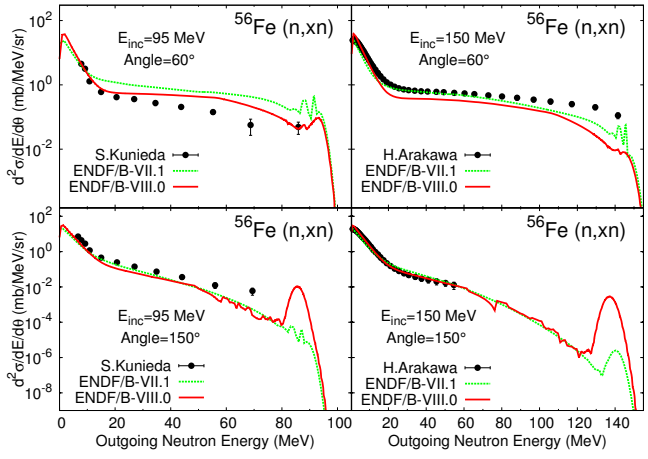

FIG. 25. (Color online) Double-differential neutron spectra for incident energies of 95 and 150 MeV at 60 and 150 degrees.

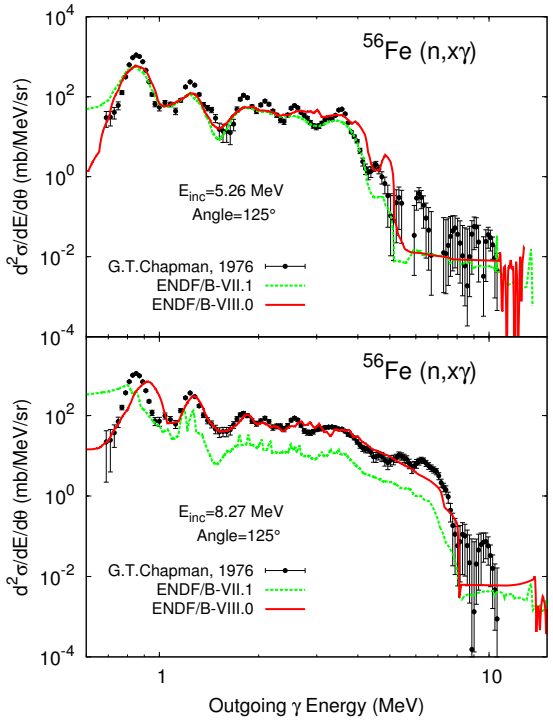

FIG. 26. (Color online) Double-differential γ spectra for incident energies of 5.26 and 8.27 MeV at 125 degrees.

VI. FILE STRUCTURE

The new iron evaluations for the three lighter isotopes consist of the resolved resonance region and the fast region. Thus, except for ^{58}Fe, the unresolved resonance regions are not present but the fast region contains empirical fluctuations up to several MeV. In the phase of assembly, the fluctuating experimental data were inserted replacing smooth cross sections or angular distributions resulting from EMPIRE calculations. In case of ^{54}Fe(n,p), ^{54}Fe(n,α) and ^{56}Fe(n,p) the IRDFF dosimetry files replaced the total cross sections for a given reaction up to 20 MeV. Partial cross sections (MT=600-649 and 800-849), calculated with EMPIRE, were renormalized to ensure consistency with the total. This renormalization was usually within the uncertainties of the dosimetry evaluation, with the difference added to the elastic channel.

There is an essential novelty in the organization of the

new evaluations which extend up to 150 MeV. So far, all evaluated files covering such high energies used standard exclusive reaction representation below 20 MeV and switched to lumped MT=5 representation above. Our files employ uniform formatting in the entire fast neutron energy range. We maintain exclusive representation for a few reactions in the whole energy range and format all the remaining reactions in MT=5 from the very beginning. The exclusive reactions are capture, elastic, inelastic, $(n,2n)$ and (n,p). The notable reaction missing in this list is (n,α) to the continuum and other reactions involving emission of a cluster. The reason for this unusual representation is the high energy range (up to 150 MeV) of the evaluation which makes it difficult to separate contributions from different reactions. Actually, EMPIRE calculates cumulative production of the residues and even though we could extract exclusive (n,α) cross section along with its exclusive α-spectrum, we have no straightforward way of producing exclusive γ-spectrum for (n,α). It is simply not possible to distinguish γ's produced by (n,α) from those produced by other reactions leading to the same residue. Therefore, we store cross sections in MF/MT=6/5 which, in combination with MF/MT=3/5, gives the production of the residues for reactions not given explicitly in MF=3. This residue production is actually the quantity measured in the activation analysis.

In case of (n,α) the situation is slightly more complicated since transitions to discrete levels are formatted in a classical way as MF/MT=3/800, 801, 802,... but MT=849 (α emission to the continuum) is formatted as part of the cumulative α-spectrum in MF/MT=6/5. Therefore, (n,α) cross sections can only be identified below threshold for other reactions populating the same residue, as a sum of cross sections in the MT=800, 801,..., 848 series plus population of the residue given by a combination of MF/MT=6/5 and MF/MT=3/5. At higher incident energies production of the residue is a sum of several reactions and one cannot interpret that as MT=107.

The only reactions which are not affected by the ambiguity described above are capture and single or multiple emissions of the same type of nucleon (*e.g.*, $(n$,elas), $(n$,inel), $(n,2n)$, (n,p)) and only these are formatted as exclusive in the current evaluations.

VII. COVARIANCES

A. ^{56}Fe Resonance Region Covariance

Essentially Fröhner's evaluation for the ^{56}Fe resonances was adopted. Unfortunately, the covariance on these parameters has since been lost. Furthermore, as noted above, a small background capture cross section was added in the region of the 24 keV resonance window. Rather than re-fitting the resonances, which would have necessitated an entire re-evaluation of the resonance region, a more pragmatic approach was taken to encoding both the resonance and background covariances. Covariances for the resolved resonance region were generated by the resonance module of the EMPIRE code. The input to the module was obtained by matching resonance parameters in the evaluation with their respective uncertainties as given in the Atlas of Neutron Resonances [30]. If such uncertainties were missing in the Atlas an educated guess based on average parameter uncertainties has been used (see Table XI). The uncertainties of the negative resonance parameters were set at the values that reproduce uncertainties of the thermal constants. The uncertainty of the scattering radius was taken into account. Following general practice, strong correlation was assumed among the Γ_γ widths. With this input EMPIRE resonance module produced a MF=32 file with covariances for the resonance parameters.

TABLE XI. Average resonance parameter percent relative uncertainties used in the resonance covariance evaluation as well as the uncertainties adopted for resonances without uncertainty estimates.

Quantity	Atlas (%) [30]	Adopted (%)
E	0.005	0
$g\Gamma_n$	12.6	18
Γ_γ	12.5	20
$g\Gamma_n^0$	5.5	10
$g\Gamma_n^1$	14.0	20
$g\Gamma_n\Gamma_\gamma/\Gamma$	14.5	20

Subsequent processing of this file with the NJOY code produced the cross section covariances in MF=33 which were incorporated in the final evaluation along with the covariances for the fast neutron region. While the total and elastic reaction uncertainties looked reasonable, we noted that this final set of MF=33 covariance files produced capture uncertainties that were systematically low. In fact, the capture uncertainties were systematically low in two separate regions: in the capture window, where the capture background was added, and near the top of the resonance region where we suspect there are missing resonances. In these two separate regions, we have been considering adding a "background covariance" to the generated MF=33 covariance. This work has not yet been completed at the time of publication of this paper and therefore we refer to the description of the evaluation in the ENDF file for details regarding the uncertainties in the resolved resonance region.

B. Fast Region Covariance

It is important to clarify that covariances in the fast neutron region assigned to the new iron evaluations refer to the *averaged* cross sections and by no means reflect the amplitude of the experimentally observed fluctuations. The uncertainties of such fluctuations, which were imposed on the averaged values, were assumed to

be of purely statistical nature and negligible compared to the uncertainties of the averaged values. This surmise has two practical implications. First, it allows for taking into account physics constraints resulting from the reaction modeling. Then, it avoids unmanageable size of the covariance matrices that would be needed to account properly for experimental datasets with thousands of points.

Covariances were determined using Kalman filter-inspired Bayesian update procedure originally coded by Kawano and Shibata in the KALMAN code [257] and more recently rewritten by S. Hoblit. This methodology combines experimental uncertainties with the model constraints imposed through the sensitivity profiles provided by the EMPIRE code. Using KALMAN, the model parameters are sequentially adjusted to each considered experiment. The resulting set of model parameters, when used in the EMPIRE code, provides averaged values of the cross sections, angular distributions, energy spectra, and energy-angle distributions that constitute the evaluation. Cross section covariances are obtained by propagating covariances of the model parameters. Therefore, all physical constraints are by construction included in the cross section covariances. These constraints result in various correlations. The most prominent condition is the unitarity which requires that the sum of all partial cross sections equals the total one. Unitarity is a principal, but not unique, reason for correlating nuclear model parameters and in consequence also cross sections for various reactions. Another important class of correlations is brought by the requirement of reproducing experimental data, which can be achieved using various combinations of parameter values. Strong correlation between two or more model parameters or evaluated quantities indicates high probability of error cancellation.

The covariances were computed for the major reaction channels represented in the evaluations, *i.e.*, total, elastic, inelastic, capture, $(n,2n)$, and (n,p). Inelastic scattering to individual discrete levels (MT=51,...,90) and to the continuum (MT=91) were combined together into MT=4. As explained in Sec. VI, we do not provide an explicit MT=107 because of the interference of other reactions at higher energies. We do provide, however, covariances for the sum of all the remaining channels (MT=5). We also calculated cross-correlations among all reactions mentioned above.

We used experimental uncertainties reported in EXFOR and determined, if possible, the long range correlations in the experimental covariance matrices from the ratio of reported systematic uncertainties to the total ones. If such information was not available from EXFOR we used default 45% correlation between different energy points for the same reaction. Since our aim was to determine covariances for the averaged cross sections, the experimental datasets showing pronounced fluctuation structure were subject to the iterative smoothing procedure before being used. In addition, datasets with excessive number of energy points were thinned to keep the total number of points below 1000 per experiment. Because this operation was performed on the already smoothed dataset there was no information loss related to dropping even 90% of the original data points.

We note that several measurements that were instrumental for establishing the recommended cross sections were not used in the uncertainty determination. This was the case for Berthold's data that defined the fluctuating structure of the total cross section in ^{56}Fe as well as for Dupont data which shaped inelastic scattering. These high energy resolution measurements were renormalized to the averaged cross sections determined by other experiments and, therefore, did not bring any information on the absolute values. Also, outliers and single energy experiments (if not of significant value) were not taken into account in determining covariances.

Special treatment has been reserved for the reactions for which IRDFF recommendations were adopted. In these cases, IRDFF cross sections were used in the evaluation procedure in place of the experimental datasets and eventually EMPIRE calculated cross sections were replaced with the IRDFF values. Therefore, it was desirable to retain, as far as possible, also IRDFF covariances. While doing it with the cross sections is straightforward, inserting IRDFF covariances in the KALMAN determined covariance matrix would break physical and mathematical consistency of the matrix. Instead of doing this we preserved KALMAN created covariances but during the procedure we adjusted weights of the IRDFF cross sections to reproduce, as closely as possible, original IRDFF uncertainties. Our off-diagonal part of the covariance matrix necessarily differs from the IRDFF since the latter is purely based on ^{56}Fe(n,p) experimental data while ours includes also physics constraints and the correlations with other reactions.

In the calculations, we adjusted the weights of each experiment to ensure that each measurement contributes about 1 to the total χ^2 independently of the number of points in the dataset. This condition turned out to be instrumental in ensuring a reasonable magnitude of the uncertainties that usually tend to be severely underestimated for the datasets with many points. The initial uncertainties of the model parameters were set large enough so that their further increase had no effect on the calculated covariances of the cross sections. It means that the final parameter covariances were fully determined by the experimental data and physics constraints and not by our prior knowledge of the parameter uncertainties. This has been possible for most of the reactions since existing measurements were sufficient to constrain model parameters. In some cases, however, lack of experimental data combined with unrestricted model parameters resulted in very large cross section uncertainties. Such expansion was controlled by allowing the model parameters to vary only within a physically sensible range (*e.g.*, as reported in RIPL-3).

In Fig. 27 we summarize relative uncertainties for the major reaction channels for ^{56}Fe in the fast neutron range

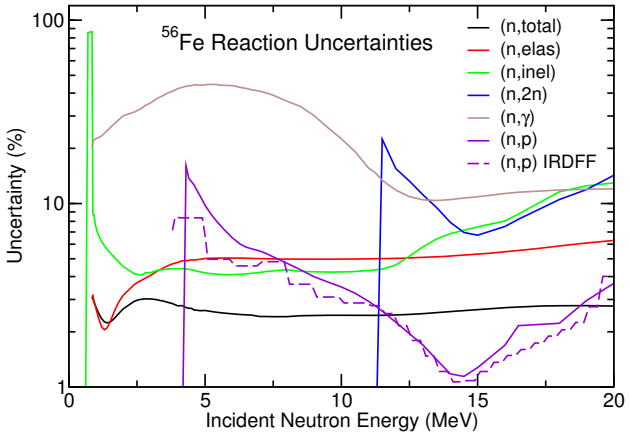

FIG. 27. (Color online) Relative uncertainties for selected reactions on ^{56}Fe. Shown is the fast neutron energy range from the first inelastic threshold up to 20 MeV. In the case of the (n,p) reaction the present uncertainties are compared with those from the IRDFF file (dashed violet line).

up to 20 MeV. One notes very high (nearly 100%) uncertainties for the inelastic at low energies. This energy range is actually below the inelastic threshold and the cross sections correspond to the ^{56}Fe$(n,\gamma n)$ reaction, *i.e.*, emission of a low energy γ followed by emission of a neutron to the ground state in ^{56}Fe. There is no place in the ENDF-6 format for the $(n,\gamma n)$ process that is neither elastic nor inelastic scattering. To preserve the unitarity we choose to store these cross sections as inelastic to the continuum (MT=91). They are orders of magnitude smaller than the regular inelastic so the high uncertainty is not unreasonable. Actual uncertainty of the inelastic in the threshold region is 9%. For the remaining part of the inelastic the uncertainties are around 4%, in good agreement with Negret's estimates, and increase up to 13% as the incident energy approaches 20 MeV.

Uncertainties for the total are slightly above 2.5%, again in good agreement with Abfalterer's data after including the systematic uncertainty. As expected, uncertainties for the elastic are nearly two times higher than for the total, except in the immediate vicinity to the inelastic threshold where total and elastic cross sections are very close and so are their uncertainties. The decrease around 2 MeV is due to the vanishing sensitivity of the total and elastic cross sections to the real volume depth of the optical potential, which happens around this energy.

For the $(n,2n)$ reaction the uncertainties start at 22% close to the reaction threshold, drop slightly below 7% in the energy range constrained by the experimental data and rise to 14% at 20 MeV.

Our knowledge of the capture is not very precise as its uncertainties reveal a broad maximum approaching 45% between 5 and 6 MeV. The position of this maximum is in the energy region where the capture cross section decreases sharply due to the competition of inelastic channels. At higher incident energies capture uncertainties decrease to about 10% as they are constrained by the experimental point at 14.2 MeV.

TABLE XII. Comparison of uncertainties (in %) for ^{56}Fe$(n$,total) and ^{56}Fe$(n$,inel) reactions obtained in three evaluations: (i) non-model fit by IRK/IPPE (1992-1995) in 41 energy groups, (ii) BROND-3 evaluation including unrecognized systematical uncertainties (7 energy groups above 1 MeV), and (iii) present ENDF/B-VIII.0 evaluation.

Reaction	E_n (MeV)	IRK/IPPE	BROND-3	ENDF/B-VIII.0
Total	1	0.8	3.5	2.8
	14.5	0.7	2.5	2.8
	20	1.5	2.8	2.8
Inelastic	1	1.8	25	8
	5	1.4	17	5
	20	9.6	14	13

In case of the dosimetry reaction ^{56}Fe(n,p), for which we used the IRDFF evaluation in place of the experimental data, we reproduce quite well the original IRDFF uncertainties (dashed line in Fig. 27). In most of the presented range the uncertainties remain below 4% and achieve a precision of 1% around 15 MeV. Only in the immediate vicinity of the threshold our uncertainties are twice higher than those reported in IRDFF. We retain that 16% is not excessive in view of the size of the cross section.

We admit that our uncertainties are on the conservative side. By requiring that each experiment contributes about one to the total χ^2 we implicitly account for the unknown systematic uncertainties and internal precision of the experiments. The former we achieve by increasing uncertainties of the experimental points to touch the average, while the latter is simulated by eliminating the typical $1/\sqrt{(n)}$ factor which decreases the uncertainty with increasing number of points (n) within an experiment. In Table XII we compare our uncertainties for total and inelastic with those reported in the IRK/IPPE evaluation [6, 7] and the Russian evaluated library BROND-3. The IRK/IPPE evaluation, which does not account for the two effects mentioned above, provides the smallest uncertainties. BROND-3 uncertainties, which include unrecognized systematic errors, are much larger than the IRK/IPPE ones. Our estimates are in between these two extremes for the two lower energies, while at 20 MeV there is a very good agreement between ENDF/B-VIII.0 and BROND-3. The major disagreement between the latter two evaluations is found at low energy inelastic where ENDF/B-VIII.0 uncertainties are three times lower than in BROND-3. This could be due to the fact that these uncertainties are driven by the recent Geel experiment which was not available at the time the BROND-3 evaluation was performed.

It is interesting to compare these uncertainties with the target accuracies required for innovative systems as specified in the WPEC Subgroup 26 report [258]. The most important ones are the inelastic cross sections, for which accuracies of 3 to 6% are requested below 2 MeV. Our un-

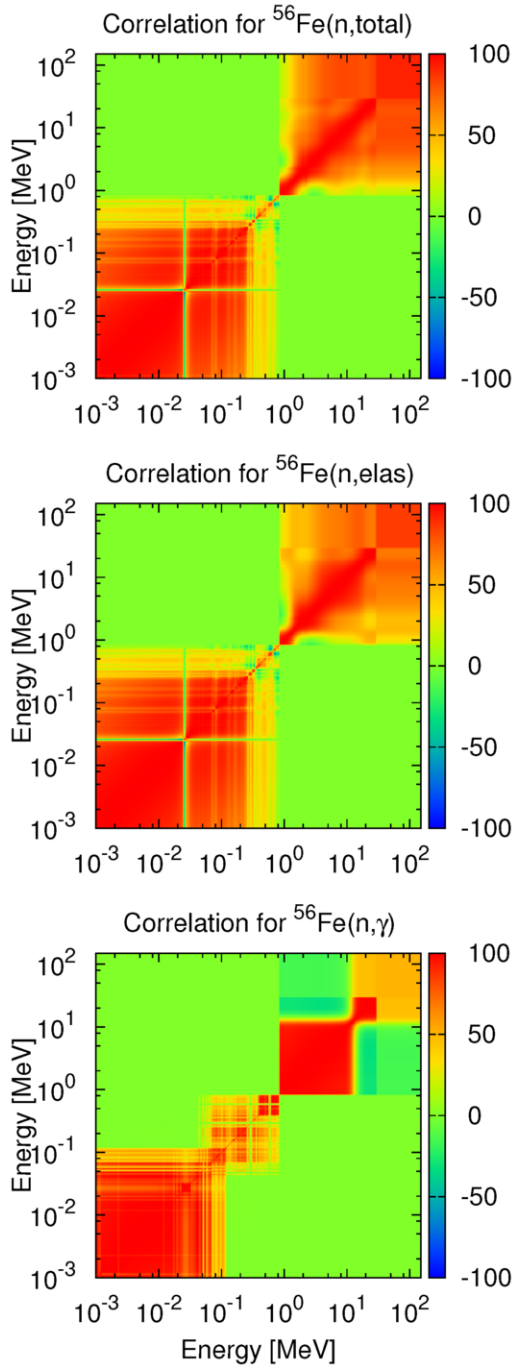

FIG. 28. (Color online) Correlation matrices for non-threshold reactions from thermal resonance regions up to 150 MeV.

certainties are about 9% at the threshold and drop down to 4.5% at 2 MeV so they are on the border of the fast system requirements. Similarly, for the elastic cross sections our uncertainties are usually well below 5% between 0.5 and 6 MeV which should satisfy most of the new designs. As already mentioned, we are not in a position to provide final capture uncertainties in the resonance region but we are skeptical about reaching required 3 to 8% uncertainty between 0.5 and 200 keV.

In Fig. 28 we present our uncertainty correlation matrices for the three non-threshold reactions - total, elastic and capture. Contrary to the uncertainties, which were still in progress when this paper was due, we do not expect major modifications to the overall structure of the correlation matrices that were estimated at the time. Therefore, in Fig. 28 we combine resolved resonance region with the fast neutron region. There is a typical lack of correlations between the resonance and fast neutron region which reflects the independence of evaluation procedures in the two regions. The correlation matrices for total and elastic are nearly identical. In the resonance region this resemblance is caused by the fact that total and elastic are very similar due to the particularly small capture in iron. One notes a green cross-hair in both plots located around 24 keV and corresponding to the well-known window of transmission in iron. This feature is so distinct that it stands on its own without any correlations. In the fast neutron range, total and elastic are essentially defined by the same optical model and the experimental data for the total. Thus, the only difference one observes are weaker correlations in the case of elastic. The fast neutron region has a chess-board pattern typical for model based covariances.

Fig. 29 shows the structure of the self-correlation matrices for the three threshold reactions (inelastic, $(n,2n)$, and (n,p)) and the lumped channel MT=5 containing all the remaining threshold reactions. The entire fast neutron range considered in the evaluation is covered. The inelastic plot bears some resemblance to a chess-board which indicates strong correlations within red boxes and weak or negative correlations among them. This type of structure is typical for the model-derived covariances and arises when the uncertainties are dominated by different model parameters in different energy regions. Therefore we conclude that, for inelastic the diagonal elements (uncertainties) are determined by the experimental data while correlations are governed by physics constraints imposed by the model. Only if high precision data are available, as in the case of the dosimetry reaction ^{56}Fe(n,p), or many reactions are mixed (as is the case of MT=5) the impact of the model is to a large extent washed out, as can be seen in two lower panels of Fig. 29. The case of the $(n,2n)$ reaction is mixed - up to 20 MeV the covariance is dominated by the experimental data while strong correlations above 20 MeV indicate a shift to the model governance.

VIII. VALIDATION

A. Criticality Benchmarks

Benchmarks that were found to be appreciably sensitive to iron were selected from the ICSBEP compilation [259] to form a 24 benchmark set used in the criticality validation. The sensitivity is a better justification

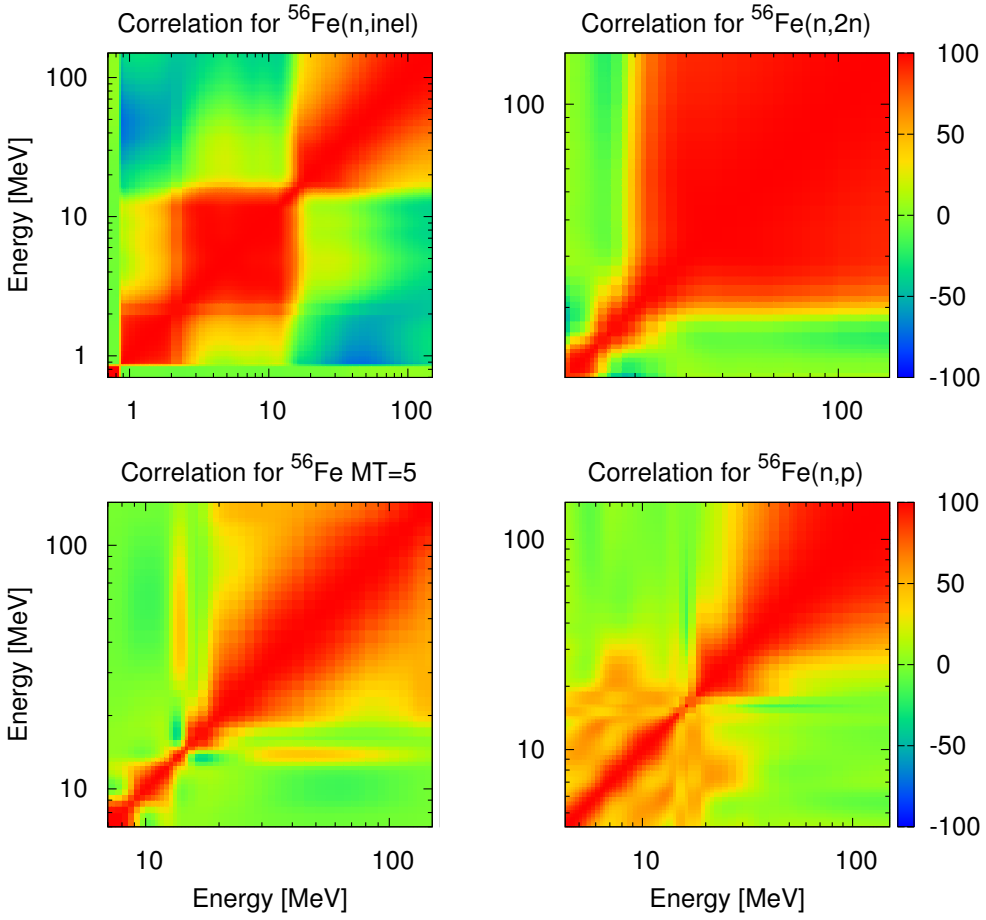

FIG. 29. (Color online) Correlation matrices for selected reactions in the fast neutron range up to 150 MeV.

than a simple presence of iron in the benchmark since it eliminates those benchmarks that do not bring any information about iron. The list of benchmarks with their ICSBEP name and the common name is given in Table XIII. The reference nuclear data for Monte Carlo calculations with the MCNP code was the ENDF/B-VII.1 library.

Most of the benchmarks are for the fast neutron spectrum (16), six are for the thermal systems and two for the intermediate ones. Fig. 30 shows the $\Delta k_{\rm eff}$, which is the difference between calculated and measured ratios of neutron gain over neutron loss ($k_{\rm eff}$), for the 24 benchmarks calculated with ENDF/B-VIII.0 (including current iron evaluations) with the results obtained for ENDF/B-VII.1, JEFF-3.2 and JENDL-4.0. Only in the case of four benchmarks (imf06, lct042-1, lct042-1, and mcf001) ENDF/B-VII.1 outperforms ENDF/B-VIII.0. For the remaining 20, the new library is either equivalent or better. The other two libraries underestimate the criticality of the first two (JENDL-4.0) or five (JEFF-3.2) fast high enriched uranium experiments (hmf) as well as five fast plutonium assemblies (pmf015, pmf025, pmf026, pmf028, pmf032). The metallic-plutonium fast benchmark pmi002 (the last on the plot) is a notorious outlier which is overcalculated by all libraries. In this case, however, the new evaluation does better than the other three. For the remaining benchmarks JEFF-3.2 and JENDL-4.0 are remarkably close to ENDF/B-VII.1. It is interesting that the two thermal benchmarks (hmt013-2, hmt015) are strongly over-predicted (about 1000 and 800 pcm respectively) by all of the tested libraries. Even more intriguing is the fact that all four libraries agree on these two cases. On the other hand, the remaining four thermal benchmarks (lct042-1, lct042-1, lct043-2, lmt015) calculate within experimental uncertainty with the three libraries while ENDF/B-VIII.0 calculates a bit lower so that the first two points fall outside the uncertainty range. The hmi01, a relatively complex zero power reactor, that is calculated with a very simplified model, is a special case. This experiment, designed specifically to test the iron evaluation, would be overcalculated by about 1500 pcm if the *ad hoc* capture background were not introduced in the range of 10-100 keV in the new ^{56}Fe evaluation.

Figure 31 allows for looking at the validation results from a different perspective. The difference between

TABLE XIII. Criticality benchmarks used to validate iron evaluations. Note that the three-letter abbreviation is being used to denote a benchmark in plots, *e.g.*, hmf-013 for HEU-MET-FAST-013.

	ICSBEP name	Common name
1	HEU-MET-FAST-013	VNIITF-CTF-SS-13
2	HEU-MET-FAST-021	VNIITF-CTF-SS-21
3	HEU-MET-FAST-024	VNIITF-CTF-SS-24
4	HEU-MET-FAST-087	VNIITF-CTF-Fe
5	HEU-MET-FAST-088	hmf088-1
6	HEU-MET-FAST-088	hmf088-2
7	HEU-MET-INTER-001	ZPR-9/34
8	HEU-MET-THERM-013	hmt013-2
9	HEU-MET-THERM-015	hmt015
10	IEU-MET-FAST-005	VNIITF-CTF-SS-5
11	IEU-MET-FAST-006	VNIITF-CTF-SS-6
12	LEU-COMP-THERM-042	lct042-1
13	LEU-COMP-THERM-042	lct042-2
14	LEU-COMP-THERM-043	IPEN/MB-01
15	LEU-MET-THERM-015	lmt015
16	MIX-COMP-FAST-001	ZPR-6/7
17	MIX-COMP-FAST-005	ZPR-9/31
18	MIX-COMP-FAST-006	ZPPR-2
19	PU-MET-FAST-015	BR-1-3
20	PU-MET-FAST-025	pmf025
21	PU-MET-FAST-026	pmf026
22	PU-MET-FAST-028	pmf028
23	PU-MET-FAST-032	pmf032
24	PU-MET-INTER-002	ZPR-6/10

the red line and the teal line represents the net effect of the new iron evaluations since effects coming from other changes in the library were eliminated. Analyzing these differences one observes that the first seven points (all hmf's and hmi01) changed in the right direction. Similarly, all pmf's at the end of the plot calculated higher, improving agreement with experimental data (except pmf028 which, however, still remains within the error band). The improvement in the criticality for pmi002 (the last point) is also due to the new iron evaluation, although this is still not enough to achieve agreement with the data. The reactivity for mcf006-s went down improving the prediction. For most of the remaining benchmarks the new iron evaluations have no effect, with notable exception of mcf001 and mcf005-s which went considerably down resulting in under-prediction of the criticality. These two are the only iron sensitive benchmarks that were worsened by the new evaluation.

The effect of other changes in the library (difference between the green line and the teal line) are most visible for hfm088-1, hfm088-2, imf006, lct042-1, lmt015, pmf015, pmf025, and pmf026 for which the reactivity was decreased. In most cases this has been counteracted by the increase of the reactivity in new iron evaluations. This was not the case, however, for imf06 and lct042-2 which were pushed down out of the uncertainty band due to changes in the remaining part of the ENDF/B-VIII.0 library. Only mcf005-s increased its reactivity significantly but this change was compensated by the

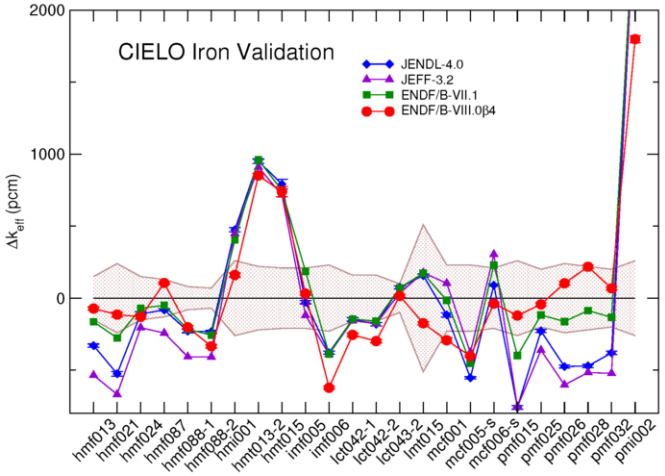

FIG. 30. (Color online) Results of the validation of ENDF/B-VIII.0 in criticality benchmarks sensitive to iron. Results for ENDF/B-VII.1, JENDL-4.0, and JEFF-3.2 are included for comparison.

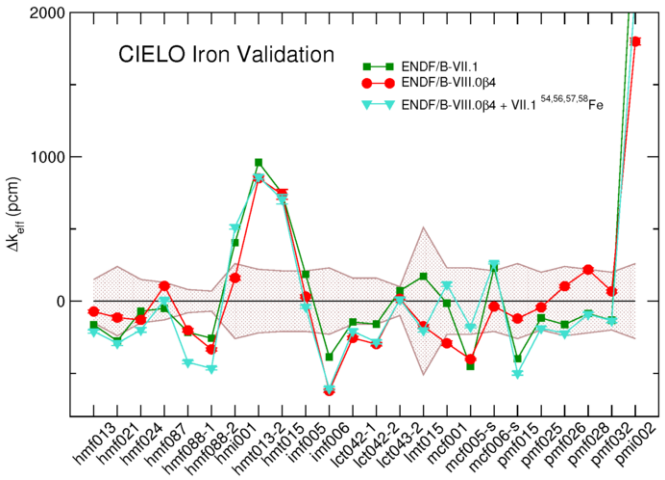

FIG. 31. (Color online) Validation of ENDF/B-VIII.0 in criticality benchmarks. This plot allows for separating the effects on the reactivities coming from the replacement of the ENDF/B-VII.1 iron evaluation from the effect introduced by the remaining changes in the ENDF/B-VIII.0 library. The difference between the red line and the teal line represents the effect of the new iron evaluations. The difference between the green line and the teal line represents the effect of the remaining changes in the ENDF/B-VIII.0 library.

decrease of the new iron evaluations so that ENDF/B-VII.1 under-prediction persists. In summary, Fig. 31 shows that new iron evaluations, when coupled to the ENDF/B-VIII.0 library, improve performance of the library on 13 benchmarks compared to ENDF/B-VII.1 iron evaluations, worsen the agreement for 3 benchmarks and maintain the performance of the remaining 8.

B. Transmission Experiments

The new evaluations were validated against so-called clean benchmarks and compared with the performance of ENDF/B-VII.1. This class of integral experiments usually have rather simple geometry, one dominating material of interest and a irradiation external source with well characterized quasi-mono-energetic or broad energy distribution. For iron there are such benchmarks with a ^{252}Cf (broad energy distribution with mean neutron energy of 2.1 MeV) source and deuterons bombarding a tritium target source (d-T) with quasi monoenergetic neutrons of 14 - 15 MeV. The geometry of the assembly is a sphere or cylindrical slab. The measured quantities are energy differential absolute fluxes (*i.e.*, normalized per 1 source neutron emitting in 4π) of the neutron and gammas leaking from the surface of assembly.

The modeling of neutron and gamma transport in the benchmarks was performed by the Monte-Carlo code MCNP-6.1 [260] using continuous energy cross sections from ENDF/B-VIII.0 and ENDF/B-VII.1. The validation of the Fe evaluated cross section was carried out against the iron spheres with ^{252}Cf and d-T sources in the center. The neutron and gamma leakage spectra from the Cf-driven 6 spheres of diameter 20 to 70 cm were measured in IPPE Obninsk by L.Trykov [261]. The measured and MCNP simulated spectra of n leaking from an Fe sphere of 60 cm diameter are compared in Fig. 32. It is seen that the largest disagreement (20 - 30%) for leaking neutrons is observed in the energy range from 1 to 10 MeV, where ENDF/B-VIII.0 demonstrates worse performance than ENDF/B-VII.1. The total cross sections for natural iron plotted in this figure show that its peaks define the dips in the leaking neutron spectrum and vice versa. The 50 mb excess of ENDF/B-VIII.0 over ENDF/B-VII.1, as shown in bottom of Fig. 32, might be a reason of larger underestimation in the 1-3 MeV interval.

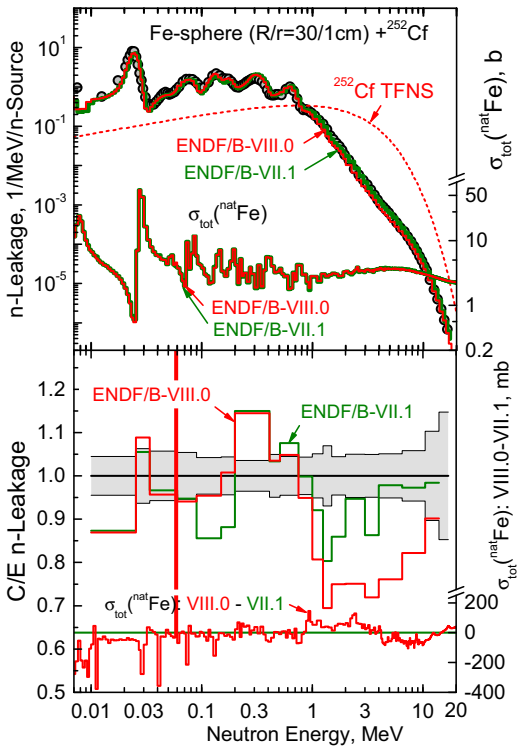

FIG. 32. (Color online) Neutron leakage spectra from an Fe sphere diameter 60 cm with ^{252}Cf source (top) and C/E ratios (bottom). Circles - experiment of L. Trykov [261]. Curves - transport calculations with ENDF/B-VIII.0 (red) and ENDF/B-VII.1 (green) cross sections. Red dashed curve - ^{252}Cf(s.f.) total fission neutron spectrum. Colour curves - corresponding total cross section for natural iron (top) and their difference (bottom).

For the same size Fe sphere the γ leakage spectra are shown in Fig. 33. We have to note that during analysis of the gamma leakage we observed large discrepancies already for the bare ^{252}Cf source and tried to improve the total gamma yield and fission spectrum used in the present Monte-Carlo simulation. From results shown in Fig. 33 we conclude that ENDF/B-VIII.0 produces slightly better results than ENDF/B-VII.1: the disagreement with experiment reaches $\approx$ 40% (compared to $\approx$ 60% for ENDF/B-VII.1) and in 4 out of 8 energy groups our results are within the uncertainty bars assigned to the experimental data (only 2 for ENDF/B-VII.1). The highest energy part of the spectra exhibits several resolved peaks at energies 6.1, 7.7 and 9.1 MeV. Tagging proper reactions in the Monte Carlo simulation allowed us to find that they are primary γ's from neutron capture reactions on ^{54}Fe and ^{56}Fe.

Figure 34 shows C/E ratios for leaking n and γ as a function of the iron sphere wall thickness. For the leaking neutrons one sees reasonable agreement with experiment in the energy interval 0.1 - 1.5 MeV while underestimation is increasing for energies between 1.5 and 10 MeV. The analytically calculated neutron attenuation *exp(-nσ(R - r))* with effective removal cross sections σ=60 mb and σ=120 mb reproduces the trend of the MCNP calculation with ENDF/B-VII.1 and ENDF/B-VIII.0, respectively.

Another experiment performed at IPPE has provided the neutron leakage spectra from 5 spheres fed by d-T neutron source [262]. The measurements were performed by Time of Flight (ToF) technique which, as was shown in Ref. [262], shifts resonances and dips in the n-leakage spectrum towards lower energies. To reduce systematic bias the time of arrival spectra were calculated by Monte-Carlo and then converted into an energy distribution. The measured and MCNP simulated spectra of neutrons leaking from an Fe sphere of 60 cm are shown in Fig. 35. It is seen that ENDF/B-VIII.0 performs better than ENDF/B-VII.1.

The fact that ENDF/B-VIII.0 describes better transmission of the 14 MeV d-T neutrons than ENDF/B-VII.1, while the opposite is true for the ^{252}Cf source spectrum, may shed some light on the reason of the ENDF/B-

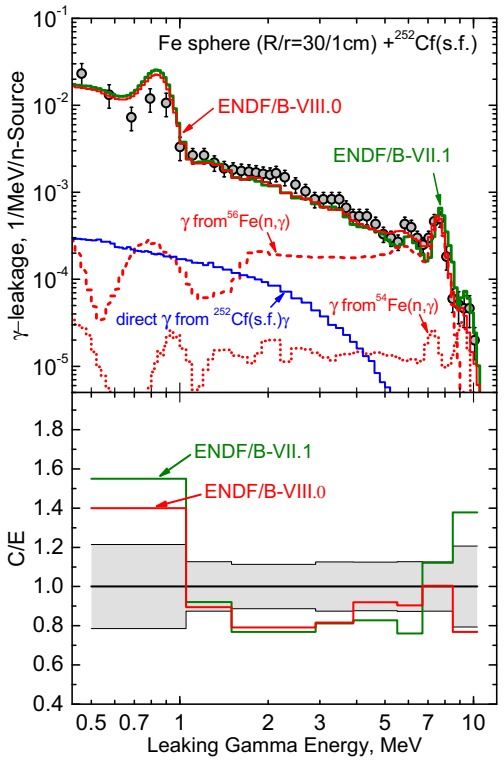

FIG. 33. (Color online) Gamma leakage spectra from an Fe sphere diameter 60 cm with ^{252}Cf source (top) and C/E ratios (bottom). Circles - experiment of L. Trykov [261]. Curves - transport calculations with ENDF/B-VIII.0 (red) and ENDF/B-VII.1 (green) cross sections. Blue curve - direct γ-rays from ^{252}Cf(s.f.) source penetrated through iron. Red dashed curves - γ-ray spectra produced by the ^{54}Fe(n,γ) and ^{56}Fe(n,γ) reactions.

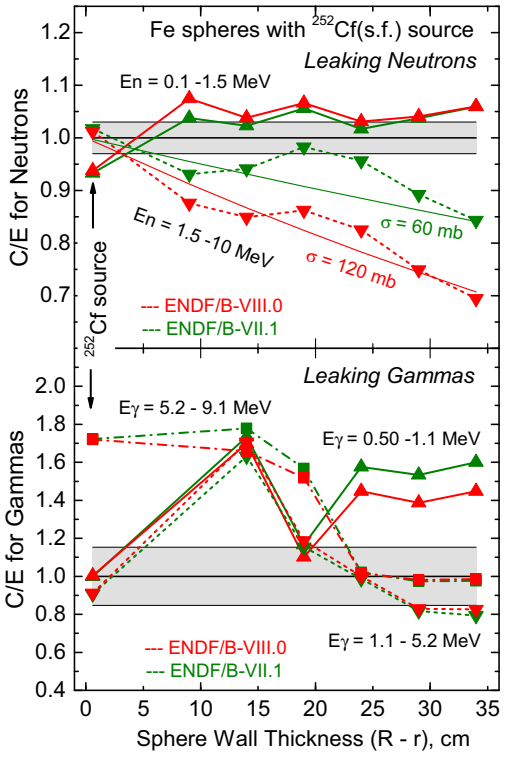

FIG. 34. (Color online) C/E ratios for neutrons (top) and gammas (bottom) leaking from bare ^{252}Cf source and Fe spheres diameter 20 - 70 cm. The transport calculations with ENDF/B-VIII.0 (red) and ENDF/B-VII.1 (green) cross sections. Thin red and green curves - analytically calculated neutron attenuation by $(R - r)$ thick Fe layer with effective removal cross sections 60 and 120 mb.

VIII.0 deficiency. In the d-T experiment with a nearly monoenergetic 14 MeV source, neutrons between 4 and 10 MeV can practically be produced only by elastic and inelastic scattering. Other energetically possible neutron producing reactions are either three orders of magnitude weaker (the case of $(n,n\alpha)$), or produce secondary neutrons below 4 MeV ($(n,2n)$ and (n,np)). The fact that ENDF/B-VIII.0 describes the experimental leakage properly is an argument in favor of the ENDF/B-VIII.0 scattering cross sections. On the other hand, in the ^{252}Cf source experiment the neutron leakage in a few MeV energy range is most likely dominated by elastic scattering of source neutrons which have continuing distribution shown as a dashed red line in Fig. 32. Therefore, one might infer that elastic cross sections and/or angular distributions in ENDF/B-VIII.0 are responsible for the underprediction of the neutron leakage in the ^{252}Cf experiment. Another possibility could be neutron capture, which in the new evaluation for ^{54}Fe has increased by a factor of two. Additional test calculations have ruled out the latter possibility leaving elastic scattering in the current evaluation to be the most likely culprit. Indeed, in the MeV range elastic cross sections for ^{56}Fe in ENDF/B-VII.1 are substantially larger than those recommended in the new evaluation, while the opposite is true for the inelastic scattering. This alone could probably make for the difference between the two evaluations, however, the new evaluation fits well experimental total and inelastic cross sections and any significant change of elastic would break this consistency. Therefore, we would rather blame elastic angular distributions, although modest adjustment of the elastic to inelastic ratio cannot be excluded. Another test calculation of the ^{252}Cf source experiment confirmed significant sensitivity of the neutron leakage to elastic angular distributions above the resonance region with more forward peaking leading to increase of the leakage. At the same time we have learned about results of a new measurement [136] of elastic angular distributions on ^{56}Fe. Fig. 36 shows that these energy-averaged results (reported energy resolution is 80 keV at 3 MeV and 170 keV at 6 MeV) agree better with our coupled-channel calculations than with our evaluated distributions. Because of the timing constraints of the CIELO project we were not able to investigate in detail potential implications of the new data but it seems that increased forward peaking of elastic scattering as measured by Ramirez *et al.* could improve performance of the evaluation in the

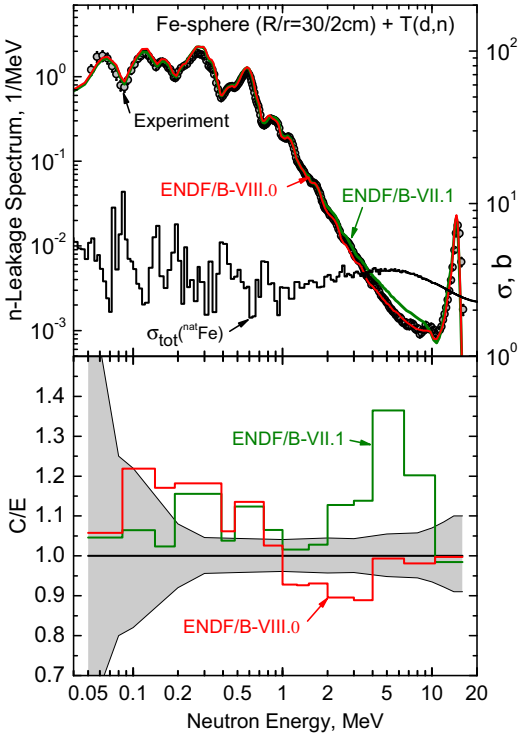

FIG. 35. (Color online) Neutron leakage spectra from an Fe sphere diameter 60 cm with a d-T source (top) and C/E ratios (bottom). Circles - experiment of S. Simakov [262]. Curves - transport calculations with ENDF/B-VIII.0 (red) and ENDF/B-VII.1 (green) cross sections. Black curve - total cross section for natural iron.

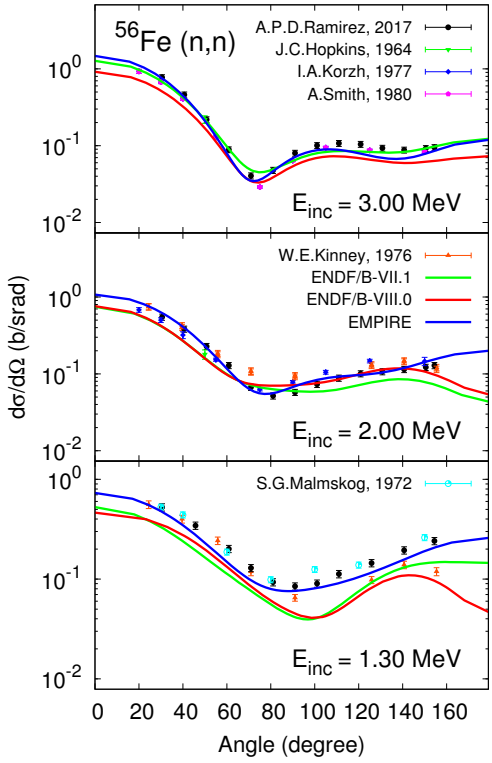

FIG. 36. (Color online) Elastic angular distributions for ^{56}Fe at several selected incident neutron energies. Recent results by Ramirez [136] are compared with the current evaluation (red line), with ENDF/B-VII.1 (green dashed line), and with the results of our CC calculations (blue line). Good agreement is observed between the energy-averaging experiment and the results of CC calculations, while higher-energy-resolution evaluations differ.

neutron leakage experiment with the ^{252}Cf spontaneous fission source.

IX. CONCLUSIONS

The CIELO collaboration has developed a new set of evaluations for isotopes of iron using recent differential measurements, state-of-the-art modeling, semi-integral data, and integral benchmarks. Between 0.85 and 4 MeV the ^{56}Fe evaluation is practically based on the experimental data. Above this range we rely on model calculations using a soft rotor optical model potential in coupled channels calculations, preequilibrium mechanism and Hauser-Feshbach formulation of the statistical model to simulate nuclear reactions all the way up to 150 MeV with the EMPIRE code. For ^{54}Fe and ^{57}Fe we have made a substantial upgrade of the resolved resonances bringing them into agreement with the most recent measurements by adding additional resonances (^{54}Fe) and matching experimental thermal quantities and Maxwellian averages.

Salient features of the new evaluations are (i) increased energy resolution for the fluctuating inelastic (and elastic) cross sections, (ii) particular attention dedicated to angular distributions, (iii) increase of the inelastic cross section on ^{56}Fe, (iv) use of the dosimetry evaluations from IRDFF, (v) consistent approach to all isotopes, and (vi) uniform formatting across the whole energy range from 0.85 up to 150 MeV.

We are generally satisfied with the fast neutron range in which the measured cross sections are reproduced quite well by the new CIELO-ENDF/B-VIII.0 evaluations. Good agreement is also found for the neutron and γ spectra as well as for angular distributions. These results are confirmed by the leakage experiment with a 14 MeV d-T neutron source. We have also improved performance in the criticality experiments although 10 measurements are still calculated outside the experimental error bar (it would be 14 with ENDF/B-VII.1 irons).

On the other hand, we concluded that experimental data, even though we can't complain about their scarcity, do not constrain sufficiently elastic angular distributions below 4 MeV, which we found to be important in calculating criticality and deep penetration experiments.

It is astonishing that four major experimental datasets which determined a large part of the current evaluation (Berthold [60], total cross section; Dupont [141] and

Nelson [143] inelastic scattering; and Kinney [74] elastic angular distributions) were never published in peer-reviewed papers. Fortunately, thanks to the commendable effort of the Nuclear Reaction Data Centers network, the respective data are available from the EXFOR [14] library. Berthold's and aforementioned, and potentially important, Cierjacks' measurements are listed there as private communications. Thus a solid monolith of experimental data for iron is not as solid as it seems to be.

Below we give a short account of those aspects which we feel fall short of fully accomplishing our goal or where our choices were motivated by the necessities of the current library that might change in future releases.

- In spite of our efforts to modernize the resolved resonance region in ^{56}Fe we were not in a position to utilize the most recent data from RPI and extend the resonance region to higher energies using the LRF=7 option in the ENDF-6 format. Several trials to improve on the resolved resonance region failed to provide improvement in the performance of the file. More work is needed to arrive to a modern evaluation of the resonance region which could replace the current one by Froehner that, apart from a few minor modifications, goes back to 1977. There is a need for reliable measurements of the capture cross sections on the minor isotopes (as well as alloying elements like Cr) in the energy range 1-25 keV. A thorough re-evaluation of the resonance parameters is needed, if significant progress is to be achieved.

- The low energy background (from 10 to 100 keV) in ^{56}Fe capture has been partially motivated by performance of the evaluation on a single integral experiment hmi001 (ZPR-34/9). This experiment is, however, highly sensitive to ^{239}Pu, as well as to ^{52}Cr and ^{58}Ni. Future evaluations of these, and possibly other materials, can modify size of the background in ^{56}Fe capture or make it even redundant.

- The thermal capture cross section for ^{56}Fe needs re-investigation in light of the recent EGAF work of Firestone *et al.* [146].

- We have done our best "bona fide" effort to reconcile experimental data on elastic angular distributions on ^{56}Fe, which resulted in less anisotropic angular distributions. These gave a modest increase/improvement of criticality for the fast Pu assemblies. It turned out later that this refinement might have come at a cost of degraded performance in the deep penetration experiments mentioned above. Indeed, more forward peaked elastic would increase transmission of ^{252}Cf fission neutrons through a thick layer of iron. The new data by Ramirez [136], which came too late to be included in the evaluation, differ from the current recommendations. Ramirez's angular distributions are more forward and more backward peaked thus could have positive impact on both the leakage and the criticality experiments. They are also in very good agreement with our coupled-channel calculations, which we have put apart in favor of the fit to experimental data taken with better energy resolution than the optical model can provide.

  Very recently, we have re-discovered ultra-fine energy resolution measurements of the elastic angular distributions on natural iron by Cierjacks [256]. This outstanding work covering an energy range from 0.489 to 3.06 MeV in nearly 1500 energy points at 10 angles has been misleadingly labeled as "spectrum averaged" in the EXFOR library. In Fig. 19 we compared two examples of the Cierjacks results with our evaluation. This comparison is too limited to allow for meaningful conclusions but the future evaluation should take these data into account.

- Our fast neutron cross sections are generally closer to the experimental data than ENDF/B-VII.1. There is, however, some uncertainty regarding partition of the fusion cross section between elastic and inelastic in the energy range from 4 to 8 MeV. Comparison of the group-averaged evaluated cross sections with the smoothed experimental data indicates that the inelastic could be lowered by 3 to 5% between 4 and 5 MeV. This would increase our elastic cross sections bringing them closer to the JENDL-4.0 and JEFF-3.2 recommendations. Between 4 MeV and 5 MeV our elastic is 120 to 150 mb lower than the average of other evaluations and a decrease of the inelastic would eliminate about half of this difference. In general, our elastic cross sections, although supported by the Kinney measurement, are lower than ENDF/B-VII.1, JENDL-4.0 and JEFF-3.2 up to 9 MeV where they merge with JENDL-4.0.

Development of a nuclear reaction data library is an iterative process combining results of the differential experiments with reaction modeling and benchmarking. Seeking to optimize library performance in the integral experiments we inevitably introduce correlations between materials. Reaction modeling brings physics related correlations among different reactions and to some extent also among materials. These correlations are mathematical representation of the fact that the same result might be obtained in various ways, *i.e.*, adjustment performed by the evaluator, or data user, is only one of many (infinite) possibilities. In the present evaluation work we were guided by sensitivity profiles available through the DICE package of the NEA Data Bank to find the most effective ways of adjusting our data to integral experiments while observing differential constraints. This helps to improve performance of the library but takes no account of the correlations. In addition, our adjustments are limited to the evaluated nuclei ignoring possible impact of deficiencies in other nuclei. There is a potential risk of overcorrection to compensate for the shortcomings in the

nuclei that are not being reevaluated. This, together with possible new experiments and advances in the modeling makes it desirable to reconsider some of the existing, although recent, evaluations when preparing a new library. We strongly believe that iron belongs to this category.

ACKNOWLEDGMENTS

Work at Brookhaven National Laboratory was sponsored by the Office of Nuclear Physics, Office of Science of the U.S. Department of Energy under Contract No. DE-AC02-98CH10886 with Brookhaven Science Associates, LLC. ORNL is managed by UT-Battelle, LLC, for the U.S. Department of Energy under Contract No. DE-AC05-00OR22725. The U.S. Department of Energy Nuclear Criticality Safety Program sponsored the work presented in this paper. Authors are grateful to the referee for a very detailed review and a number of comments and suggestions that not only increased value of the paper but also indicated possible improvements in a future evaluation. In particular, we are thankful for the data presented in Table XII.

[1] M. B. Chadwick, M. Herman, P. Obložinský *et al.*, "ENDF/B-VII.1 nuclear data for science and technology: Cross sections, covariances, fission product yields and decay data," Nucl. Data Sheets **112**, 2887 (2011).

[2] M. Chadwick, E. Dupont, E. Bauge *et al.*, "The CIELO collaboration: Neutron reactions on 1H, 16O, 56Fe, 235,238U and 239Pu," Nucl. Data Sheets **118**, 1 (2014).

[3] M. Chadwick, R. Capote, A. Trkov *et al.*, "The CIELO collaboration summary results: International evaluations of neutron reactions on oxygen, iron, uranium and plutonium," Nucl. Data Sheets **148**, 188–212 (2018).

[4] C. Fu and D. Hetrick, "Update of ENDF/B-V Mod4 iron: Neutron-producing reaction cross sections and energy-angle correlations," Report ENDF 341, Oak Ridge National Laboratory (1986).

[5] M. B. Chadwick, P. G. Young, S. Chiba *et al.*, "Cross-section evaluations to 150 MeV for accelerator-driven systems and implementation in MCNPX," Nucl. Sci. Eng. **131**, 293 (1999).

[6] H. Vonach, S. Tagesen, M. Wagner, and V. Pronyaev, "Evaluation of the fast neutron cross sections of 56Fe including complete covariance information," Physics Data 13-7, Fachinformationszentrum, Karlsruhe (1992).

[7] V. Pronyaev, S. Tagesen, H. Vonach, and S. Badikov, "Evaluation of the fast neutron cross sections of 52Cr and 56Fe including complete covariance information," Physics Data 13-8, Fachinformationszentrum, Karlsruhe (1995).

[8] D. A. Brown, G. P. A. Nobre, and M. Herman, "Brief history of iron isotope evaluations in the ENDF/B library," Report BNL-114315-2017-IR, Brookhaven National Laboratory (2017).

[9] M. Herman, R. Capote, B. V. Carlson, P. Obložinský, M. Sin, A. Trkov, H. Wienke, and V. Zerkin, "EMPIRE: Nuclear reaction model code system for data evaluation," Nucl. Data Sheets **108**, 2655 (2007).

[10] M. B. Chadwick, P. G. Young, R. E. MacFarlane, P. Moller, G. M. Hale, R. C. Little, A. J. Koning, and S. Chiba, "LA150 documentation of cross sections, heating, and damage," Report Los Alamos National Laboratory LA-UR-99-1222 (1999).

[11] D. Brown, M. Chadwick, R. Capote *et al.*, "ENDF/B-VIII.0: The 8^{th} major release of the nuclear reaction data l ibrary with CIELO-project cross sections and new standards and thermal scattering data," Nucl. Data Sheets **148**, 1–141 (2018).

[12] H. I. Liou, R. E. Chrien, R. C. Block, and U. N. Singh, "The transmission of neutrons through iron-56 at 24.37 keV," Nucl. Sci. Eng. **70**, 150 (1979).

[13] R. R. Spencer, J. H. Todd, N. M. Larson, and L. W. Weston, "The ORNL neutron-capture cross section facility," vol. **1**, 99 (1994). Conf. on Nucl. Data for Sci. and Techn., Gatlinburg 1994.

[14] N. Otuka, E. Dupont, V. Semkova *et al.*, "Towards a more complete and accurate experimental nuclear reaction data library (EXFOR): International collaboration between nuclear reaction data centres (NRDC)," Nucl. Data Sheets **120**, 272 (2014).

[15] S. F. Mughabghab, *Atlas of Neutron Resonances, Vol.1 and 2* (Elsevier, Amsterdam 2018).

[16] R. B. Firestone, T. Belgya, M. Krtička, F. Bečvář, L. Szentmiklosi, and I. Tomandl, "Thermal neutron capture cross section for ^{56}Fe(n,γ)," Phys. Rev. C **95**, 014328 (2017).

[17] K. Shibata, O. Iwamoto, T. Nakagawa, N. Iwamoto *et al.*, "JENDL-4.0: A new library for nuclear science and engineering," J. Nucl. Sci. Tech. **48**, 1 (2011).

[18] "The JEFF-3.1 nucelar data library," JEFF Report 21, OECD NEA, Paris 2006.

[19] I. Dillmann, R. Plag, F. Käppeler, and T. Rauscher, "Kadonis v0.3 - the third update of the "Karlsruhe Astrophysical Database of Nucleosynthesis in Stars"," in *EFNUDAT Fast Neutrons - scientific workshop on neutron measurements, theory and applications*, (Geel, Belgium) (2009). http://www.kadonis.org/.

[20] T. Wang, M. Lee, G. Kim, Y. Oh, W. Namkung, T.-I. Ro, Y.-R. Kang, M. Igashira, and T. Katabuchi, "Measurement of keV-neutron capture cross-sections and capture γ-ray spectra of ^{56}Fe and ^{57}Fe," Nucl. Inst. Meth. Phys. Res. B **268**, 440 (2010).

[21] F. Corvi, G. Fioni, A. Mauri, and T. Babeliowsky, "The 30 keV Averaged Neutron Capture Cross Sections of ^{56}Fe and ^{60}Ni," AIP Conf. Proc. **238**, 906 (1991).

[22] F. Corvi, G. Fioni, A. Mauri, and K. Athanassopulos, *Resonance Neutron Capture in Structural Materials*, 44. Springer Verlag, Berlin, Heidelberg (1992).

[23] F. Kaeppeler, K. Wisshak, and L. D. Hong, "Neutron capture resonances in ^{56}fe and ^{58}Fe in the energy range from 10 to 100 keV," Nucl. Sci. Eng. **84**, 234 (1983).

[24] F. Corvi, A. Brusegan, R. Buyl, G. Rohr, R. Shelley, and T. van der Veen, "High resolution neutron capture

cross section measurements of ^{56}Fe," in *Nuclear Data for Science and Technology* (K. H. Böckhoff, ed.), p.131, Central Bureau for Nuclear Measurements, Geel, Belgium, Reidel (1982). Conf. on Nucl. Data for Sci. and Technol., Antwerp 1982.

[25] B. J. Allen and A. R. d. L. Musgrove, "S-wave resonance parameters in the structural materials," in *Neutron Data of Structural Materials for Fast Reactors* (K. Böckhoff, ed.), p. 447 (Pergamon Press, Oxford 1977).

[26] B. J. Allen, A. R. d. L. Musgrove, J. W. Boldeman, M. J. Kenny, and R. L. Macklin, "Resonance neutron capture in ^{56}Fe," Nucl. Phys. A **269**, 408 (1976).

[27] M. S. Pandey, J. A. Harvey, J. B. Garg, and W. M. Good, "Dependence of level spacing of the isotopes of iron upon parity," Progress Report 5025 (1975), Oak Ridge National Laboratory.

[28] E. Cornelis, L. Mewissen, and F. Poortmans, "Neutron resonance structure of ^{54}Fe and ^{56}Fe from high resolution total cross section experiments," p. 135 (1982). Conf. on Nucl. Data for Sci. and Technol., Antwerp 1982.

[29] L. C. Leal, H. Derrien, N. M. Larson, and R. Q. Wright, "R-matrix analysis of 235U neutron transmission and cross-section measurements in the 0- to 2.25-keV energy range," Nucl. Sci. Eng. **131**, 230 (1999).

[30] S. F. Mughabghab, *Atlas of Neutron Resonances, Resonance Parameters and Thermal Cross Sections, Z = 1-100* (Elsevier, Amsterdam 2006).

[31] G. Giubrone, *Neutron capture measurement of 54Fe and 57Fe at CERN n-TOF*, PhD thesis, University of Valencia (2014).

[32] A. Wallner, K. Buczak, T. Belgya *et al.*, "Precise measurement of the thermal and stellar ^{54}Fe(n,γ)^{55}Fe cross sections via accelerator mass spectrometry," Phys. Rev. C (2017), accepted.

[33] L. Coquard, F. Kaeppeler, I. Dillmann, A. Wallner, K. Knie, and W. Kutschera, "Determination of the stellar (n,γ) cross section of Fe-54 with accelerator mass spectrometry," (Geneva, Switzerland), (274) (2006). Proceedings "Nuclei in the Cosmos-IX", CERN, Geneva, 2006.

[34] A. Brusegan, F. Corvi, G. Rohr, R. Shelley, T. van der Veen, C. Van der Vorst, and B. J. Allen, "^{54}Fe neutron capture cross section," in *Nuclear Data for Science and Technology* (K. H. Böckhoff, ed.), p. 127, Central Bureau for Nuclear Measurements, Geel, Belgium, Reidel (1982). Conf. on Nucl. Data for Sci. and Technol., Antwerp 1982.

[35] B. J. Allen, A. R. d. L. Musgrove, J. W. Boldeman, and R. L. Macklin, "Valence neutron capture in ^{54}Fe," Nucl. Phys. A **283**, 37 (1977).

[36] H. Beer, R. R. Spencer, and A. Ernst, "The s-process near the iron seed - some improved capture cross sections," Astron. Astrophys. **37**, 197 (1974).

[37] H. Beer and R. R. Spencer, "keV neutron radiative capture and total cross section of ^{50,52,53}Cr, ^{54,57}Fe, and ^{62,64}Ni," Nucl. Phys. A **240**, 29 (1975).

[38] S. F. Mughabghab, M. Divadeenam, and N. E. Holden, *Neutron Cross Sections, Vol.1, Neutron Resonance Parameters and Thermal Cross Sections, Part A, Z = 1-60.* Academic Press, New York 1981.

[39] G. Rohr and K. N. Muller, "Untersuchungen an Neutronenresonanzen im ^{57}Fe," Zeit. Physik **227**, 1 (1969).

[40] S. Raman, G. G. Slaughter, W. M. Good, J. A. Harvey, J. B. McGrory, and D. Larson, "1$^-$ States in ^{58}Fe," 277 (1974). 2-nd Symp. Neutr. Capt. Gamma-Ray Spectroscopy, Petten 1974.

[41] "KADoNiS – the Karlsruhe Astrophysical Database of Nucleosynthesis in Stars, v.1.0," (2017); Available at http://exp-astro.physik.uni-frankfurt.de/kadonis1.0/.

[42] G. Rohr, A. Brusegan, F. Corvi, R. Shelley, T. van der Veen, and C. Van der Vorst, "Resonance parameters of ^{57}Fe," in *Nuclear Data for Science and Technology* (K. H. Böckhoff, ed.), p.139, Central Bureau for Nuclear Measurements, Geel, Belgium, Reidel (1982). Conf. on Nucl. Data for Sci. and Technol., Antwerp 1982.

[43] B. J. Allen, A. R. d. L. Musgrove, R. Taylor, and R. L. Macklin, "Neutron Capture Cross Section of ^{57}Fe," in *Neutron Data of Structural Materials for Fast Reactors* (K. Böckhoff, ed.), p. 476 (Pergamon Press, Oxford 1977).

[44] D. C. Moxon, "The thermal activation cross section of 58Fe," Report 6261, AEAT (2001).

[45] M. Moxon, "Evaluation of the resonance region for 58Fe," Report INDC(UK)-089, IAEA, Vienna 2004.

[46] S. F. Mughabghab, "Thermal Neutron Capture Cross Sections, Resonance Integrals and g-factors," Report INDC(NDS)-440, IAEA, Vienna 2003.

[47] R. W. Hockenbury, Z. M. Bartolome, J. R. Tatarczuk, W. R. Moyer, and R. C. Block, "Neutron radiative capture in Na, Al, Fe, and Ni from 1 to 200 keV," Phys. Rev. **178**, 1746 (1969).

[48] L. D. Hong, H. Beer, and F. Käppeler, "Capture and Total Cross Section Measurements on ^{58}Fe Below 325 keV," in *Neutron Data of Structural Materials for Fast Reactors* (K. Böckhoff, ed.), p. 624 (Pergamon Press, Oxford 1977).

[49] J. B. Garg, S. Jain, and J. A. Harvey, "Neutron total cross section and resonance parameters of ^{58}Fe," Phys. Rev. C **18**, 1141 (1978).

[50] B. J. Allen and R. L. Macklin, "Resonance neutron capture in ^{58}Fe," J. Phys. G **6**, 381 (1980).

[51] D. B. Gayther, B. Thom, M. C. Moxon, and J. E. Jolly, "Capture Cross-Sections Of Structural Materials Measured With The Harwell Large Liquid Scintillator," Report 11583, A.E.R.E. Harwell (1985). Supercedes data in D.B. Gayther, M.C. Moxon, J.E. Jolly, Report A.E.R.E. Harwell, UK, No.26, p.21 (1979).

[52] D. B. Gayther, B. W. Thomas, and M. C. Moxon, "Capture Cross-Section Measurements on Natural Iron and Nickel," in *Neutron Data of Structural Materials for Fast Reactors* (K. Böckhoff, ed.), p. 547 (Pergamon Press, Oxford 1977).

[53] A. Borella, *Determination of the neutron resonance parameters for ^{206}Pb and of the thermal neutron capture cross section for ^{206}Pb and ^{209}Bi*, PhD thesis, Gent University, Belgium (2005).

[54] M. Heil, F. Käppeler, E. Uberseder, R. Gallino, and M. Pignatari, "Neutron capture cross sections for the weak *s* process in massive stars," Phys. Rev. C **77**, 015808 (2008).

[55] E. M. Zsolnay, R. Capote, H. Nolthenius, and A. Trkov, "Summary description of the new international reactor dosimetry and fusion file (IRDFF release 1.0)," Report INDC(NDS)-0616, IAEA, Vienna 2012.

[56] R. Capote, K. I. Zolotarev, V. G. Pronyaev, and A. Trkov, "Updating and extending the IRDF-2002 dosimetry library," J. ASTM Int. **9**, 1 (2012).

[57] A. Daskalakis, E. Blain, B. McDermott, R. Bahran, Y. Danon, D. Barry, R. Block, M. Rapp, B. Epping, and G. Leinweber, "Quasi-differential elastic and inelastic neutron scattering from iron in the MeV energy range," Annals Nucl. Energy **110**, 603 (2017).

[58] W. P. Abfalterer, R. W. Finlay, and S. M. Grimes, "Level widths and level densities of nuclei in the $32 < A < 60$ mass region inferred from fluctuation analysis of total neutron cross sections," Phys. Rev. C **62**, 064312 (2000).

[59] W. P. Abfalterer, F. B. Bateman, F. S. Dietrich, R. W. Finlay, R. C. Haight, and G. L. Morgan, "Measurement of neutron total cross sections up to 560 MeV," Phys. Rev. C **63**, 044608 (2001).

[60] K. Berthold, C. Nazareth, G. Rohr, and H. Weigman, "Total cross section of natural Fe," Private communication (1994).

[61] K. Berthold, C. Nazareth, G. Rohr, and H. Weigman, "High-resolution Fe transmission data from Geel," Private communication (1995).

[62] J. R. Beyster, M. Walt, and E. W. Salmi, "Interaction of 1.0-, 1.77-, 2.5-, 3.25-, and 7.0-MeV neutrons with nuclei," Phys. Rev. **104**, 1319 (1956).

[63] D. G. Foster, and D. W. Glasgow, "Neutron total cross sections, 2.5 - 15 MeV, experimental," Phys. Rev. C **3**, 576 (1971).

[64] J. B. Garg, J. Rainwater, and W. W. a. Havens, "Neutron resonance spectroscopy: Ti, Fe, and Ni," Phys. Rev. C **3**, 2447 (1971).

[65] J. A. Harvey and D. C. Larson, Private communication (1974).

[66] J. A. Harvey, Private communication (1975).

[67] J. A. Harvey, H. A. Mook, N. W. Hill, and O. Shahal, "Solid state effects on thermal neutron cross sections and on low energy resonances," p. 961 (1982). Conf. on Nucl. Data for Sci. and Technol., Antwerp 1982.

[68] J. A. Harvey, F. G. Perey, and J. A. Hill, "The 56Fe 1.15 keV resonance parameters from transmission measurements at ORELA," Report 33 (1984). US DOE Nuclear Data Committee Reports.

[69] N. Nereson and S. Darden, "Average neutron total cross sections in the 3- to 12-MeV region," Phys. Rev. **89**, 775 (1953).

[70] C. M. Perey, F. G. Perey, J. A. Harvey, N. W. Hill, and N. M. Larson, "^{56}Fe and ^{60}Ni resonance parameters," p. 41 (1991). Conf. on Nucl. Data for Sci. and Technol., Juelich 1991.

[71] R. B. Schwartz, R. A. Schrack, and H. T. Heaton, "MeV total neutron cross sections," Report 138 (1974). National Bureau of Standards Monograph.

[72] A. B. Smith, D. Lister, and J. F. Whalen, "Microscopic neutron scattering cross-sections for reactor design," vol. **1**, 399 (1966). Conf. Nuclear Data For Reactors, Paris 1966.

[73] W. E. Kinney and F. G. Perey, "Neutron elastic- and inelastic-scattering cross sections for 56Fe in the energy range 4.19 to 8.56 MeV," Report 4515 (1970), Oak Ridge National Laboratory.

[74] W. E. Kinney and J. W. Mcconnell, "High resolution neutron scattering experiments at ORELA," p. 1319 (1976). Int. Conf. on Interact. of Neutr. with Nuclei, Lowell 1976.

[75] D. Schmidt, W. Mannhart, H. Klein, and R. Nolte, "Elastic and inelastic neutron scattering on elemental iron," Report 20 (1994). Phys. Techn. Bundesanst., Neutronenphysik Reports.

[76] Zo-In-Ok, V. G. Nikolenko, A. B. Popov, and G. S. Samosvat, "The neutron integral and differential cross-sections in the energy region below 440 keV," Report 85 (1985), Joint Inst. for Nucl. Res., Dubna, USSR.

[77] R. A. Zuhr and K. Min, "Differential elastic scattering cross sections of Fe and Ni from 10 to 700 keV," Nucl. Phys. A **237**, 29 (1975).

[78] R. W. Benjamin, P. S. Buchanan, and I. L. Morgan, "Gamma rays produced in the ^{56}Fe(n,n'γ)^{56}Fe reaction," Nucl. Phys. **79**, 241 (1966).

[79] V. M. Besotosnyj, V. M. Gorbachev, L. M. Suvorov, and M. S. Shvecov, "Cross section of gamma-rays production at inelastic interaction of 14 MeV neutrons with different nuclei," Report 19 (1975). Yadernye Konstanty.

[80] W. E. Kinney and F. G. Perey, "High-resolution fast-neutron gamma-ray production cross sections for iron up to 2100 keV," Nucl. Sci. Eng. **63**, 418 (1977).

[81] A. Smith and P. Guenther, "Scattering of MeV neutrons from elemental iron," Nucl. Sci. Eng. **73**, 186 (1980).

[82] D. L. Smith, "Fast neutron gamma-ray production from elemental iron energies less than/equal to 2 MeV," Report 20 (1976), Argonne National Laboratory.

[83] A. Borella, A. Brusegan, M. C. Moxon, G. Aerts, F. Gunsing, P. Siegler, and P. Schillebeeckx, "High-resolution neutron total and capture cross-section measurements on ^{206}Pb," p. 1539 (2004). Conf. on Nucl. Data for Sci.and Techn., Santa Fe 2004.

[84] A. Borella, F. Gunsing, S. Kopecky, I. Ivanov, C. Mihailescu, M. Moxon, A. J. M. Plompen, C. Sage, P. Schillebeeckx, P. Siegler, and I. Sirakov, "Advances in neutron-induced resonance reaction cross section studies at GELINA," vol. **1**, 547 (2007). Conf. on Nucl. Data for Sci. and Technology, Nice 2007.

[85] C. Le Rigoleur, A. Arnaud, and J. Taste, "Mesures en valeur absolue des sections efficaces de capture radiativedes neutrons par le ^{23}Na, Cr, ^{55}Mn, Fe, Ni, ^{103}Rh, Ta, ^{197}Au, ^{238}U dans le domaine de 10 A 600 keV," Report 4788 (1976). Centre d'Etudes Nucleaires, Saclay.

[86] M. C. Moxon, Private communication (1964).

[87] E. Barnard, J. A. M. De Villiers, C. A. Engelbrecht, D. Reitmann, and A. B. Smith, "High resolution fast neutron cross-sections of iron," Nucl. Phys. A **118**, 321 (1968).

[88] A. Begum and R. B. Galloway, "Polarisation in 2.9 MeV neutron elastic scattering by W, Tl, Bi and U," Jour. Phys. G **7**, 535 (1981).

[89] D. M. Chittenden II, D. G. Gardner, and R. W. Fink, "New isotope of manganese; cross sections of the iron isotopes from 14.8-MeV neutrons," Phys. Rev. **122**, 860 (1961).

[90] J. C. Ferrer, J. D. Carlson, and J. Rapaport, "Neutron elastic scattering at 11 MeV and the isospin dependence of the neutron-nucleus optical potential," Nucl. Phys. A **275**, 325 (1977).

[91] L. F. Hansen, F. S. Dietrich, B. A. Pohl, C. H. Poppe, and C. Wong, "Test of microscopic optical model potentials for neutron elastic scattering at 14.6 MeV over a wide mass range," Phys. Rev. C **31**, 111 (1985).

[92] S. F. Hicks, J. R. Vanhoy, A. J. French *et al.*, "Studies of 54,56Fe neutron scattering cross sections," EPJ Web Conf. **93**, 02002 (2015).

[93] E. L. Hjort, F. P. Brady, J. L. Romero, J. R. Drummond,

D. S. Sorenson, J. H. Osborne, B. McEachern, and L. F. Hansen, "Measurements and analysis of neutron elastic scattering at 65 MeV," PHYS. REV. C **50**, 275 (1994).

[94] M. Ibaraki, H. Nakashima, S. I. Meigo, M. Baba, Y. Nauchi, T. Miura, Y. Hirasawa, S. Tanaka, and N. Hirakawa, "Measurements of elastic scattering cross sections of carbon, iron and lead for 75 MeV neutrons," Conference Report 182/U (1998). Japanese report to the INDC, IAEA, Vienna.

[95] M. Ibaraki, H. Nakashima, S. I. Meigo, M. Baba, T. Miura, Y. Hirasawa, T. Hiroishi, T. Aoki, and S. Tanaka, "Measurements of elastic scattering and total non-elastic cross sections for 40-80 MeV neutrons at TIARA," Conference Report 185/U (1999). Japanese report to the INDC, IAEA, Vienna.

[96] M. Ibaraki, M. Baba, T. Miura, Y. Hirasawa, Y. Nauchi, H. Nakashima, S. I. Meigo, O. Iwamoto, and S. Tanaka, "Experimental method for neutron elastic scattering cross-section measurement in 40-90 MeV region at TIARA," NUCL. INST. METH. PHYS. RES. A **446**, 536 (2000).

[97] A. Jacquot and C. Rousseau, "Fast neutron scattering cross sections of iron," NUCL. PHYS. **84**, 239 (1966).

[98] A. Langsdorf, , R. O. Lane, and J. E. Monahan, "Angular distributions of scattered neutrons," PHYS. REV. **107**, 1077 (1957).

[99] N. Olsson, B. Trostell, E. Ramstrom, B. Holmqvist, and F. S. Dietrich, "Microscopic and conventional optical model analysis of neutron elastic scattering at 21.6 MeV over a wide mass range," NUCL. PHYS. A **472**, 237 (1987).

[100] X. Ruan, H. Huang, J. Jiang *et al.*, "Measurement of secondary neutron emission double differential cross section for natural iron induced by 8.17 MeV neutron," AT. ENERGY SCI. TECHNOL. **43**, 793 (2009).

[101] A. B. Smith, "Neutron scattering and models: Iron," NUCL. PHYS. A **605**, 269 (1996).

[102] A. Takahashi, M. Gotoh, Y. Sasaki, and H. Sugimoto, "Double and single differential neutron emission cross sections at 14.1 MeV for natFe, 16O and and natNi," Report 92 (1992). Osaka Univ., OKTAVIAN Reports.

[103] V. M. Bondar, I. N. Kadenko, B. E. Leshchenko, Y. N. Onishchuk, V. A. Plujko, and A. N. Gorbachenko, "Cross section of prompt gamma-ray production by fast neutrons on iron and bismuth nuclei," BULL. RUSS. ACAD. SCI. - PHYS. **73**, 1511 (2009).

[104] D. Hermsdorf, S. Sassonoff, D. Seeliger, and K. Seidel, "Absolute differentielle Neutronenemissionsquerschnitte fur Ti, V und Cr bei 14 MeV Einschussenergie," KERNENERGIE **17**, 176 (1974).

[105] D. Hermsdorf, S. Sassonoff, D. Seeliger, and K. Seidel, "Absolute differentielle Neutronenemissionsquerschnitte fur Mn, Fe, Co, Ni, Cu und Zn bei 14 MeV Einschussenergie," KERNENERGIE **17**, 259 (1974).

[106] D. Hermsdorf, A. Meister, S. Sassonoff, D. Seeliger, and K. Seidel, "Absolute differentielle Neutronenemissionsquerschnitte fur Na, Mg, Al, Si, P und S bei 14 MeV Einschussenergie," KERNENERGIE **18**, 83 (1975).

[107] D. Hermsdorf, A. Meister, S. Sassonoff, D. Seeliger, and K. Seidel, "Absolute differentielle Neutronenemissionsquerschnitte fur Ga, Se, Br, Zr, Nb, Cd, In, Sn, Sh, J, Ta, W, Au, Hg, Pb und Bi bei 14 MeV Einschussenergie," KERNENERGIE **19**, 241 (1976).

[108] Kokooo, I. Murata, and A. Takahashi, "Measurements of double-differential cross sections of charged particles emission reactions for several structural elements of fusion power reactors by 14.1 MeV incident neutrons," NUCL. SCI. ENG. **132**, 16 (1999).

[109] S. Matsuyama, T. Ito, M. Baba, N. Ito, H. Iide, T. Okubo, and N. Hirakawa, "Measurement of double-differential (DDX) and energy differential neutron emission cross sections for Fe-nat at En=14.1 MeV neutron energy," Report 92 (1992). JAERI-M Reports.

[110] E. Raeymackers, I. Slypen, S. Benck, J. P. Meulders, N. Nica, and V. Corcalciuc, "Experimental cross-sections for light charged particle emission induced by neutrons with energies between 25 and 65 MeV incident on ^{nat}Fe, ^{59}Co, ^{209}Bi, and ^{nat}U," AT. DATA NUCL. DATA TABLES **87**, 231 (2004).

[111] D. Soda, S. Matsuyama, M. Ibaraki, M. Baba, S. Iwasaki, and N. Hirakawa, "Measurements of double-differential neutron emission cross sections for 18 and 11.5 MeV neutrons," Conference Report 96 (1995). JAERI Conference proceedings.

[112] G. Stengl, M. Uhl, and H. Vonach, "Gamma competition in the decay of unbound states in ^{56}Fe produced by the ^{56}Fe(n,n') reaction with 14 MeV neutrons," NUCL. PHYS. A **290**, 109 (1977).

[113] A. Takahashi, I. Murata, Kokooo, S. Ogino, Y. Murakami, H. Nishizawa, and T. Kondo, "A time-of-flight spectrometer with pulse-shape discrimination for the measurement of double-differential charged-particle emission cross sections," NUCL. INST. METH. PHYS. RES. A **401**, 93 (1997).

[114] T. Vilaithong, D. Boonyawan, S. Konklong, W. Pairsuwan, and S. Singkarat, "Measurement of double differential neutron emission cross sections of Fe induced by 14.1 MeV neutrons," NUCL. INST. METH. PHYS. RES. A **332**, 561 (1993).

[115] B. Ye, Y. Fan, Z. Wang, R. Han, and Z. Xiao, "Proton emission in reaction of 14.6-MeV neutrons with natural iron," NUCL. SCI. ENG. **122**, 136 (1996).

[116] H. Arakawa, T. Kajimoto, S. Noda, T. Watanabe, N. Shigyo, K. Ishibashi, S. Kunieda, and R. C. Haight, "Neutron-production double-differential cross sections for 150 MeV neutron-incidence on Fe," Conference Report 2008 (2008). JAEA Conference proceedings.

[117] N. S. Biryukov, B. V. Zhuravlev, N. V. Kornilov, A. P. Rudenko, O. A. Salnikov, and V. I. Trykova, "Neutron spectra and angular distributions from the reactions ^{181}Ta(p,n)^{181}W and ^{181}Ta(n,n')^{181}Ta," YADERNAYA FIZIKA **26**, 1146 (1977).

[118] V. Blideanu, F. R. Lecolley, J. F. Lecolley *et al.*, "Nucleon-induced reactions at intermediate energies: New data at 96 MeV and theoretical status," PHYS. REV. C **70**, 014607 (2004).

[119] Q. Bujia, T. Hongqing, Z. Zuying, Z. Chenwei, K. Zunjian, S. Zhengqiang, S. Guanren, and X. Haihong, "Neutron double differential cross sections of 238U, 209Bi and Fe at 10 MeV," AT. ENERGY SCI. TECHNOL. **33**, 497 (1999).

[120] J. K. Dickens, G. L. Morgan, G. T. Chapman, T. A. Love, E. Newman, and F. G. Perey, "Cross sections for gamma-ray production by fast neutrons for 22 elements between Z = 3 and Z = 82," NUCL. SCI. ENG. **62**, 515 (1977).

[121] D. M. Drake, J. C. Hopkins, C. S. Young, and H. Conde, "Gamma-ray production cross sections for fast neutron

interactions with several elements," Nucl. Sci. Eng. **40**, 294 (1970).
[122] M. Drosg, R. C. Haight, and D. M. Drake, "Double-differential gamma-ray production: cross sections and spectra of Al, Si and Fe for 8.51, 10.00, 12.24 and 14.24 MeV neutrons," Report 02 (2002), Los Alamos Scientific Laboratory.
[123] S. Hlavac, P. Obložinský, and R. Antalik, "γ-decay of states in ^{55,56}Fe excited in the reaction (n,xnγ) on ^{56}Fe at E(n)=14.6 MeV," Izv. Rossiiskoi Akademii Nauk, Ser.Fiz. **46**, 903 (1982).
[124] E. L. Hjort, F. P. Brady, J. R. Drummond, B. McEachern, J. H. Osborne, J. L. Romero, D. S. Sorenson, and H. H. K. Tang, "Measurements of 65 MeV Fe,Sn, and Pb(n,n'x) continuum cross sections," Phys. Rev. C **53**, 237 (1996).
[125] J. L. Kammerdiener, "Neutron spectra emitted by ^{239}Pu, ^{238}U, ^{235}U, Pb, Nb, Ni, Al, and C irradiated by 14 MeV neutrons," Report 51232 (1972). Lawrence Rad. Laboratory (Berkeley and Livermore).
[126] S. Kunieda, T. Watanabe, N. Shigyo, K. Ishibashi, D. Satoh, Y. Iwamoto, T. Nakamura, and R. C. Haight, "Measurement of neutron-production double-differential cross sections for continuous-energy-neutron-incidence on Fe and Pb by liquid organic scintillator," vol. **1**, 1058 (2004). Conf. on Nucl. Data for Sci. and Techn., Santa Fe 2004.
[127] N. Shigyo, S. Kunieda, T. Watanabe, S. Noda, K. Ishibashi, Y. Iwamoto, D. Satoh, T. Nakamura, and R. C. Haight, "Measurement of continuous-energy neutron-incident neutron-production cross section," vol. **1**, 924 (2004). Conf. on Nucl. Data for Sci. and Techn., Santa Fe 2004.
[128] A. Takahashi, J. Yamamoto, K. Oshima, M. Ueda, M. Fukazawa, Y. Yanagi, J. Miyaguchi, and K. Sumita, "Measurements of double differential neutron emission cross sections for fusion reactor candidate elements," Jour. Nucl. Sci. Techn. **21**, 577 (1984).
[129] J. A. Harvey, Private communication (1987).
[130] C. M. Perey, F. G. Perey, J. A. Harvey, N. W. Hill, and N. M. Larson, "^{56}Fe and ^{60}Ni resonance parameters," 41 (1991). Conf. on Nucl. Data for Sci. and Technol., Juelich 1991.
[131] A. I. Tutubalin, A. P. Klyucharev, V. P. Bozhko, V. Y. Golobnya, G. P. Dolya, G. A. Zachepilo, and A. S. Kachan, "Total neutron cross section for the isotopes 54-Fe and 56-Fe," Report 11 (1973). Yadernye Konstanty.
[132] V. N. Vinogradov, E. V. Gai, A. N. Glukhovets, N. S. Rabotnov, A. I. Stupak, M. Z. Tarasko, and O. A. Shcherbakov, "Measurement of total neutron cross sections of the isotopes ^{54}Fe and ^{56}Fe by the time-of-flight method in the energy range 1-70 keV and ^{56}Fe by the time-of-flight method in the energy range 1-70 keV," Yadernaya Fizika **26**, 936 (1977).
[133] P. Boschung, J. T. Lindow, and E. F. Shrader, "Scattering of fast neutrons by ^{12}C, ^{54}Fe, ^{56}Fe, ^{58}Ni, and ^{60}Ni," Nucl. Phys. A **161**, 593 (1971).
[134] S. M. El-Kadi, C. E. Nelson, F. O. Purser, R. L. Walter, A. Beyerle, C. R. Gould, and L. W. Seagondollar, "Elastic and inelastic scattering of neutrons from ^{54,56}Fe and ^{63,65}Cu. (i). measurements from 8 to 14 MeV and a spherical optical model analysis," Nucl. Phys. A **390**, 509 (1982).
[135] W. E. Kinney, *Neutron Elastic and Inelastic Scattering from ^{56}Fe from 4.60 to 7.55 MeV*, PhD thesis (1968).
[136] A. P. D. Ramirez, M. T. McEllistrem, S. Mukhopadhyay *et al.*, "Neutron cross section measurements for ^{56}Fe," Phys. Rev. C **95**, 064605 (2017).
[137] L. A. Rayburn and E. O. Wollen, "Total neutron cross sections at 1.44 eV," Nucl. Phys. **61**, 381 (1965).
[138] W. L. Rodgers, E. F. Shrader, and J. T. Lindow, "Neutron scattering from C12, Fe54, Fe56, Cu65, Ni58, and Ni60," Progress Report 1573 (1967). Chicago Operations Office, Atomic Energy Commission.
[139] T. Schweitzer, D. Seeliger, and K. Seidel, "Differentielle elastische und unelastische Streuquerschnitte für Magnesium, Silizium, Eisen und Wismut bei einer Neutroneneinschussenergie von 3,4 MeV," Kernenergie **20**, 174 (1977).
[140] R. Beyer, R. Schwengner, R. Hannaske, A. R. Junghans, R. Massarczyk, M. Anders, D. Bemmerer, A. Ferrari, A. Hartmann, T. Kogler, M. Roder, K. Schmidt, and A. Wagner, "Inelastic scattering of fast neutrons from excited states in ^{56}Fe," Nucl. Phys. A **927**, 41 (2014).
[141] E. Dupont, P. Ribon, H. Weigmann, and G. Vanpraet, "High resolution measurement of the neutron inelastic scattering cross section of ^{56}Fe," p. 529 (1997). Conf. on Nucl. Data for Sci. and Techn., Trieste 1997.
[142] I. A. Korzh, V. A. Mishchenko, N. M. Pravdivy, N. T. Sklyar, D. A. Bazavov, and V. P. Lunyov, "Inelastic scattering of neutrons by nuclei Mo-94,Mo-96, Mo-98 near the first 2+level excitation threshold," Ukrainskii Fizichnii Zhurnal **39**, 785 (1994).
[143] R. O. Nelson, N. Fotiades, M. Devlin, J. A. Becker, P. E. Garrett, and W. Younes, "Cross-section standards for neutron-induced gamma-ray production in the MeV energy range," vol. **1**, 838 (2004). Conf. on Nucl. Data for Sci. and Techn., Santa Fe 2004.
[144] A. Negret, C. Borcea, P. Dessagne, M. Kerveno, A. Olacel, A. J. M. Plompen, and M. Stanoiu, "Cross-section measurements for the ^{56}Fe(n,xnγ) reactions," Phys. Rev. C **90**, 034602 (2014).
[145] F. G. Perey, W. E. Kinney, and R. L. Macklin, "High resolution inelastic cross section measurements for Na, Si, and Fe," **1**, 191 (1971). 3-rd Conf. Neutron Cross-Sections and Tech., Knoxville 1971.
[146] R. B. Firestone, T. Belgya, M. Krticka, F. Becvar, L. Szentmiklosi, and I. Tomandl, "Thermal neutron capture cross section for ^{56}Fe (n,γ)," Phys. Rev. C **95**, 014328 (2017).
[147] R. L. Macklin, P. J. Pasma, and J. H. Gibbons, "Resonance neutron capture and transmission in sulfur, iron, and lead," Phys. Rev. **136**, B695 (1964).
[148] D. L. Bowers and L. R. Greenwood, "Analysis of long-lived isotopes by liquid scintillation spectrometry," J. Radioanal. Nucl. Chem. **123**, 461 (1988).
[149] V. Corcalciuc, B. Holmqvist, A. Marcinkowski, and G. A. Prokopets, "A study of the neutron induced reactions for ^{19}F, ^{56}Fe and ^{50}Co in the energy interval 16 to 22 MeV," Nucl. Phys. A **307**, 445 (1978).
[150] J. Frehaut and G. Mosinski, "Measurement of the (n,2n) cross-sections for ^{56}Fe, ^{59}Co, ^{89}Y, ^{169}Tm, ^{175}Lu, ^{181}Ta, ^{197}Au, ^{209}Bi, ^{238}U and of the (n,3n) cross-section for ^{238}U from threshold to 15 MeV incident neutron energy," Report 4627 (1974). Centre d'Etudes Nucleaires, Saclay.
[151] N. I. Molla and S. M. Qaim, "A systematic study of

(n,p) reactions at 14.7 MeV," Nucl. Phys. A **283**, 269 (1977).
[152] A. Wallner, K. Buczak, C. Lederer *et al.*, "Production of long-lived radionuclides 10Be, 14C, 53Mn, 55Fe, 59Ni and 202gPb in a fusion environment.," J. Korean Phys. Soc. **59**, 1378 (2011).
[153] R. Wenusch and H. Vonach, "(n,2n) cross-section measurements on Mn-55, Co-59, Cr-52, Fe-56 and Zn-68 for 14 MeV neutrons (in German)," Oesterr. Akad. Wiss., Math-Naturw. Kl., Anzeiger **99**, 1 (1962).
[154] S. K. Saraf, C. E. Brient, P. M. Egun, S. M. Grimes, V. Mishra, and R. S. Pedroni, "Cross sections and spectra for the ^{54}Fe and ^{56}Fe(n,xp) and (n,xa) reactions between 8 and 15 MeV," Nucl. Sci. Eng. **107**, 365 (1991).
[155] Z. Wang, X. Fan, L. Zhang, H. Bai, J. Chen, G. Zhang, Y. M. Gledenov, M. V. Sedysheva, L. Krupa, and G. Khuukhenkhuu, "Cross sections of the ^{56}Fe (n,a)^{53}Cr and ^{54}Fe (n,a)^{51}Cr reactions in the MeV region," Phys. Rev. C **92**, 044601 (2015).
[156] S. M. Grimes, R. C. Haight, K. R. Alvar, H. H. Barschall, and R. R. Borchers, "Charged-particle emission in reactions of 15-MeV neutrons with isotopes of chromium, iron, nickel, and copper," Phys. Rev. C **19**, 2127 (1979).
[157] S. M. Qaim and G. Stocklin, "Investigation of (n,t) reactions at 14.6 MeV and an analysis of some systematic trends in the cross-section data," Nucl. Phys. A **257**, 233 (1976).
[158] S. M. Qaim and G. L. Stocklin, "A systematic investigation of (n,t) reactions at 14-15 MeV on medium and heavy mass nuclei," J. Inorg. Nucl. Chem. **35**, 19 (1973).
[159] J. Cabe, M. Laurat, P. Yvon, and G. Bardolle, "Recherche d'une structure intermediaire dans les sections efficaces totales neutroniques," Nucl. Phys. A **102**, 92 (1967).
[160] J. Cabe, M. Laurat, and P. Yvon, "Section efficace neutronique du chrome de 500 keV a 1200 keV," Comptes Rendus **258**, 1478 (1964).
[161] S. Mellema, R. W. Finlay, F. S. Dietrich, and F. Petrovich, "Microscopic and conventional optical model analysis of fast neutron scattering from ^{54,56}Fe," Phys. Rev. C **28**, 2267 (1983).
[162] A. Ohrn, J. Blomgren, P. Andersson *et al.*, "Elastic scattering of 96 MeV neutrons from iron, yttrium, and lead," Phys. Rev. C **77**, 024605 (2008).
[163] A. I. Tutubalin, A. P. Klyucharev, V. P. Bozhko, V. Y. Golovnya, G. P. Dolya, A. S. Kachan, and N. A. Shlyakhov, "Elastic scattering of 14.7 MeV neutrons on iron, cobalt and nickel isotopes," **vol.3**, 62 (1973). 2-nd Conf. on Neutron Physics, Kiev 1973.
[164] R. Fischer, G. Traxler, M. Uhl, and H. Vonach, "^{56}Fe(n,a)^{53}Cr and ^{60}Ni(n,a)^{57}Fe Reactions at E(n) = 14.1 MeV," Phys. Rev. C **30**, 72 (1984).
[165] R. Fischer, G. Traxler, M. Uhl, H. Vonach, and P. Maier-Komor, "^{55}Mn(n,a)^{53}Cr and ^{59}Co(n,a) reactions at E(n)=14.1 MeV," Phys. Rev. C **34**, 460 (1986).
[166] S. M. Grimes, R. C. Haight, K. R. Alvar, H. H. Barschall, and R. R. Borchers, "Charged-particle emission in reactions of 15-MeV neutrons with isotopes of chromium, iron, nickel, and copper," Phys. Rev. C **19**, 2127 (1979).
[167] Y. E. Kozyr and G. A. Prokopets, "Radiative transitions from unbound states of Fe and Co nuclei," Yadernaya Fizika **27**, 616 (1978).
[168] A. A. Lychagin, S. P. Simakov, B. V. Devkin *ez al.*, "Study of reaction ^{56}Fe(n,n'γ) with 14.1-MeV neutrons," Yadernaya Fizika **45**, 1226 (1987).
[169] A. Marcinkowski, R. W. Finlay, G. Randers-Pehrson, C. E. Brient, R. Kurup, S. Mellema, A. Meigooni, and R. Tailor, "Neutron emission cross sections at 25.7 MeV: ^{51}V,^{56}Fe,^{65}Cu,^{93}Nb, and ^{209}Bi," Nucl. Sci. Eng. **83**, 13 (1983).
[170] A. Marcinkowski, R. W. Finlay, G. Randers-Pehrson, C. E. Brient, J. E. O'Donnell, and K. Stankiewicz, "Neutron emission spectra and angular distributions at 25.7 MeV neutron bombarding energies," Nucl. Phys. A **402**, 220 (1983).
[171] I. C. Sagrado Garcia, J. F. Lecolley, F. R. Lecolley *et al.*, "Neutron production in neutron-induced reactions at 96 MeV on ^{56}Fe and ^{208}Pb," Phys. Rev. C **84**, 044619 (2011).
[172] I. C. Sagrado Garcia, G. Ban, V. Blideanu *et al.*, "(n,xn) measurements at 96 MeV," vol. **2**, 1035 (2007). Conf. on Nucl. Data for Sci. and Technology, Nice 2007.
[173] S. M. Sterbenz, F. B. Bateman, T. M. Lee *et al.*, "The ^{56}Fe (n,xa) reaction from threshold to 30 MeV," vol. **1**, 314 (1994). Conf. on Nucl. Data for Sci. and Techn., Gatlinburg 1994.
[174] A. P. Degtyarev, B. E. Leshchenko, V. A. Plyuyko, and G. A. Prokopets, "Angular distribution of neutron groups from (n,xn) reactions on ^{56}Fe,^{59}Co,^{93}Nb,^{115}In,^{209}Bi and ^{238}U at incident energy e_0=14.6 MeV," Yadernaya Fizika **34**, 299 (1981).
[175] T. Ronnqvist, H. Conde, N. Olsson *et al.*, "The ^{54,56}Fe(n,p)^{54,56}Mn reactions at E(n) = 97 MeV," Nucl. Phys. A **563**, 225 (1993).
[176] U. Abbondanno, R. Giacomich, M. Lagonegro, and G. Pauli, "Gamma rays resulting from nonelastic processes of 14.2 MeV neutrons with sodium, magnesium, silicon, sulphur, titanium, chromium and iron," J. Nucl. Energy **27**, 227 (1973).
[177] L. Cranberg and J. S. Levin, "Neutron scattering at 2.45 MeV by a time-of-flight method," Phys. Rev. **103**, 343 (1956).
[178] M. Hyakutake, M. Matoba, T. Tonai, J. Niidome, and S. Nakamura, "Scattering of 14.1 MeV neutrons from Fe," J. Phys. Soc. Jpn. **38**, 606 (1975).
[179] B. Jonsson, K. Nyberg, and I. Bergqvist, "High resolution measurements of gamma rays produced by 15 MeV neutrons," Arkiv foer Fysik **39**, 295 (1969).
[180] S. Mellema, R. W. Finlay, and F. S. Dietrich, "Neutron inelastic scattering from ^{54,56}Fe," Phys. Rev. C **33**, 481 (1986).
[181] A. Mittler, J. Nardini, and G. P. Couchell, *Measurements of neutron inelastic scattering cross sections for natural iron* , PhD thesis (1975).
[182] N. Olsson, E. Ramstrom, and B. Trostell, "Neutron elastic and inelastic scattering from Mg, Si, S, Ca, Cr, Fe and Ni at E(n) = 21.6 MeV," Nucl. Phys. A **513**, 205 (1990).
[183] H. Sakane, Y. Kasugai, F. Maekawa, Y. Ikeda, and K. Kawade, "Measurement of discrete gamma-ray production cross sections for interactions of 14 MeV neutron with Mg, Al, Si, Ti, Fe, Ni, Cu, Nb, Mo and Ta," Conference Report 182 (1999). Japanese report to the INDC, IAEA, Vienna.
[184] M. Salama, "Inelastic scattering of fast neutrons from

iron," ATOMKERNENERGIE **37**, 221 (1981).
[185] K. Tsukada, S. Tanaka, Y. Tomita, and M. Maruyama, "Elastic and inelastic scattering of fast neutrons from iron, nickel and tungsten," NUCL. PHYS. A **125**, 641 (1969).
[186] S. Xiamin, S. Ronglin, X. Jinjiang, W. Yongshun, and D. Dazhao, "Measurements of the induced gamma ray cross sections by 14.2 MeV neutrons with Fe,Ni,Cu," CHIN. J. NUCL. PHYS. **4**, 120 (1982).
[187] T. Yamamoto, Y. Hino, S. Itagaki, and K. Sugiyama, "Gamma-ray production cross sections for interactions of 14.8 MeV neutrons with O, Na, Al, Cl, Cr, Fe, Ni, Cu and Pb," JOUR. NUCL. SCI. TECHNOL. **15**, 797 (1978).
[188] W. Yongshun, S. Ronglin, S. Xiamin, X. Jinqiang, and D. Dazhao, "Production cross sections of discrete gamma-rays resulting from interaction of 14.2 MeV neutrons with Pb and Bi," CHIN. J. NUCL. PHYS. **4**, 299 (1982).
[189] S. Zong-Ren, S. Xia-Min, Z. Xian-Tang, L. Zhi-Rong, X. Jin-Qiang, S. Rong-Lin, and D. Da-Zhao, "Gamma-ray production cross sections from interactions of 14.9 MeV neutrons with C, F, Al, Si, Fe and Cu," CHIN. J. NUCL. PHYS. **1**, 45 (1979).
[190] E. G. Bilpuch, L. W. Weston, C. D. Bowman, A. K. Furr, P. F. Nichols, and H. W. Newson, "Narrow neutron resonances in the keV region," BULL. AM. PHYS. SOC. **3**, 164(B3) (1958).
[191] C. D. Bowman, E. G. Bilpuch, and H. W. Newson, "s- and p-wave neutron spectroscopy. Part VIII. Subshell effect on nuclear level spacing near A = 50," ANNALS PHYS. (NEW YORK) **17**, 319 (1962).
[192] R. F. Carlton, J. A. Harvey, and B. Castel, "Single particle strength in ^{55}Fe," BULL. AM. PHYS. SOC. **30**, 1252 (1985).
[193] P. T. Guenther, D. L. Smith, A. B. Smith, and J. F. Whalen, "Total, scattering and γ-ray-production cross sections for few-MeV neutrons on ^{54}Fe," ANNALS NUCL. ENERGY **13**, 601 (1986).
[194] V. N. Vinogradov, E. V. Gai, A. N. Glukhovets, N. S. Rabotnov, A. I. Stupak, M. Z. Tarasko, and O. A. Shcherbakov, "Measurement of total neutron cross sections of the isotopes ^{54}Fe and ^{56}Fe by the time-of-flight method in the energy range 1-70 keV," YADERNAYA FIZIKA **26**, 936 (1977).
[195] I. A. Korzh, V. A. Mishchenko, and N. M. Pravdivyi, "Fast neutron elastic and inelastic scattering cross sections of ^{54}Fe," ATOMNAYA ENERGIYA **62**, 417 (1987).
[196] C. Shull and E. Wollan, "Coherent scattering amplitudes as determined by neutron diffraction," PHYS. REV. **81**, 527 (1951).
[197] Z. Y. Bao and F. Kaeppeler, "Neutron capture cross sections for s-process studies," AT. DATA NUCL. DATA TABLES **36**, 411 (1987).
[198] Z. Y. Bao, H. Beer, F. Käppeler, F. Voss, K. Wisshak, and T. T. Rauscher, "Neutron cross sections for nucleosynthesis studies," AT. DATA NUCL. DATA TABLES **76**, 70 (2000).
[199] H. Beer, F. Voss, and R. R. Winters, "On the calculation of Maxwellian-averaged capture cross sections," ASTROPHYS. JOURNAL, SUPPL. **80**, 403 (1992).
[200] M. Bormann, H. K. Feddersen, H. H. Holscher, W. Scobel, and H. Wagner, "(n,2n) Anregungsfunktionen fur ^{54}Fe, ^{70}Ge, ^{74}Se, ^{85}Rb, ^{86,88}Sr, ^{89}Y, ^{92}Mo, ^{204}Hg im Neutronenenergiebereich 13-18 MeV," ZEIT. PHYSIK A **277**, 203 (1976).
[201] C. Carles, "Measurement of (n,2n) reaction cross sections produced by 14 MeV neutrons," COMPTES RENDUS **257**, 659 (1963).
[202] A. Ercan, M. N. Erduran, M. Subasi, E. Gueltekin, G. Tarcan, A. Baykal, and M. Bostan, "14.6 MeV neutron induced reaction cross section measurements," p. 376 (1991). Conf. on Nucl. Data for Sci. and Technol., Juelich 1991.
[203] A. Fessler, "Activation cross sections and isomeric cross section ratios in neutron induced reactions on Cr-, Fe- and Ni-isotopes in the energy range 9 to 21 MeV," Report 3502 (1998), Kernforschungsanlage, Juelich.
[204] Z. Muyao, Z. Yongfa, W. Chuanshan *et al.*, "Shell effect from the cross section of the (n,2n) reaction produced by 14.6 MeV neutrons," CHIN. J. NUCL. PHYS. **9**, 34 (1987).
[205] G. R. Pansare and V. N. Bhoraskar, "Measurement of 79Br(n,2n)78Br, 63Cu(n,2n)62Cu, 58Ni(n,2n)57Ni, 54Fe(n,2n)53Fe, 50Cr(n,2n)49Cr, 46Ti(n,2n)45Ti reaction cross-sections at 14.7 MeV neutron energy," INT. J. MOD. PHYS. E **2**, 259 (1993).
[206] H. Pollehn and H. Neuert, "Bestimmung von Wirksungsquerschnitten einiger Kernreaktionen durch 14 MeV Neutronen nach einer Aktivierungsmethode," ZEIT. NATURFORSCHUNG, SECT. A **16**, 227 (1961).
[207] S. M. Qaim, "Activation cross sections, isomeric cross-section ratios and systematics of (n,2n) reactions at 14-15 MeV," NUCL. PHYS. A **185**, 614 (1972).
[208] L. A. Rayburn, "14-MeV (n,2n) cross sections of N^{14}, P^{31}, K^{39}, Ti^{46}, Cr^{50} and Fe^{54}," BULL. AM. PHYS. SOC. **3**, 365(G13) (1958).
[209] L. A. Rayburn, "14.4 MeV (n,2n) cross sections," PHYS. REV. **122**, 168 (1961).
[210] J. C. Robertson, B. N. Audric, and P. Kolkowski, "The ^{56}Fe(n,p)^{56}Mn and ^{27}Al(n,a)^{24}Na cross sections at 14.78 MeV," J. NUCL. ENERGY **27**, 139 (1973).
[211] T. B. Ryves, P. Kolkowski, and K. J. Zieba, "Cross section measurements of ^{56}Fe(n,p)^{56}Mn, ^{63}Cu(n,2n)^{62}Cu and ^{65}Cu(n,2n)^{64}Cu between 14 and 19 MeV," METROL. **14**, 127 (1978).
[212] T. B. Ryves, P. Kolkowski, and K. J. Zieba, "Cross section measurements of ^{14}N(n,2n)^{13}N, ^{19}F(n,2n)^{18}F, ^{54}Fe(n,2n)^{53}Fe, ^{27}Al(n,p)^{27}Mg and ^{27}Al(n,a)^{24}Na," JOUR. PHYS. G **4**, 1783 (1978).
[213] H. Sakane, Y. Kasugai, M. Shibata, T. Iida, A. Takahashi, T. Fukahori, and K. Kawade, "Measurement of activation cross-sections for (n,2n) reactions producing short-lived nuclei in the energy range between 13.5 and 14.9 MeV," ANNALS NUCL. ENERGY **28**, 1175 (2001).
[214] S. R. Salisbury and R. A. Chalmers, "Fe^{54}(n,p), (n,a), and (n,2n) cross sections," PHYS. REV. **140**, B305 (1965).
[215] Y. Uwamino, T. S. Soewarsono, H. Sugita, Y. Uno, T. Nakamura, T. Shibata, M. Imamura, and S. I. Shibata, "High-energy p-Li neutron field for activation experiment," NUCL. INST. METH. PHYS. RES. A **389**, 463 (1997).
[216] M. Viennot, M. Berrada, G. Paic, and S. Joly, "Cross-section measurements of (n,p) and (n,np + pn + d) reactions for some titanium, chromium, iron , cobalt, nickel and zinc isotopes around 14 MeV," NUCL. SCI. ENG. **108**, 289 (1991).
[217] G. P. Dolya, A. P. Klyucharev, V. P. Bozhko, V. Y.

Golovnya, A. S. Kachan, and A. I. Tutubalin, "Differential and integral cross-sections for (n,alfa) reactions on nuclei Fe-54,-56,-57,-58 and Ni-58,-60,-62 at neutron energy 14.7 MeV," **vol.4**, 173 (1975). 3-rd All-Union Conf. on Neutron Phys., Kiev 1975.

[218] R. S. Pedroni, C. R. Howell, G. M. Honore, H. G. Pfutzner, R. C. Byrd, R. L. Walter, and J. P. Delaroche, "Energy dependence of the deformed optical potential for neutron scattering from ^{54,56}Fe and ^{58,60}Ni up to 80 MeV," PHYS. REV. C **38**, 2052 (1988).

[219] A. I. Tutubalin, A. P. Klyucharev, V. P. Bozhko, V. Y. Golovnya, G. P. Dolya, A. S. Kachan, and N. A. Shlyakhov, "Elastic scattering of 14.7 MeV neutrons on iron, cobalt and nickel isotopes," **vol.3**, 62 (1973). 2-nd Conf. on Neutron Physics, Kiev 1973.

[220] G. Bassini, L. Colli, E. Gadioli, and I. Iori, "The (n,d) reaction on Fe^{54}," NUCL. PHYS. **36**, 471 (1962).

[221] R. W. Benjamin and I. L. Morgan, "γ-rays from fast-neutron scattering in ^{54}Fe," PHYS. REV. **163**, 1252 (1967).

[222] W. M. Good, D. Paya, R. Wagner, and T. Tamura, "Total cross sections for kilovolt neutrons of even-odd nuclei in the region of the 3s strength-function resonances," PHYS. REV. **151**, 912 (1966).

[223] J. A. Harvey, Private communication (1987).

[224] C. T. Hibdon, "No title," Progress Report 4963 (1953), Argonne National Laboratory.

[225] M. S. Pandey, J. A. Harvey, J. B. Garg, and W. M. Good, "Dependence of level spacing of the isotopes of iron upon parity," Progress Report 5025 (1975), Oak Ridge National Laboratory.

[226] D. M. Chittenden II, D. G. Gardner, and R. W. Fink, "New isotope of manganese; cross sections of the iron isotopes from 14.8-MeV neutrons," PHYS. REV. **122**, 860 (1961).

[227] A. Ercan, M. N. Erduran, M. Subasi, E. Gueltekin, G. Tarcan, A. Baykal, and M. Bostan, "14.6 MeV neutron induced reaction cross section measurements," 376 (1991). Conf. on Nucl. Data for Sci. and Technol., Juelich 1991.

[228] A. Fessler, A. J. M. Plompen, D. L. Smith, J. W. Meadows, and Y. Ikeda, "Neutron activation cross-section measurements from 16 to 20 MeV for isotopes of F, Na, Mg, Al, Si, P, Cl, Ti, V, Mn, Fe, Nb, Sn and Ba," NUCL. SCI. ENG. **134**, 171 (2000).

[229] A. A. Filatenkov, "Neutron activation cross sections measured at kri in neutron energy region 13.4 - 14.9 MeV," Report 0460 (2016). USSR report to the INDC, IAEA, Vienna.

[230] F. Habbani and G. Paic, "Measurements of (n,p) and (n,np) cross-sections for some Fe isotopes at 14.7 MeV," APPL. RADIAT. ISOT. **39**, 1041 (1988).

[231] Y. Kasugai, H. Yamamoto, K. Kawade, Y. Ikeda, Y. Uno, and H. Maekawa, "Activation cross section measurement of reactions producing short-lived nuclei at neutron energy between 13.4 MeV and 14.9 MeV," 935 (1994). Conf. on Nucl. Data for Sci. and Techn., Gatlinburg 1994.

[232] J. J. Singh, "Neutron reaction cross sections of iron at 14.5 MeV," TRANS. AMER. NUCL. SOC. **15**, 147 (1972).

[233] H. Beer, L. D. Hong, and F. Kaeppeler, "A measurement of the total neutron cross section of iron-58 in the energy range from 7 to 325 keV," NUCL. SCI. ENG. **67**, 184 (1978).

[234] D. M. Chittenden II, D. G. Gardner, and R. W. Fink, "New isotope of manganese; cross sections of the iron isotopes from 14.8-MeV neutrons," PHYS. REV. **122**, 860 (1961).

[235] N. C. Dyer and J. H. Hamilton, "^{56}Fe and ^{58}Fe(n,p) cross sections for 14.4 MeV neutrons," J. INORG. NUCL. CHEM. **34**, 1119 (1972).

[236] L. I. Klochkova, B. S. Kovrigin, V. N. Kuritsin, N. S. Lavrova, E. V. Cherepanov, and V. A. Shibaev, "Study of the (n,p),(n,np) reactions on ^{27}Al, ^{50}Cr, ^{54}Fe, ^{58}Fe at 14.1 MeV neutron energy," p. 342 (1981). 31-st Conf. Nucl. Spectr. and Nucl. Struct., Samarkand 1981.

[237] A. D. Majdeddin, V. Semkova, R. Doczi, C. M. Buczko, and J. Csikai, "Investigations on (n,alpha) cross sections in the 14 MeV region.," Report 031 (1997). Hungarian report to the INDC, IAEA, Vienna.

[238] R. Li, W. Sun, E. Soukhovitskii, J. Quesada, and R. Capote, "Dispersive coupled-channels optical-model potential with soft-rotator couplings for Cr, Fe and Ni isotopes," PHYS. REV. C **87**, 054611 (2013).

[239] W. Sun, R. Li, E. Soukhovitskii, J. Quesada, and R. Capote, "Fully Lane-consistent dispersive optical model potential for even Fe isotopes based on a soft-rotator model," NUCL. DATA SHEETS **118**, 191 (2014).

[240] A. J. Koning and J. P. Delaroche, "Local and global nucleon optical models from 1 keV to 200 MeV," NUCL. PHYS. A **713**, 231 (2003).

[241] V. Avrigeanu, P. E. Hodgson, and M. Avrigeanu, "Global optical potentials for emitted alpha particles," PHYS. REV. C **49**, 2136 (1994).

[242] H. An and C. Cai, "Global deuteron optical model potential for the energy range up to 183 MeV," PHYS. REV. C **73**, 054605 (2006).

[243] F. B. Jr. and G. Greenlees, "Annual Report," J.H.Williams Laboratory, Univ. Minnesota 1969.

[244] A. Iwamoto and K. Harada, "Mechanism of cluster emission in nucleon-induced preequilibrium reactions," PHYS. REV. C **26**, 1821 (1982).

[245] C. Kalbach, "Systematics of continuum angular distributions: Extensions to higher energies," PHYS. REV. C **37**, 2350 (1988).

[246] C. Kalbach and F. M. Mann, "Phenomenology of continuum angular distributions. I. Systematics and parametrization," PHYS. REV. C **23**, 112 (1981).

[247] J. M. Blatt and L. C. Biedenharn, "The angular distribution of scattering and reaction cross sections," REV. MOD. PHYS. **24**, 258 (1952).

[248] H. M. Hofmann, J. Richert, J. W. Tepel, and H. A. Weidenmüller, "Direct reactions and Hauser-Feshbach theory," ANN. PHYS. **90**, 403 (1975).

[249] P. A. Moldauer, "Evaluation of the fluctuation enhancement factor," PHYS. REV. C **14**, 764 (1976).

[250] C. A. Engelbrecht and H. A. Weidenmüller, "Hauser-Feshbach theory and Ericson fluctuations in the presence of direct reactions," PHYS. REV. C **8**, 859 (1973).

[251] R. Capote, M. Herman, P. Obložinský *et al.*, "RIPL – reference input parameter library for calculation of nuclear reactions and nuclear data evaluations," NUCL. DATA SHEETS **110**, 3107 (2009).

[252] N. Fotiades, R. O. Nelson, and M. Devlin, "First 3^- excited state of ^{56}Fe," PHYS.REV. C **81**, 037304 (2010).

[253] E. Cornelis, L. Mewissen, and F. Poortmans, "Total neutron cross section of Fe-54 and Fe-56 in the energy range 500 keV to 19 MeV," Private communication; EX-

FOR:22316 (1995).
[254] A. Hibden, Report ANL-4963, Argonne National Laboratory 1953. Data from V. McLane, Neutron Cross Sections, Vol. 2 (Academic Press, 1988).
[255] J. B. Garg, S. Jain, and J. A. Harvey, "Neutron total cross section and resonance parameters of ^{58}Fe," PHYS. REV. C **18**, 1141 (1978).
[256] S. W. Cierjacks, I. Schouky, and F. Voss, "Investigation of s-wave resonances and a possible doorway state in Fe below 850 keV," Private communication (1978).
[257] T. Kawano and K. Shibata, "Covariance evaluation system," JAERI data/code, Japan Atomic Energy Research Institute, Tokai, Japan (1997).
[258] M. Salvatores *et al.*, "Uncertainty and target accuracy assessment for innovative systems using recent covariance data evaluations," WPEC Subgroup 26, OECD-NEA, Paris 2008.
[259] J. Bess*et al.*, "International criticality safety benchmark evaluation project," OECD-NEA, Paris.
[260] Monte Carlo Code Group, "A general Monte Carlo N-particle (MCNP) transport code, ver. 6.1," unpublished.
[261] L. Trykov, J. Kolevatov, A. Nikolaev, I. Buryan, M. Marek, B. Yanskiy, M. Tikhiy, and P. Otopal, "Experimental researches of outflow spectra of neutron and gamma radiations for spheres from iron," Preprint 943, IPPE, Obninsk 1979.
[262] S. P. Simakov, B. V. Devkin, M. G. Kobozev, A. A. Lychagin, V. A. Talalaev, and A. A. Androsenko, "14 MeV facility and research in IPPE," Report INDC(CCP)-351, IAEA, Vienna 1993.